Journal of Physics: Condensed Matter

TOPICAL REVIEW

The Hubbard dimer: a density functional case study of a many-body problem

To cite this article: D J Carrascal *et al* 2015 *J. Phys.: Condens. Matter* **27** 393001

View the article online for updates and enhancements.

Related content

- Exact maps in density functional theory for lattice models
  Tanja Dimitrov, Heiko Appel, Johanna I Fuks et al.
- Charge transfer in time-dependent density functional theory
  Neepa T Maitra
- Transport through correlated systems with density functional theory
  S Kurth and G Stefanucci

Recent citations

- Kinetic-Energy Density-Functional Theory on a Lattice
  Iris Theophilou *et al*
- Density functional theory of electron transfer beyond the Born-Oppenheimer approximation: Case study of LiF
  Chen Li *et al*
- Justin C. Smith *et al*

IOP ebooks™

Bringing you innovative digital publishing with leading voices to create your essential collection of books in STEM research.

Start exploring the collection - download the first chapter of every title for free.

This content was downloaded from IP address 130.120.229.69 on 23/07/2018 at 14:09

IOP Publishing Journal of Physics: Condensed Matter
J. Phys.: Condens. Matter **29** (2017) 019501 (1pp) doi:10.1088/0953-8984/29/1/019501

Corrigendum: The Hubbard dimer: a density functional case study of a many-body problem (2015 *J. Phys.: Condens. Matter* **27** 393001)

D J Carrascal[1,2], J Ferrer[1,2], J C Smith[3] and K Burke[3]

[1] Department of Physics, Universidad de Oviedo, 33007 Oviedo, Spain
[2] Nanomaterials and Nanotechnology Research Center, Oviedo, Spain
[3] Departments of Chemistry and of Physics, University of California, Irvine, CA 92697, USA

E-mail: dj.carrascal@gmail.com

Received 20 September 2016
Accepted for publication 6 October 2016
Published 10 November 2016

Three equations are incorrect. First, equation (56) should read

$$E_C \sim -U(1-|n_1-1|)^2/2, \quad U \gg 2\,t \tag{56}$$

so that it agrees with equation (B.12). Equation (114) is missing an addition sign and the correct form is

$$g_1 = g_0 + \left(u\,\frac{\partial h}{\partial g} - 1\right)\frac{\partial g(\lambda)}{\partial \lambda}\bigg|_{\substack{g=g_0\\ \lambda=1}} \tag{114}$$

where we have also clarified that the rhs is evaluated at $g = g_0$. Lastly, equation (115) reads

which differs from equation (115) in the paper by several factors of u. Although figure 22 of the paper was reproduced using the correct equations, we found that numerical errors yielded an incorrect result for the case $U = 0.2$. We reproduce this figure again to be consistent with the exact results obtained using the formulation above.

To clarify, all instances of the argument (λ) in section 6 imply (λU).

$$\frac{\partial g(\lambda)}{\partial \lambda}\bigg|_{\substack{g=g_0\\ \lambda=1}} = \frac{(1-\rho)\,(1+\rho)^3\,u^2[(3\,\rho/2 - 1 + \rho\,(1+\rho)^3\,u\,a_2(u))\,a_{12} - \rho\,(1+(1+\rho)^3\,u\,a_1(u))\,a_{22}]}{2\,g_0\,(1+(1+\rho)^3\,u\,a_2(u))^2} \tag{115}$$

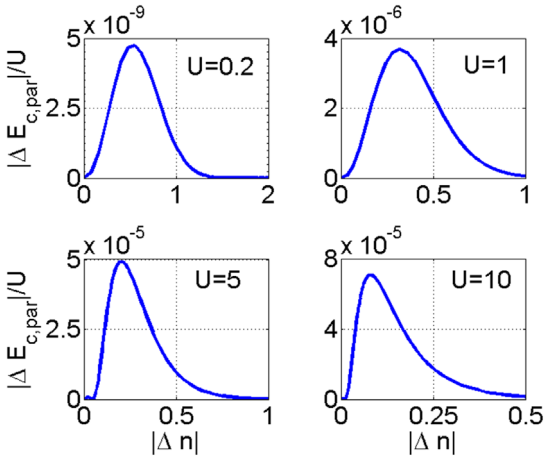

Figure 22. Error in $E_{C,par}(\rho)/U$ for different U and $2\,t$ as a function of $|\Delta n|$.

 © 2016 IOP Publishing Ltd Printed in the UK

IOP Publishing Journal of Physics: Condensed Matter
J. Phys.: Condens. Matter **27** (2015) 393001 (34pp) doi:10.1088/0953-8984/27/39/393001

Topical Review

The Hubbard dimer: a density functional case study of a many-body problem

D J Carrascal[1,2], J Ferrer[1,2], J C Smith[3] and K Burke[3]

[1] Department of Physics, Universidad de Oviedo, 33007 Oviedo, Spain
[2] Nanomaterials and Nanotechnology Research Center, Oviedo, Spain
[3] Departments of Chemistry and of Physics, University of California, Irvine, CA 92697, USA

E-mail: dj.carrascal@gmail.com

Received 9 April 2015, revised 24 July 2015
Accepted for publication 4 August 2015
Published 17 September 2015

Abstract

This review explains the relationship between density functional theory and strongly correlated models using the simplest possible example, the two-site Hubbard model. The relationship to traditional quantum chemistry is included. Even in this elementary example, where the exact ground-state energy and site occupations can be found analytically, there is much to be explained in terms of the underlying logic and aims of density functional theory. Although the usual solution is analytic, the density functional is given only implicitly. We overcome this difficulty using the Levy–Lieb construction to create a parametrization of the exact function with negligible errors. The symmetric case is most commonly studied, but we find a rich variation in behavior by including asymmetry, as strong correlation physics vies with charge-transfer effects. We explore the behavior of the gap and the many-body Green's function, demonstrating the 'failure' of the Kohn–Sham (KS) method to reproduce the fundamental gap. We perform benchmark calculations of the occupation and components of the KS potentials, the correlation kinetic energies, and the adiabatic connection. We test several approximate functionals (restricted and unrestricted Hartree–Fock and Bethe ansatz local density approximation) to show their successes and limitations. We also discuss and illustrate the concept of the derivative discontinuity. Useful appendices include analytic expressions for density functional energy components, several limits of the exact functional (weak- and strong-coupling, symmetric and asymmetric), various adiabatic connection results, proofs of exact conditions for this model, and the origin of the Hubbard model from a minimal basis model for stretched H_2.

Keywords: density functional theory, Hubbard model, strongly correlated electron systems

(Some figures may appear in colour only in the online journal)

1. Introduction

In condensed matter, the world of electronic structure theory can be divided into two camps: the weakly and the strongly correlated. Weakly correlated solids are almost always treated with density-functional methods as a starting point for ground-state properties [28, 31, 36, 49, 110]. Many-body (MB) approximations such as GW might then be applied to find properties of the quasi-particle spectrum, such as the gap [14, 182, 228]. This approach is 'first-principles', in the sense that it uses the real-space Hamiltonian for the electrons in the field of the nuclei, and produces a converged result that is independent of the basis set, once a sufficiently large basis set is used. Density functional theory (DFT) is known to be exact in principle, but the usual approximations often fail when correlations become strong [44].

 © 2015 IOP Publishing Ltd Printed in the UK

On the other hand, strongly correlated systems are most often treated via lattice Hamiltonians with relatively few parameters [47, 114]. These simplified Hamiltonians can be easier to deal with, especially when correlations are strong [47, 53]. Even approximate solutions to such Hamiltonians can yield insight into the physics, especially for extended systems [212]. However, such Hamiltonians can rarely be unambiguously derived from a first-principles starting point, making it difficult (if not impossible) to say how accurate such solutions are quantitatively or to improve on that accuracy. Moreover, methods that yield approximate Green's functions are often more focused on response properties or thermal properties rather than on total energies in the ground-state.

On the other hand, the ground-state energy of electrons plays a much more crucial role in chemical and material science applications [152, 166]. Very small energy differences determine geometries and sometimes qualitative properties, such as the nature of a transition state in a chemical reaction [56, 91, 128] or where a molecule is adsorbed on a surface [17, 165]. An error of 0.05 eV changes a reaction rate by a factor of 5 at room temperature. Thus quantum chemical development has focused on extracting extremely accurate energies for the ground and other eigenstates [64, 88, 111, 197, 249]. This is routinely achieved for molecules using coupled-cluster methods (CCSD(T)) and reasonable basis sets [185, 213]. Such methods are called *ab initio*, but are not yet widespread for solids, where quantum Monte Carlo (QMC) is more often used [60, 226]. DFT calculations for molecules are usually much less computationally demanding, but the errors are less systematic and less reliable [167].

However, many materials of current technological interest are both chemically complex and strongly correlated. Numerous metal oxide materials are relevant to novel energy technologies, such as TiO_2 for light-harvesting [164] or LiO compounds for batteries [83, 218]. For many cases, DFT calculations find ground-state structures and parameters, but some form of strong correlation method, such as introducing a Hubbard U or applying dynamical mean field theory (DMFT), is needed to correctly align bands and predict gaps [12, 69]. There is thus great interest in developing techniques that use insights from both ends, such as DFT + U and dynamical mean field theory [13, 95, 115, 116, 118, 119].

There are two different approaches to combining DFT with lattice Hamiltonians [37]. In the first, more commonly used, the lattice Hamiltonian is taken as given, and a density function(al) theory is constructed for that Hamiltonian [81]. We say function(al), not functional, as the density is now given by a list of occupation numbers, rather than a continuous function in real space. The parenthetical reminds us that although everything is a function, it is analogous to the functionals of real-space DFT. We will refer to this method as SOFT, i.e. site-occupation function(al) theory [204], although in the literature it is also known as lattice density functional theory [101]. While analogs of the basic theorems of real-space DFT can be proven such as the Hohenberg-Kohn (HK) theorems and the Levy constrained search formulation for SOFT, it is by no means clear [86] how such schemes might converge to the real-space functionals as more and more orbitals (and hence parameters) are added. Alternatively, one may modify efficient solvers of lattice models so that they can be applied to real-space Hamiltonians (as least in 1D), and use them to explore the nature of the exact functionals and the failures of present approximations [214, 236]. While originally formulated for Hubbard-type lattices, SOFT has been extended and applied to many different models include quantum-spin chains [7], the Anderson impurity model [40, 221], the 1D random Fermi–Hubbard model [247], and quantum dots [199].

These two approaches are almost orthogonal in philosophy. In the first, one finds approximate function(al)s for lattice Hamiltonians, and can then perform Kohn–Sham (KS) DFT calculations on much larger (and more inhomogeneous) lattice problems [33], but with all the usual caveats of DFT treatments (am I looking at interesting physics or a failure of an uncontrolled approximation?). For smaller systems, one can often also compare approximate DFT calculations with exact results, results which would be prohibitively expensive to calculate on real-space Hamiltonians. The dream of lattice models in DFT is that lessons we learn on the lattice can be applied to real-space calculations and functional developments. To this end, work has been done on understanding self-interaction corrections [233], and on wedding TDDFT and DMFT methods for application to more complex lattices (e.g. 3D Hubbard) [105]. And while it is beyond the scope of this current review, much work has been done on developing and applying density-matrix functional theory for the lattice as well [142–145, 195, 196]. While such results can be very interesting, it is often unclear how failures of approximate lattice DFT calculations are related to failures of the standard DFT approximations in the real world.

There is much interest in extracting excited-state information from DFT, and time-dependent (TD) DFT [192] has become a very popular first-principles approach [32, 151, 224]. Because exact solutions and useful exact conditions are more difficult for TD problems, there has been considerable research using lattices. TD-SOFT can be proven for the lattice in much the same way SOFT is proven from ground-state DFT. This generalization is worked out carefully in [55, 220]. An adiabatic approximation for TDSOFT was introduced in [227]. Applications of TD-SOFT typically involve Hubbard chains both with and without various types of external potentials [15, 106, 107, 149, 222]. However, TD-SOFT has also been applied to the dimer to understand the effects of the adiabatic approximation in TD-DFT [66–68], strong correlation [222], and TD-LDA results for stretched H_2 in real-space [16]. Unfortunately, we will already fill this article simply discussing the ground-state SOFT problem, and save the TD case for future work.

To get the basic idea, consider figure 1. It shows the asymmetric Hubbard dimer in two different regimes. In this work we use asymmetric to mean differing on-site potentials. On the left, the Hubbard U energy is considerably larger than the difference in on-site potentials and the hopping energy t. This is the case most often analyzed, where strong correlations drive the system into the Mott–Hubbard regime if U is also

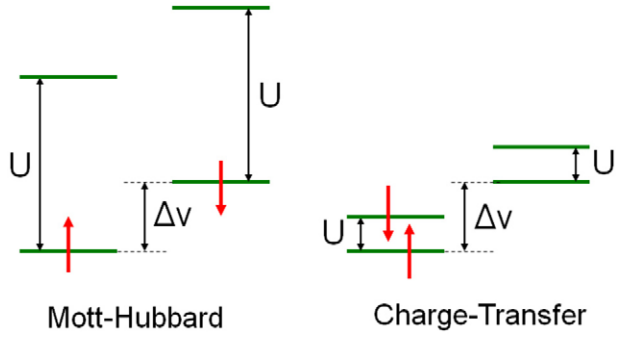

Figure 1. Many-body view of two distinct regimes of the asymmetric Hubbard dimer. On the left, the charging energy is much greater than the difference in on-site potentials. On the right, the situation is reversed.

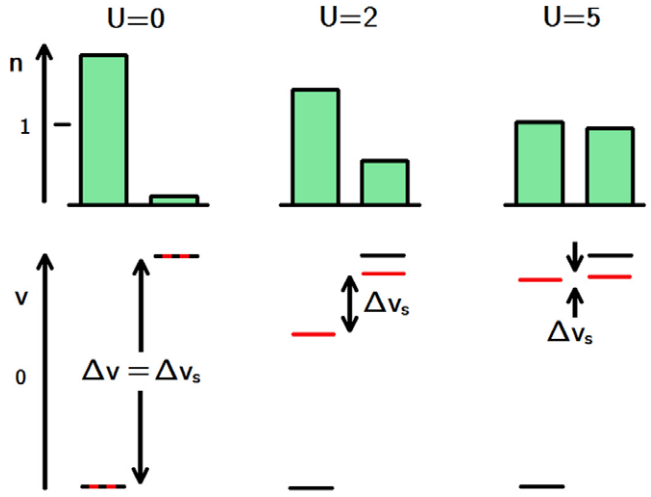

Figure 2. DFT view: occupations n and potentials v of an asymmetric half-filled Hubbard dimer as a function of U. The on-site potential difference Δv is shown in black and the KS on-site potential difference Δv_S is in red. The second and third panels correspond to the situations of figure 1.

considerably larger than t. The on-site occupations are in this case close to 1. On the right panel, U is in contrast smaller than the on-site potential difference Δv, and here the dimer stays in the charge-transfer regime, where both electrons mostly sit in the same deeper well. This is the many-body view of the physics of an asymmetric Hubbard dimer.

Now we turn to the KS-DFT viewpoint. Here, we replace the interacting Hubbard dimer ($U \neq 0$) with a non-interacting ($U = 0$) tight-binding dimer, called the KS system, that reproduces the Hubbard occupations. In figure 2, we take the asymmetric dimer with the same on-site potential difference, but we vary U. We plot the occupations, showing how, as U increases, their difference decreases. But we also plot the on-site potentials of the Kohn–Sham model, Δv_S, that are chosen to reproduce the occupations of the interacting system with a given value of U. As U increases, the KS on-site potential difference reduces and the offset from 0 increases. The middle panel corresponds to the charge-transfer conditions of figure 1, while the last panel corresponds to the Mott–Hubbard conditions of figure 1. The basic theorems of DFT show that if we know the energy as a function(al) of the density, we can determine the occupations by solving effective tight-binding equations, the KS equations, and then find the *exact* ground-state energy. This is not mean-field theory. It is instead a horribly contorted logical construction, that is wonderfully practical for computations of ground-state quantities. Inside this article, we give explicit formulas for the energy functional of the Hubbard dimer.

We perform a careful study of the Hubbard dimer, to show the differences between SOFT and real-space DFT. We show how it is *necessary* to introduce inhomogeneity into the site occupations in order to find the exact density function(al) explicitly. In section 2.1 we explain the logic of the KS DFT approach in excruciating detail in order to both illustrate the concepts to those unfamiliar with the method and to give explicit formulas for anyone doing SOFT calculations. We elucidate the differences between the KS and the many-body Green's functions in section 4.3. Next, in sections 4 and 5 we discuss in detail both concepts and tools for strong correlation, and explain how the gap problem appears in DFT. We construct the adiabatic connection formula for the exact function(al) in section 5.2, showing how it is quantitatively similar to those of real-space DFT. We use the theory to construct a simple parametrization for the exact function(al) for this problem in section 6, where we also demonstrate the accuracy of our formula by finding ground-state energies and densities by solving the KS equations with our parametrization. In section 7.1, we study the broken-symmetry solutions of Hartree–Fock theory, showing that these correctly yield both the strongly-correlated limit and the approach to this limit for strong correlation. In section 7.2 we present BALDA (Bethe-ansatz local density approximation), a popular approximation for lattice DFT, and in section 7.3 we compare the accuracy of BALDA and Hartree–Fock to each other. We discuss fractional particle number and the derivative discontinuity in section 8. Finally, we end with a discussion of our results in section 9. In table 1 we list our notation for the Hubbard dimer, as well as many standard DFT definitions.

Our purpose here is several-fold. Perhaps most importantly, this article is intended to explain the logic of modern DFT to our friends who are more familiar with strongly correlated lattice systems. We believe this should be equally useful to any researcher interested in many-electron systems such as traditional quantum chemists, or atomic and molecular physicists, since we use and explain the simplest model of strong correlation to illustrate many of the basic techniques of modern DFT. There are many more tricks and constructions, but we save those for future work.

Secondly, the article forms an essential reference for those researchers interested in SOFT, possibly in very different contexts and applied to very different models. It shows precisely how concepts from first-principles calculations are realized in lattice models. Third, we give many exact results for this simple model, expanding in many different limits, showing that even in this simple case, there are orders-of-limits issues. Fourth, we use DFT techniques to find a simple but extremely accurate parametrization of the exact function(al) for this model. Even though the

Table 1. Standard DFT definitions and our Hubbard dimer notation.

Definition	Description
Generic DFT	
$\Psi[n]$	Many-body wfn of density n
$\Phi[n]$	Kohn–Sham wfn of density n
$F = T + V_{ee}$	Hohenberg–Kohn functional
$E_{XC} = F - T_S - U_H$	Exchange-correlation energy
$E_X = \langle\Phi\vert\hat{V}_{ee}\vert\Phi\rangle - U_H$	Exchange energy
$E_X = -U_H/2$	Exchange energy for 2 electrons
$E_C = T_C + U_C$	Total correlation energy
$T_C = T - T_S$	Kinetic correlation energy
$U_C = V_{ee} - U_H - E_X$	Potential correlation energy
$U_{XC}(\lambda) = U_{XC}^{\lambda}/\lambda$	Adiabatic connection integrand
$T_C = E_C - \mathrm{d}E_C^{\lambda}/\mathrm{d}\lambda\vert_{\lambda=1}$	Method to extract T_C from E_C
$U_C = \mathrm{d}E_C^{\lambda}/\mathrm{d}\lambda\vert_{\lambda=1}$	Method to extract U_C from E_C
$\hat{h}_S = -\nabla^2/2 + v_S$	Kohn–Sham hamiltonian
$v_S = v + v_H + v_{XC}$	Kohn–Sham one-body potential
$E_C^{trad} = E - E^{HF}$	Quantum chemical corr. energy
SOFT Hubbard	
n_1, n_2	Occupations at sites 1, 2
$N = n_1 + n_2$	Total number of electrons
$\Delta n = n_2 - n_1$	Occupation difference
$\Delta m = m_2 - m_1$	Magnetization difference
v_1, v_2	On-site potentials
$\bar{v} = (v_1 + v_2)/2 = 0$	On-site potential average
$\Delta v = v_2 - v_1$	On-site potential difference
$\Delta v_{XC} = v_{XC,2} - v_{XC,1}$	XC potential difference
$U_H = U(N^2 + \Delta n^2)/4$	Hartree energy
$E_{HX} = U(N^2 + \Delta n^2)/8$	Hartree-Exchange energy
$T_S = -t\sqrt{(2-\vert N-2\vert)^2 - \Delta n^2}$	Single particle hopping energy
Dimensionless variables	
$\epsilon = E/2t$	Energy in units of hopping
$u = U/2t$	Hubbard U in units of hopping
$\nu = \Delta v/2t$	Pot. diff. in units of hopping
$\rho = \vert\Delta n\vert/2$	Reduced density difference
$\bar{\rho} = 1 - \rho$	Asymmetry parameter

model can be solved analytically, the function(al) cannot be expressed explicitly. Thus our parametrization provides an ultra-convenient and ultra-accurate expression for the exact function(al) for this model, that can be used in the ever increasing applications of SOFT. Finally, we examine several standard approximations to SOFT, including both restricted and unrestricted mean field theory, and the BALDA, and we find surprising results.

2. Background

In this section we briefly introduce real-space DFT, and the logical underpinnings for everything that follows. Then we discuss the mean-field approach to the Hubbard model as well as a few well-known results and limits for the Hubbard dimer. Throughout this section we use atomic units for all real-space expressions so all energies are in Hartree and all distances are in Bohr.

2.1. Density functional theory

We restrict ourselves to non-relativistic systems within the Born-Oppenheimer approximation with collinear magnetic fields [51]. Density functional theory is concerned with efficient methods for finding the ground-state energy and density of N electrons whose Hamiltonian contains three contributions:

$$\hat{H} = \hat{T} + \hat{V}_{ee} + \hat{V}. \tag{1}$$

The first of these is the kinetic energy operator, the second is the electron–electron repulsion, while the last is the one-body potential,

$$\hat{V} = \sum_{i=1}^{N} v(\mathbf{r}_i). \tag{2}$$

Only N and $v(\mathbf{r})$ change from one system to another, be they atoms, molecules or solids. In 1964, Hohenberg and Kohn proved that for a given electron–electron interaction, there was at most one $v(\mathbf{r})$ that could give rise to the ground-state one-particle density $n_0(\mathbf{r})$ of the system, thereby showing that all ground-state properties of that system were uniquely determined by $n_0(\mathbf{r})$ [98]. The ground-state energy E_0 could then be found by splitting the variational principle into two steps via the Levy–Lieb constrained search approach [129, 132]. First, the universal functional F is determined,

$$F[n] = \min_{\Psi\to n}\langle\Psi\vert\,\hat{T} + \hat{V}_{ee}\,\vert\Psi\rangle = T[n] + V_{ee}[n] \tag{3}$$

where the minimization is over all normalized, antisymmetric Ψ with one-particle density $n(\mathbf{r})$. This establishes a one-to-one connection between wavefunctions and ground-state densities, and enables us to define the minimizing wavefunction functional $\Psi[n_0]$. Then the ground-state energy is determined by a second minimization step of the energy functional $E[n]$,

$$E_0 = \min_n\{E[n]\} = \min_n\left\{F[n] + \int \mathrm{d}^3r\, n(\mathbf{r})\, v(\mathbf{r})\right\}. \tag{4}$$

This shows that E_0 can be found from a search over one-particle densities $n(\mathbf{r})$ instead of many-body wavefunctions Ψ, provided that the functional $F[n]$ is known. The Euler equation corresponding to the above minimization for fixed N is simply

$$\frac{\delta F[n]}{\delta n(\mathbf{r})}\Big|_{n_0(\mathbf{r})} = -v(\mathbf{r}). \tag{5}$$

Armed with the exact $F[n]$, the solution of this equation yields the exact ground-state density which, when inserted back into $F[n]$, yields the exact ground-state energy.

To increase accuracy and construct $F[n]$, modern DFT calculations use the Kohn–Sham (KS) scheme that imagines a fictitious set of non-interacting electrons with the same ground-state density as the real Hamiltonian [112]. These electrons satisfy the KS equations:

$$\left\{-\frac{1}{2}\nabla^2 + v_S(\mathbf{r})\right\}\phi_i(\mathbf{r}) = \epsilon_i\,\phi_i(\mathbf{r}), \tag{6}$$

where $v_S(\mathbf{r})$ is defined as the unique potential that generates single-electron orbitals $\phi_i(\mathbf{r})$ that reproduce the ground-state density of the real system,

$$n_0(\mathbf{r}) = \sum_{occ} |\phi_i(r)|^2. \tag{7}$$

To relate these to the interacting system, we write

$$F[n] = T_S[n] + U_H[n] + E_{XC}[n]. \tag{8}$$

T_S is the non-interacting (or KS) kinetic energy, given by

$$T_S[n] = \frac{1}{2}\int d^3 \sum_{i=1}^{N} |\nabla\phi_i(\mathbf{r})|^2 = \min_{\Phi\to n}\langle\Phi|\,\hat{T}|\Phi\rangle, \tag{9}$$

where we have assumed the KS wavefunction (as is almost always the case) is a single Slater determinant Φ of single-electron orbitals. The second expression follows from equation (3) applied to the KS system, it emphasizes that T_S is a functional of $n(\mathbf{r})$, and the minimizer defines $\Phi[n_0]$, the KS wavefunction as a density functional. Then $U_H[n]$ is the classical electrostatic self-repulsion of $n(\mathbf{r})$,

$$U_H[n] = \frac{1}{2}\int \mathrm{d}^3r \int \mathrm{d}^3r' \frac{n(\mathbf{r})\,n(\mathbf{r}')}{|\mathbf{r}-\mathbf{r}'|}, \tag{10}$$

and E_{XC} is called the exchange-correlation energy, and is *defined* by equation (8).

Lastly, we differentiate equation (8) with respect to the density. Applying equation (5) to the KS system tells us

$$v_S(\mathbf{r}) = -\frac{\delta T_S[n]}{\delta n(\mathbf{r})}, \tag{11}$$

yielding

$$v_S(\mathbf{r}) = v(\mathbf{r}) + v_H(\mathbf{r}) + v_{XC}(\mathbf{r}) \tag{12}$$

where $v_H(\mathbf{r})$ is the classical electrostatic potential and

$$v_{XC}(\mathbf{r}) = \frac{\delta E_{XC}}{\delta n(\mathbf{r})} \tag{13}$$

is the exchange-correlation potential. This is the single most important result in DFT, as it closes the set of KS equations. Given any expression for E_{XC} in terms of $n_0(\mathbf{r})$, either approximate or exact, the KS equations can be solved self-consistently to find $n_0(\mathbf{r})$ for a given $v(\mathbf{r})$. Under standard conditions, and with the exact functional, they always converge [237].

However, we also note that, just as in all such schemes, the energy of the KS electrons *does* not match that of the real system. This 'KS energy' i.e. the energy of the KS electrons, is

$$E_S[n] = \sum_i \epsilon_i = T_S + V_S, \tag{14}$$

but the actual energy is

$$E_0 = F[n_0] + V[n_0] = T_S[n_0] + U_H[n_0] + E_{XC}[n_0] + V[n_0] \tag{15}$$

where $n_0(\mathbf{r})$ and $T_S[n_0]$ have been found by solving the KS equations, and inserted into this expression. Thus, in terms of the KS orbital energies, there are double-counting corrections, which can be deduced from equations (14) and (15):

$$E_0 = E_S - U_H[n_0] + E_{XC}[n_0] - \int \mathrm{d}^3r\, n_0(\mathbf{r})\, v_{XC}[n_0](\mathbf{r}). \tag{16}$$

We emphasize that, with the *exact* $E_{XC}[n_0]$, solution of the KS equations yields the *exact* ground-state density and energy, and this has been done explicitly in model cases [237], but is computationally exorbitant. The practical use of the KS scheme is that simple, physically motivated approximations to $E_{XC}[n_0]$ often yield usefully accurate results for E_0, bypassing direct solution of the many-electron problem.

For the remainder of this article, we drop the subscript 0 for notational convenience, and energies will be assumed to be ground-state energies, unless otherwise noted. For many purposes, it is convenient to split E_{XC} into a sum of exchange and correlation contributions. The definition of the KS exchange energy is simply

$$E_X[n] = \langle\Phi[n]|\hat{V}_{ee}|\Phi[n]\rangle - U_H[n]. \tag{17}$$

The remainder is the correlation energy functional

$$E_C[n] = F[n] - \langle\Phi[n]|\,\hat{T} + \hat{V}_{ee}\,|\Phi[n]\rangle, \tag{18}$$

which can be decomposed into kinetic T_C and potential U_C contributions (see equations (75) and (76) in section 5). Additionally, all practical calculations generalize the preceding formulas for arbitrary spin using spin-DFT [20].

For just one particle ($N = 1$), there is no electron–electron repulsion, i.e. $V_{ee} = 0$. This means

$$E_X = -U_H, \quad E_C = 0, \qquad (N = 1), \tag{19}$$

i.e. the self-exchange energy exactly cancels the Hartree self-repulsion. Since there is no interaction, $F^0[n] = T[n] = T_S[n]$, and for one electron we know the explicit functional:

$$T_S = T^W = \int \mathrm{d}^3r\, |\nabla n|^2/(8n), \tag{20}$$

which is called the von Weisacker functional [240]. For two electrons in a singlet ($N = 2$),

$$E_X = -U_H/2, \qquad T_S = T^W, \qquad (N = 2), \tag{21}$$

but the correlation components are non-zero and non-trivial.

Many popular forms of approximation exist for $E_{XC}[n]$, the most common being the local density approximation (LDA) [20, 112, 179], the generalized gradient approximation (GGA) [22, 102, 126, 172, 174], and hybrids of GGA with exact exchange from a Hartree–Fock calculation [4, 23, 94, 175]. The computational ease of DFT calculations relative to more accurate wavefunction methods usually allows much larger systems to be calculated, leading to DFT's immense popularity today [183]. However, all these approximations fail in the paradigm case of stretched H_2, the simplest example of a strongly correlated system [18, 44, 92].

2.2. The Hubbard model

The Hubbard Hamiltonian is possibly the most studied, and simplest, model of a strongly correlated electron system. It was initially introduced to describe the electronic properties of narrow-band metals, whose conduction bands are formed by d and f orbitals, so that electronic correlations become important [61, 100]. The model was used to describe ferromagnetic, antiferromagnetic and spin-spiral instabilities and phases, as well as the metal-insulator transition in metals and oxides, including high-T_c superconductors [47, 127]. The

Hubbard model is both a qualitative version of a physical system depending on what terms are built in [11, 205] and also a testing-ground for new techniques since the simpler forms of the Hubbard model are understood very well [26, 27, 96, 97].

The model assumes that each atom in the lattice has a single orbital. The Hamiltonian is typically written as [54, 82, 153, 216]

$$\hat{H} = \sum_{i,\sigma} v_{i\sigma}\, \hat{n}_{i\sigma} - \sum_{i\,j\,\sigma} (t_{ij}\, \hat{c}^{\dagger}_{i\,\sigma}\, \hat{c}_{j\,\sigma} + \text{h.c.}) + \sum_{i} U_i\, \hat{n}_{i\uparrow}\, \hat{n}_{i\downarrow} \quad (22)$$

where at its simplest the on-site energies are all equal $v_{i\sigma} = 0$ as well as the Coulomb integrals $U_i = U$. Further, the hopping integrals t_{ij} typically couple only nearest neighbor atoms and are equal to a single value t.

We note that here the interaction is of ultra-short range, so that two electrons only interact if they are on the same lattice site. Further, they must have opposite spins to obey the Pauli principle. Simple examples of building in more complicated physics include using next-nearest-neighbor hoppings or nearest neighbors Coulomb integrals for high-T_c cuprate calculations and magnetic properties [48, 50, 138], and varying on-site potentials used to model confining potentials [189]. Also, adding more orbitals per site delivers multi-band Hubbard models, where Coulomb correlations may be added to some or all of the orbitals. The Hubbard model has an analytical solution in one dimension, via Bethe ansatz techniques [133, 134].

If the Hubbard U is small enough, a paramagnetic mean-field (MF) solution provides a reasonable description of the model in dimensions equal or higher than two. As an example, the Hubbard model in a honeycomb lattice can describe correctly a number of features of gated graphene samples [93]. However, for large U or in one dimension, more sophisticated approaches are demanded, which go beyond the scope of this article [61, 134].

We describe briefly the well-known broken-symmetry MF solution, where the populations of up- and down-spin electrons can differ. The standard starting point for the MF solution neglects completely quantum fluctuations:

$$(\hat{n}_{i\uparrow} - n_{i\uparrow})\,(\hat{n}_{i\downarrow} - n_{i\downarrow}) = 0, \qquad \text{(MF)} \quad (23)$$

where $n_{i\sigma} = \langle \hat{n}_{i\sigma} \rangle$, so that

$$\hat{V}^{\text{MF}}_{\text{ee}} = \sum_{i} U\, (n_{i\uparrow}\, \hat{n}_{i\downarrow} + n_{i\downarrow}\, \hat{n}_{i\uparrow} - n_{i\uparrow}\, n_{i\downarrow}). \quad (24)$$

The MF hamiltonian is then just an effective single-particle problem

$$\hat{H}^{\text{MF}} = \sum_{i\sigma} \hat{h}^{\text{eff}}_{i\sigma}, \quad (25)$$

$$\hat{h}^{\text{eff}}_{i\sigma} = v^{\text{MF}}_{i\sigma}\, \hat{n}_{i\sigma} - t \sum_{j} (\hat{c}^{\dagger}_{i\sigma} \hat{c}_{j\sigma} + \text{h.c.}), \quad (26)$$

where $v^{\text{MF}}_{i\sigma} = v_{i\sigma} + U\, n_{i\bar{\sigma}}$. This $\hat{H}^{\text{MF}}$ can be easily diagonalized if one assumes space-homogeneity of the occupations $n_{i,\sigma} = n_{\sigma}$. For large U, the broken symmetry solution (often ferromagnetic) has lower energy than the paramagnetic solution.

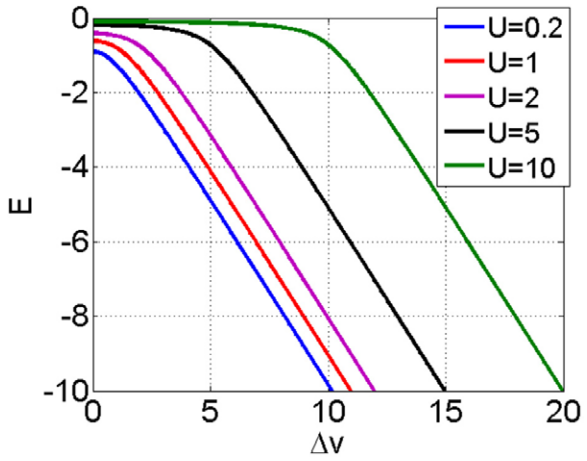

Figure 3. Ground-state energy of Hubbard dimer as a function of Δv for several values of U and $2\,t = 1$.

2.3. The two-site Hubbard model

We now specialize to a simple Hubbard dimer model with open boundaries, but we allow different on-site spin-independent energies by introducing a third term that produces asymmetric occupations,

$$\hat{H} = -t \sum_{\sigma} (\hat{c}^{\dagger}_{1\sigma} \hat{c}_{2\sigma} + \text{h.c}) + U \sum_{i} \hat{n}_{i\uparrow}\, \hat{n}_{i\downarrow} + \sum_{i} v_i \hat{n}_i \quad (27)$$

where we have made the choices $t_{12} = t^{*}_{21} = t$ and $v_1 + v_2 = 0$. Our notation for this Hamiltonian can be found in table 1. Specifically, the two-site model is useful in comparing approximate methods [147] or investigating highly local properties [34] due to its conceptual simplicity. Recently, the two-site model was realized experimentally using ultracold techniques with the hopes of experimentally building more arbitrary Hubbard models in the future [160]. This model was carefully investigated in a DFT context by Requist and Pankratov [187, 188].

It is straightforward to find an analytic solution of the model for any integer occupation N. However, we specialize to the particle sub-space $N = 2$, $S_z = 0$ in what follows unless otherwise stated. We expand the Hamiltonian in the basis set $[|1\uparrow\ 1\downarrow\rangle, |1\uparrow\ 2\downarrow\rangle, |1\downarrow\ 2\uparrow\rangle, |2\uparrow\ 2\downarrow\rangle]$:

$$\hat{H} = \begin{pmatrix} 2v_1 + U & -t & t & 0 \\ -t & 0 & 0 & -t \\ t & 0 & 0 & t \\ 0 & -t & t & 2v_2 + U \end{pmatrix} \quad (28)$$

The eigenstates are three singlets and a triplet state. The ground-state energy corresponds to the lowest-energy singlet, and can be found analytically. The expressions are given in appendix A. The wavefunction, density difference, and individual energy components are also given there. We plot in figure 3 the ground-state energy as a function of Δv for several values of U, while in figure 4, we plot the occupations.

When $U = 0$, we have the simple tight-binding result, for which the ground-state energy is

$$E = -\sqrt{(2\,t)^2 + \Delta v^2} \qquad (U = 0), \quad (29)$$

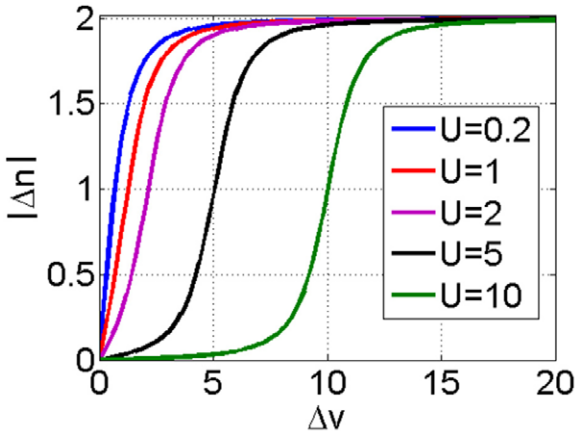

Figure 4. Ground-state occupation of Hubbard dimer as a function of Δv for several values of U and $2\,t = 1$.

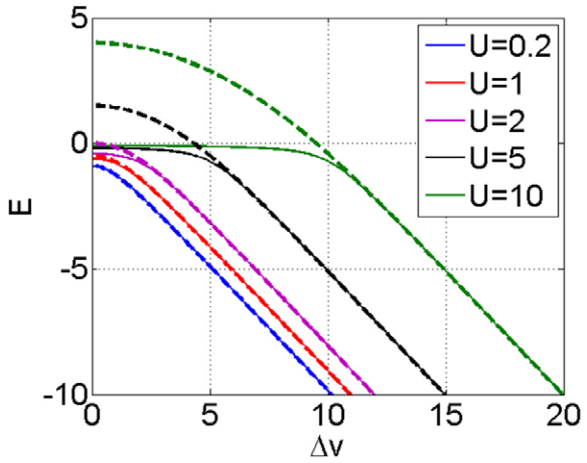

Figure 5. Ground-state energy of the Hartree–Fock Hubbard dimer (thick dashed line) and exact ground-state of the Hubbard dimer (thin solid line) as a function of Δv for several values of U and $2\,t = 1$.

$$\Delta n = -2\,\Delta v/\sqrt{(2\,t)^2 + \Delta v^2} \qquad (U = 0). \tag{30}$$

where Δn is defined in table 1. If there is only one electron, these become smaller by a factor of 2. The curves for $U = 0.2$ are indistinguishable (by eye) from the tight-binding result. We may simplify the expressions by introducing an effective hopping parameter,

$$\tilde{t} = t\sqrt{1 + (\Delta v/(2\,t))^2} \tag{31}$$

which accounts for the asymmetric potential. Then

$$\begin{aligned} E &= -2\tilde{t}, \qquad (U = 0), \\ \Delta n &= -\Delta v/\tilde{t}, \end{aligned} \tag{32}$$

i.e. the same equations as when $\Delta v = 0$.

In the other extreme, as U grows, we approach the strongly correlated limit. For a given Δv, as U increases, Δn decreases as in figures 2 and 4, see also figure 1 in [187], and the magnitude of the energy shrinks. Typically, the $E(\Delta v)$ curve morphs from the tight-binding result towards two straight lines for U large:

$$E \simeq (U - \Delta v)\,\Theta(\Delta v - U), \qquad U \gg 2\,t, \tag{33}$$

$$\Delta n \simeq -2\,\Theta(\Delta v - U), \qquad U \gg 2\,t. \tag{34}$$

We also have a simple well-known result for the symmetric limit, $\Delta v = 0$, where

$$E = -\sqrt{(2t)^2 + (U/2)^2} + U/2, \qquad (\Delta n = \Delta v = 0). \tag{35}$$

This vanishes rapidly with $1/U$ for large U. Its behavior is different from the case with finite Δv. Results for various limits and energy components are given in appendix A.

2.4. Quantum chemistry

Traditional quantum chemical methods (often referred to as *ab initio* by their adherents) usually begin with the solution of the Hartree–Fock equations [215]. For our Hubbard dimer, these are nothing but the mean-field equations of section 2.2. Expressing the paramagnetic HF Hamiltonian of equation (26) for two sites yields a simple tight-binding Hamiltonian and eigenvalue equation describing a single-particle in an effective potential:

$$v_i^{\text{eff}}(n_i) = v_i + U n_i/2. \tag{36}$$

with an eigenvalue:

$$\epsilon^{\text{eff}} = \left(U - \sqrt{(\Delta v^{\text{eff}})^2 + (2\,t)^2}\right)/2. \tag{37}$$

Writing $\phi^{\text{eff}} = (c_1, c_2)^T$, then

$$\Delta n = 2\,(c_2^2 - c_1^2) = 2\,\frac{\xi^2 - 1}{\xi^2 + 1}, \tag{38}$$

where $x = \Delta v^{\text{eff}}/2\,t$, and $\xi = \sqrt{x^2 + 1} - x$. Equation (38) is quartic in Δn and can be solved algebraically to find Δn as a function of Δv explicitly (appendix E). Just as in KS, the HF energy is not simply twice the orbital energy, there is a double-counting correction:

$$\begin{aligned} E^{\text{MF}} &= 2\epsilon^{\text{eff}} - U_{\text{H}} \\ &= \frac{U}{2}\left(1 - \left(\frac{\Delta n}{2}\right)^2\right) - 2\,t\sqrt{1 + x^2}. \end{aligned} \tag{39}$$

These energies are plotted in figure 5. We see that for small U, HF is very accurate, but much less so for $2\,t \ll U \ll \Delta v$. In fact, the HF energy becomes positive in this region, unlike the exact energy, which we prove is never positive in appendix C. The molecular orbitals often used in chemical descriptions have traditionally been those of HF calculations, despite the fact that HF energies are usually far too inaccurate for most chemical energetics [25]. (They have now largely been supplanted by KS orbitals.) In quantum chemical language, the paramagnetic mean-field solution is called restricted HF (RHF) because the spin symmetry is restricted to that of the exact solution, i.e. $S_z = 0$. For large enough U, the broken-symmetry, or unrestricted, solution is lower, and is labeled UHF, which we discuss in section 7.1.

Accurate ground-state energies, especially as a function of nuclear positions, are central quantities in chemical electronic

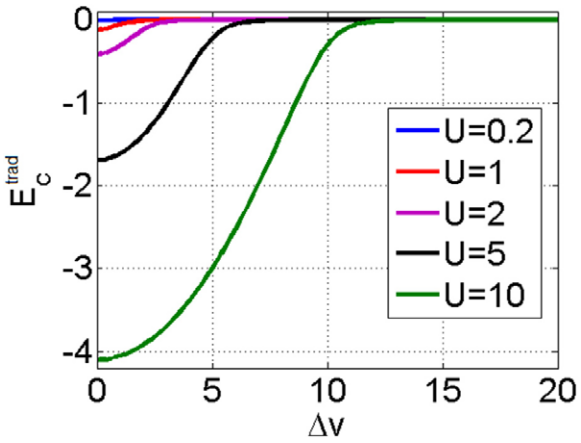

Figure 6. Correlation energy E_C^{trad} of Hubbard dimer as a function of Δv for several values of U and 2 $t = 1$.

structure calculations [215]. Most such systems are weakly correlated unless the bonds are stretched. The correlation energy of traditional quantum chemistry is defined as just the error made by the (restricted) HF solution:

$$E_C^{trad} = E - E^{HF}. \tag{40}$$

This is plotted in figure 6. This is always negative, by the variational principle. Many techniques have been highly developed over the decades to go beyond HF. These are called model chemistries, and for many small molecules, errors in energy differences of less than 1 kcal mol^{-1} (0.05 eV) are now routine [21, 161].

Usually E_C^{trad} is a small fraction of E for weakly correlated systems. For example, for the He atom, $E = -77.5$ eV, but $E_C^{trad} = -1.143$ eV. This is the error made by a HF calculation. In figure 6 we plot E_C^{trad} just as we plotted E in figure 5. We see that for strong correlation E_C^{trad} becomes large ($\sim -U/2$ for $\Delta v \ll U$), much larger than E. However, E is much smaller, and so any strongly correlated method should reproduce E accurately. In fact, one can already see difficulties for weakly correlated approximations in this limit. For weak correlation, a small percent error in E_C^{trad} yields a very small error in E, but produces an enormous error in E in the strong correlation limit. For an infinitely stretched molecular bond, $t \to 0$ while U remains finite, so only one electron is on each site. Thus $E \to 0$, so we can think of E as the ground-state electronic energy relative to the dissociated limit, i.e. the binding energy.

Because HF is accurate for E when correlation is weak, and because quantum chemistry focuses on energy differences, the error is often measured in terms of the accuracy of the exchange-correlation together (if both are approximated as in most DFT calculations). For 2 electrons having $S_z = 0$, the exact exchange is trivial, and so we will focus on approximations to the correlation energy.

Notice the slight difference in definition of correlation energy between DFT (equation 18) and quantum chemistry (equation (40)) [78, 194, 225]. In DFT, all quantities are defined on a given density, usually the exact density of the problem, whereas in quantum chemistry, the HF energy is evaluated on the density that minimizes the HF energy. For weakly correlated systems, this difference is extremely small [73], but is not so small for large U. And, one can prove, $E_C^{trad} \geqslant E_C^{DFT}$ [78], (see appendix C).

We close by emphasizing the crucial difference in philosophy between DFT and traditional approaches. In many-body theory, mean-field theory is an approximation to the many-body problem, yielding an approximate wavefunction and energy which are expected to be reasonably accurate for small U. In DFT, this treatment arises from approximating F for small U, and so should yield an accurate KS wavefunction and expectation values for small U. Thus, only one-body properties that depend only on position are expected to be accurate, and their accuracy can be improved by further improving the approximation to F. For large U, such an approximation fails, but there is still an exact F that yields an exact answer.

3. Site-occupation function theory (SOFT)

In this section, we introduce the site-occupation function theory for the Hubbard dimer [40, 42, 81, 187, 188, 203, 204]. If we want a physical system where this arises, think of stretched H_2 [154]. We imagine a minimal basis set of one function per atom for the real Hamiltonian. We choose these basis functions to be 1s orbitals centered on each nucleus, but symmetrically orthonormalized. Then each operator in real-space contributes to the parameters in the Hubbard Hamiltonian as seen in appendix F.

It is reasonably straightforward to establish the validity of SOFT for our dimer. So long as each occupation can come from only one value of Δv, for a fixed U, there is a one-to-one correspondence between Δn and Δv, and all the usual logic of DFT follows. But note that $\hat{T}$ and $\hat{V}$ in SOFT do *not* correspond to the real-space kinetic energy and potential energy. For example, the hopping energy is negative, whereas the real-space kinetic energy is positive. This means that all theorems of DFT to be used must be reproven for the lattice model. More importantly, the SOFT does not become real-space DFT in some limit of complete basis sets (in any obvious way). We will however apply the same logic as real-space DFT, with the hopping energy in SOFT playing the role of the kinetic energy in DFT, and the on-site energy in SOFT playing the role of the one-body potential. The interaction term obviously plays the role of $\hat{V}_{ee}$. Many of the elementary equations and figures in these sections have appeared elsewhere, e.g. [37, 67, 68, 187, 188], some of them as static versions of time-dependent results.

3.1. Non-interacting warm-up exercise

To show how SOFT works, begin with the $U = 0$ case, i.e. tight-binding of two non-interacting electrons. The ground-state is always a spin singlet. From the non-interacting solution, we can solve for Δv in terms of Δn

$$\Delta v = -\frac{2\,t\,\Delta n}{\sqrt{4 - \Delta n^2}}, \tag{41}$$

and substitute back into the kinetic energy expectation value to find

$$T(n_1, n_2) = -2\,t\,\sqrt{n_1 n_2}. \tag{42}$$

This is the universal density function(al) for this non-interacting problem (see equation (3)), and can be used to solve every non-interacting dimer.

To solve this $N = 2$ problem in the DFT way, we note that T is playing the role of $F(n_1, n_2)$. So the exact function(al) here is

$$F(n_1) = -2\,t\sqrt{n_1 n_2}, \qquad (U = 0), \tag{43}$$

from which we can calculate all the quantities of interest using a DFT treatment. Note that everything is simply a function(al) of n_1 since $n_2 = (N - n_1)$, or alternatively a function(al) of Δn. When N is fixed the formulas look like usual DFT when we use Δn.

We then construct the total energy function(al):

$$E(n_1) = F(n_1) + \Delta v\,\Delta n/2, \qquad (U = 0) \tag{44}$$

and minimize with respect to n_1 for a given Δv to find the ground-state energy and density:

$$E = -\sqrt{(2\,t)^2 + \Delta v^2}, \tag{45}$$

$$\Delta n = -2\,\Delta v/\sqrt{(2\,t)^2 + \Delta v^2}. \tag{46}$$

Both of these agree with the traditional approach and recover equations (29) and (30). The $N = 1$ result is half as great as equations (45) and (46).

We can deduce several important lessons from this example. First, we need to vary the one-body potential (in this case, the on-site energy difference) to make the density change through all possible values, in order to find the function(al), since it requires knowing the one-to-one correspondence for all possible densities. Second, if we really change the atoms in our 2-electron stretched molecule, of course the minimal basis functions would change, and *both* t and Δv would differ. But here we keep t fixed, and vary Δv simply to explore the function(al), even if we are only interested in solving the symmetric problem. (Real-space DFT does not suffer from this problem, as the kinetic and repulsion operators are universal). Third, we are reminded that the hopping and on-site operators in no sense represent the actual kinetic and one-body potential terms—they are a mixture of each. Finally, although we 'cheated' and *extracted* the kinetic energy function(al) from knowing the solutions, if someone had given us the formula, it would allow us to solve every possible non-interacting Hubbard dimer by minimizing over densities. And an approximation to that formula would yield approximate solutions to all those problems.

3.2. The interacting functional

For the interacting case, we cannot analytically write down the exact function(al) $F(n_1)$ at $N = 2$ in closed form. Although we have analytic formulas for both E and Δn as functions of Δv, the latter cannot be explicitly inverted to yield an analytic formula for $F(\Delta n)$. However, we can plot the function(al), by simply plotting $F = E - V$ as a function of n_1, and see how it evolves from the $U = 0$ case to stronger interaction. The spin state is always a singlet. We plot in figure 7 the F-function(al) as a function of n_1 for several values of U. As U increases we can see F appears to tend to $U|1 - n_1|$.

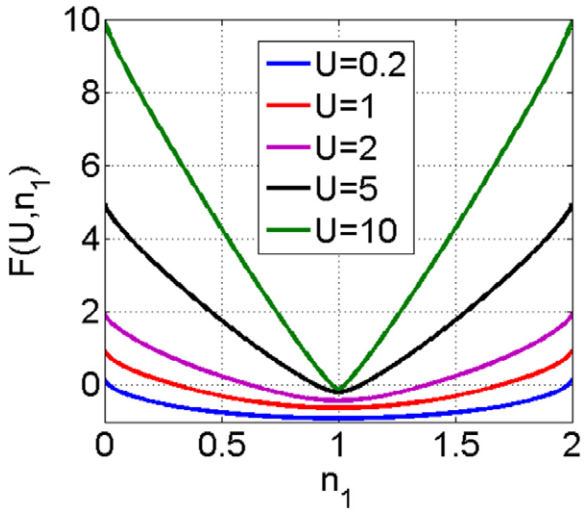

Figure 7. F-function(al) of Hubbard dimer as a function of n_1 for several values of U and $2t = 1$.

For any real problem the Euler equation for a given Δv is

$$\frac{\mathrm{d}F(n_1)}{\mathrm{d}n_1} - \frac{\Delta v}{2} = 0, \tag{47}$$

and the unique $n_1(\Delta v)$ is found that satisfies this. Then

$$E(\Delta v) = F(n_1, \Delta v) + \Delta v \Delta n(\Delta v)/2. \tag{48}$$

The oldest form of DFT (Thomas–Fermi theory [57, 219]) approximates both $T(n_1)$ and $V_{\mathrm{ee}}(n_1)$ and so leads to a crude treatment of the energetics of the system. A variation on this was used in [33] to enable extremely large calculations.

3.3. Kohn–Sham method

The modern world uses the KS scheme, and not pure DFT [28]. The scheme in principle allows one to find the *exact* ground-state energy and density of an interacting problem by solving a non-interacting one. This scheme is what produces such high accuracy while using simple approximations in DFT calculations today. Next, we see how the usual definitions of KS-DFT should be made for our dimer.

The heart of the KS method is the fictitious system of non-interacting electrons whose density matches with the ground-state density of the interacting system. For our two-electron system, the KS system is that of non-interacting electrons ($U = 0$) with an on-site potential difference Δv_{S}, *defined* to reproduce the exact Δn of the real system. This is just the tight-binding problem with an effective on-site potential difference, and is illustrated in figure 2.

As stated in section 2.1, in KS-DFT one conventionally extracts the Hartree contribution from the electron–electron repulsion. There are deep reasons for doing so, which center

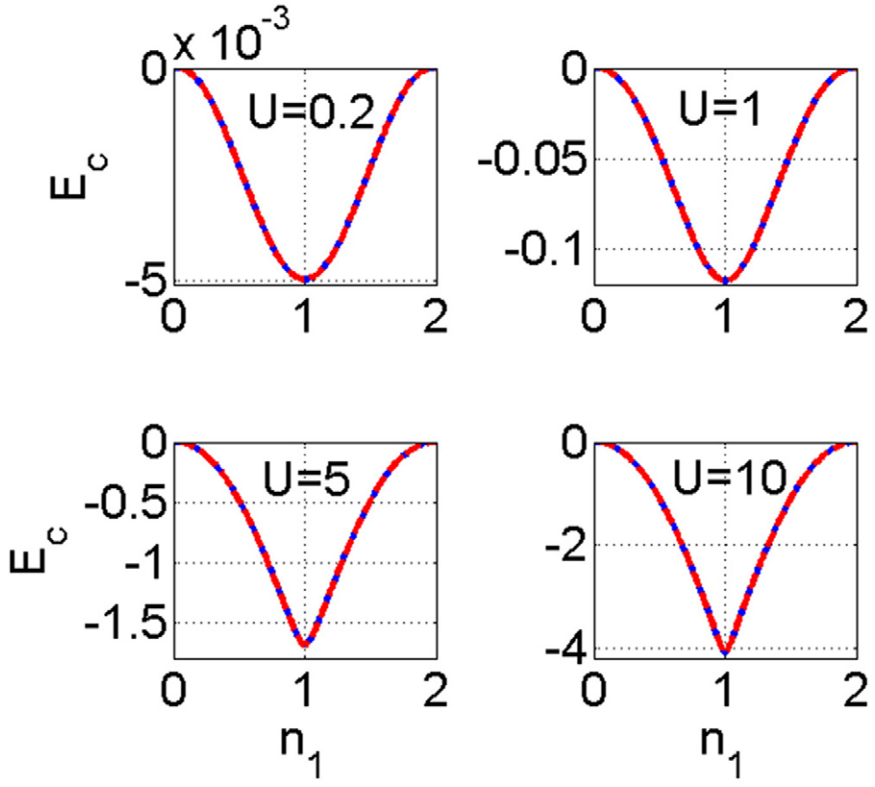

Figure 8. Plot of exact $E_{\rm C}$ (blue line) and $E_{\rm C,par}$ (red dashed line) for different U and $2\,t = 1$.

on the remnant, the XC energy, being amenable to local and semilocal-type approximations [30, 183]. To see how the Hartree energy should be defined here, rewrite the electron–electron repulsion as:

$$\hat{V}_{\rm ee} = \frac{U}{2}\sum_i (\hat{n}_i^2 - \hat{n}_{i\uparrow}^2 - \hat{n}_{i\downarrow}^2). \tag{49}$$

This form mimics the treatment in DFT. The first term depends only on the total (i.e. spin-summed) density, akin to Hartree in real-space DFT. The remaining terms cancel the self-interaction that arises from using the total density for the electron–electron interaction. For the $N = 2$ dimer, this decomposition results in

$$U_{\rm H}(\Delta n) = \frac{U}{2}(n_1^2 + n_2^2), \tag{50}$$

and

$$E_{\rm X}(\Delta n) = -\frac{U}{4}(n_1^2 + n_2^2), \tag{51}$$

which satisfies $E_{\rm X} = -U_{\rm H}/2$ for $N = 2$ as in real-space DFT for a spin singlet, equation (23). Together, the Hartree-Exchange is

$$E_{\rm HX}(\Delta n) = \frac{U}{4}(n_1^2 + n_2^2) = \frac{U}{2}\left(1 + \left(\frac{\Delta n}{2}\right)^2\right). \tag{52}$$

In appendix B we see that the leading order in the U expansion of the F-function(al) yields the same result. A typical mean field treatment of $\hat{V}_{\rm ee}$ also results in equation (52). In DFT there is always self-exchange, even for one or two particles. In many-body theory, exchange means only exchange between different electrons. Despite this semantic difference, both approaches yield the same leading-order-in-U expression for the dimer, which we call $E_{\rm HX}$ here (but is often called just Hartree in many-body theory).

For the dimer, from equation (42), the KS kinetic energy is just

$$T_{\rm S}(n_1) = -2\,t\sqrt{n_1 n_2}, \tag{53}$$

so that $F^{\rm HF}(n_1) = T_{\rm S}(n_1) + E_{\rm HX}(n_1)$ as in section 2.4. We can then define the correlation energy function from equation (18), so that

$$E_{\rm C}(n_1) = F(n_1) - T_{\rm S}(n_1) - E_{\rm HX}(n_1). \tag{54}$$

In figure 8, we plot the correlation energy as a function of n_1. For small U,

$$E_{\rm C} \sim -U^2(1 - (n_1 - 1)^2)^{5/2}/8 \qquad U \ll 2\,t \tag{55}$$

which is much smaller than the Hartree-exchange contribution, and is a relatively small contribution to E. But as U increases,

$$E_{\rm C} \sim -U(1 - (n_1 - 1)^2)/2, \qquad U \gg 2\,t \tag{56}$$

with a cusp at half-filling. Combined with $E_{\rm HX}$, this creates F for large U as in figure 7.

Inserting this result into equation (47), we find that the KS electrons have a non-interacting Hamiltonian:

$$\hat{h}_{\rm S}\,|\phi\rangle = \epsilon_{\rm S}\,|\phi\rangle, \tag{57}$$

where this KS Hamiltonian is

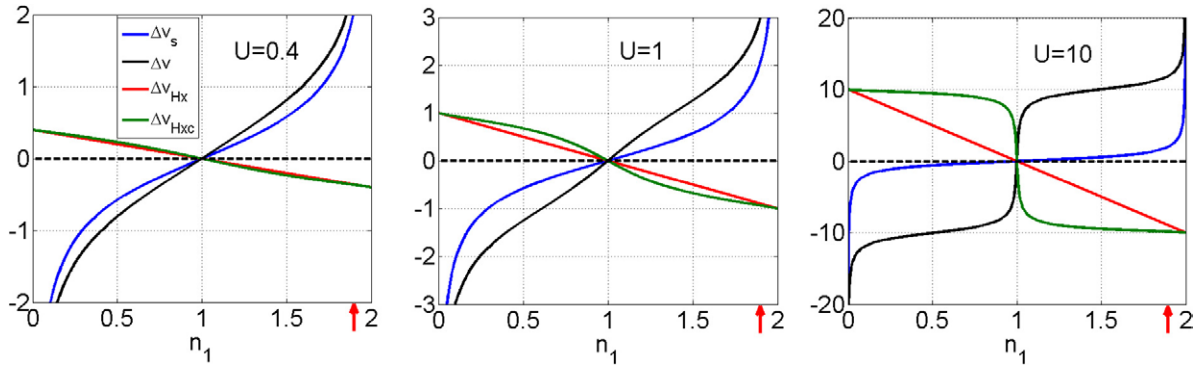

Figure 9. Plots of Δv_S (blue) and its components, Δv (black), $U\Delta n/2$ (red), and $\Delta v_C + U\Delta n/2$ (green) plotted against n_1 for various U and $2\,t = 1$. The arrows indicate the occupations used in figure 2. (See also figures 5 and 6 of [187]).

$$\hat{h}_S(\Delta n) = -t(\hat{c}_1^\dagger \hat{c}_2 + \text{h.c.}) + \sum_i v_{s,i}(\Delta n)\hat{n}_i. \tag{58}$$

The KS potential difference is

$$\Delta v_S(\Delta n) = \Delta v + U\Delta n/2 + \Delta v_C(\Delta n), \tag{59}$$

where

$$\Delta v_C = -2\,\mathrm{d}E_C(n_1)/\mathrm{d}n_1, \tag{60}$$

the analog of equation (13). For any given form of the (exchange-)correlation energy, differentiation yields the corresponding KS potential. If the exact expression for $E_C(n_1)$ is used, this potential is guaranteed [237] to yield the exact ground-state density when the KS equations are iterated to convergence via a simple algorithm.

In figure 9, we plot several examples of the dependence of the potentials in the KS system as a function of n_1, which range from weakly ($U = 0.4$) to strongly ($U = 10$) correlated cases. In each curve, the black line is the actual on-site potential difference as a function of occupation of the first site. The blue line is the KS potential difference, which is the on-site potential needed for two non-interacting ($U = 0$) particles to produce the given n_1. This is found by inverting the tight-binding equation for the density, equation (41). Their difference is the Hartree-exchange-correlation on-site potential, denoted by the red line. Finally, the green line is just Hartree-exchange, which ignores correlation effects. For $U = 0.4$, we see that the difference between blue and black is quite small, and almost linear. Indeed the Hartree-exchange contribution is always linear (see equation (59)). Here the red is indistinguishable by eye from the green, showing how small the correlation contribution to the potential is. This means the HF and exact densities will be virtually (but not quite) identical. When we increase U to $2\,t$, we see a similar pattern, but now the red line is noticeably distinct from the green. For any given n_1, the blue curve is smaller in magnitude than the black. This is because turning on U pushes the two occupation numbers closer, and so their KS on-site potential difference is smaller. Again, the red curve is larger in magnitude than the green, showing that HF does not suppress the density difference quite enough. In our final panel, $U = 20\,t$, and the effects of strong correlation are clear. Now there is a huge difference between black and blue curves. Because U is so strong, the density difference is close to zero for most n_1, making the blue curve almost flat except at the edges. In the KS scheme, this is achieved by the red curve being almost flat, except for a sudden change of sign near $n_1 = 1$. These effects give rise to the Δv_S values shown in figure 2. This effect is completely missed in HF.

To emphasize the role of correlation, in figure 10, we plot the correlation potential alone, which is the difference between the red and green curves in figure 9. Values from the blue curves for $\Delta v = 2$ were used to make figure 2. Δv_C is an odd function of n_1. In the weak- and strong-coupling limits we can write down simple expressions for Δv_C (see appendix B.2):

$$\Delta v_C \approx \frac{5\,U^2\Delta n}{32\,t}(1-(\Delta n/2)^2)^{3/2} \qquad (U \ll 2\,t) \tag{61}$$

$$\Delta v_C \approx U(1-|\Delta n/2|)\,sgn(\Delta n) \qquad (U \gg 2\,t). \tag{62}$$

These correspond to the 1st and 4th panels in figure 10. For small U, it is of order U^2 (see appendix B), and has little effect. As U increases, it becomes proportional to U, and becomes almost linear in U, with a large step near $n_1 = 1$. If we now compare this figure with figure 8, we see that it is simply the derivative of the previous $E_C(n_1)$ curve, as stated in equation (60).

The self-consistent KS equations, equations (57) and (58), have, in this case, precisely the same form as those of restricted HF (or mean-field theory), equations (26) and (36), but with whatever additional dependence on n_1 occurs due to $\Delta v_C(n_1)$. When converged, the ground-state energy is found simply from:

$$E(n_1) = T_S(n_1) + V_{ext}(n_1) + U_H(n_1) + E_{XC}(n_1). \tag{63}$$

The energy can alternatively be extracted from the KS orbital energy via equation (16):

$$E = 2\epsilon_S + (E_C - \Delta v_C\Delta n/2 - E_{HX}), \tag{64}$$

where the second term is the double-counting correction. But note the crucial difference here. We consider HF an approximate solution to the many-body problem whereas DFT, with the exact correlation function(al), yields the exact energy and on-site occupation, but not the exact wavefunction.

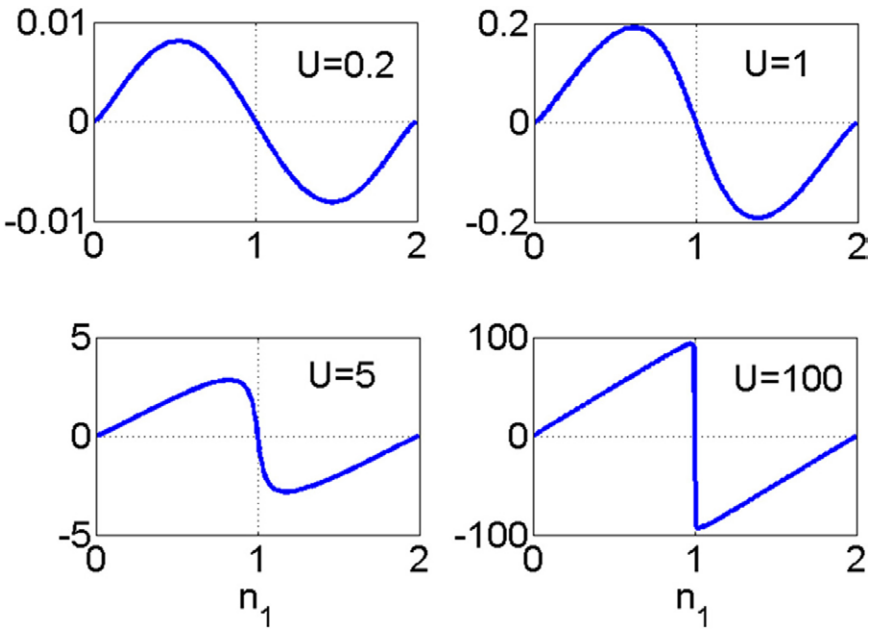

Figure 10. Plot of $\Delta v_{\rm C}$ for different U and $2\,t = 1$.

4. The fundamental gap

Now that we have carefully defined what exact KS DFT is for this model, we immediately apply this knowledge to investigate a thorny subject on the border of many-body theory and DFT, namely the fundamental gap of a system.

4.1. Background in real space

Begin with the ionization energy of an N-electron system:

$$I = E(N-1) - E(N) \tag{65}$$

is the energy required to remove one electron entirely from a system. We can then define the electron affinity as the energy gained by adding an electron to a system, which is also equal to the ionization energy of the $(N+1)$-electron system:

$$A = E(N) - E(N+1). \tag{66}$$

In real-space, I and $A \geqslant 0$. For systems which do not bind an additional electron, such as the He atom, $A = 0$. The charge, or fundamental, gap of the system is then

$$E_g = I - A, \tag{67}$$

and for many materials, E_g can be used to decide if they are metals ($E_g = 0$) or insulators ($E_g > 0$) [109]. The spectral function of the single-particle Green's function has a gap equal to E_g. For Coulombic matter, E_g has always been found to be non-negative, but no general proof has been given.

Now we turn to the KS system of the N-electron system. We denote the highest occupied (molecular) orbital as $\epsilon^{\rm HOMO}$ and the lowest unoccupied one as $\epsilon^{\rm LUMO}$. Then the DFT version of Koopmans' theorem [8, 9, 39, 176, 177, 208] shows that

$$\epsilon^{\rm HOMO} = -I, \tag{68}$$

by matching the decay of the density away from any finite system in real space, in the interacting and KS pictures. However, this condition applies only to the HOMO, not to any other occupied orbitals, or unoccupied ones. The LUMO level is not at $-A$, in general. Define the KS gap as

$$E_{gs} = \epsilon^{\rm LUMO} - \epsilon^{\rm HOMO}. \tag{69}$$

Then E_{gs} does not match the true gap, even with the exact XC functional [19, 193]. We write

$$E_g = E_{gs} + \Delta_{\rm XC} \tag{70}$$

where $\Delta_{\rm XC} \neq 0$, and is called the derivative discontinuity contribution to the gap (for reasons that will be more apparent later) [171, 173]. In general, $\Delta_{\rm XC}$ appears to always be positive, i.e. the KS gap is smaller than the true gap. In semiconductors with especially small gaps, such as germanium, approximate KS gaps are often zero, making the material a band metal, but an insulator in reality. The classic example of a chain of H atoms becoming a Mott–Hubbard insulator when the bonds are stretched is demonstrated unambiguously in [214].

While this mismatch occurs for all systems, it is especially problematic for DFT calculations of insulating solids. For molecules, one can (and does) calculate the gap (called the chemical hardness in molecular systems [166]) by adding and removing electrons. But with periodic boundary conditions, there is no simple way to do this for solids. Even with the exact functional, the KS gap does not match the true gap, and there's no easy way to calculate E_g in a periodic code. In fact, popular approximations like LDA and GGA mostly produce good approximations to the KS gap, but yield $\Delta_{\rm XC} = 0$ for solids. Thus there is no easy way to extract a good approximation to the true gap in such DFT calculations. The standard method for producing accurate gaps for solids has long been to perform a GW calculation [14], an approximate calculation

of the Green's function, and read off its gap. This works very well for most weakly correlated materials [200]. Such calculations are now done in a variety of ways, but usually employ KS orbitals from an approximate DFT calculation. Recently, hybrid functionals like HSE06 [94] have been shown to yield accurate approximate gaps to many systems, but these gaps are a mixture of the quasiparticle (i.e. fundamental) gap, and the KS gap. Their exchange component produces the fundamental gap at the HF level, which is typically a significant overestimate, which then compensates for the 'too small' KS gap. While this balance is unlikely to be accidental, no general explanation has yet been given.

4.2. Hubbard dimer gap

For our half-filled Hubbard dimer, we can easily calculate both the $N \pm 1$-electron energies, the former via particle-hole symmetry from the latter [40]. In figure 11, we plot $-I$,$-A$, ϵ^{HOMO}, and ϵ^{LUMO} for $U = 1$ when $2\,t = 1$, as a function of Δv. We see that A (and even sometimes I) can be negative here. (This cannot happen for real-space calculations, as electrons can always escape to infinity, so a bound system always has $A \geqslant 0$.) The HOMO level is always at $-I$ according to equation (68) but the LUMO is not at $-A$. Here it is smaller than $-A$, and we find this result for all values of U and Δv. The true gap is $I - A$, but the KS gap is $\epsilon^{\mathrm{LUMO}} + I$, which is always smaller. Thus $\Delta_{\mathrm{XC}} \geqslant 0$, just as for real systems.

Figure 11 is typical of weakly correlated systems, where Δ_{XC} is small but noticeable. In figure 12, we repeat the calculation with $U = 10\,t$, where now $E_g \gg E_{gs}$ at $\Delta v = 0$, but we still see the difference become tiny when $\Delta v > U$. In both figures, Δ_{XC} is the difference between the red line and the green dashed line. In all cases, $\Delta_{\mathrm{XC}} \geqslant 0$, and this has always been found to be true in real-space DFT, but has never been proven in general.

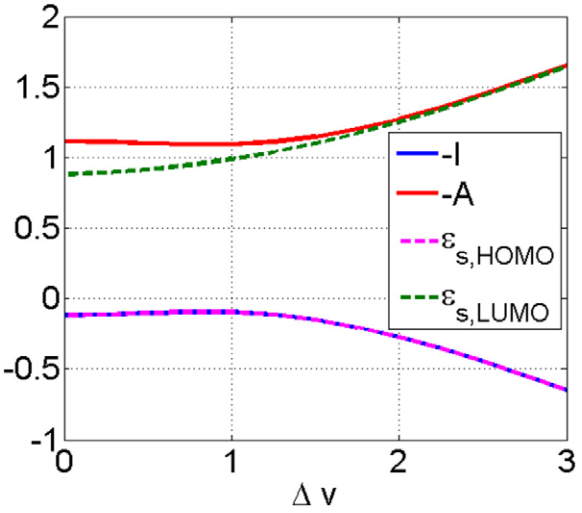

Figure 11. Plot of $-A$, $-I$, ϵ^{HOMO}, and ϵ^{LUMO} as a function of Δv with $U = 1$ and $2\,t = 1$.

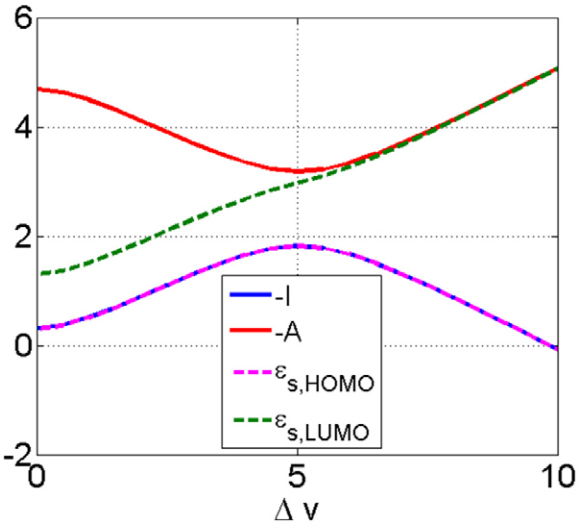

Figure 12. Plot of $-A$, $-I$, ϵ^{HOMO}, and ϵ^{LUMO} as a function of Δv with $U = 5$ and $2\,t = 1$.

4.3. Green's functions

To end this section, we emphasize the difference between the KS and many-body approaches to this problem by calculating their spectral functions [163]. We define the many-body retarded single-particle Green's function as

$$G_{ij\sigma\sigma'}(t - t') = -\mathrm{i}\,\theta(t - t')\langle\Psi_0|\{\hat{c}_{i\sigma}(t), \hat{c}^{\dagger}_{j\sigma'}(t')\}\,|\Psi_0\rangle \quad (71)$$

where i, j label the site indices, σ, σ' the electron spins, and $\{A, B\} = AB + BA$. For the Hubbard dimer at $N = 1$ and 3, $|\Psi_0\rangle$ is a degenerate Kramers doublet and we choose here the spin-$\uparrow$ partner. Fourier transforming into frequency, we find for the diagonal component:

$$G_\sigma(\omega) = G_{11\sigma\sigma}(\omega) = \sum_\alpha \frac{|M^\alpha_{1\sigma}|^2}{\omega + E^N - E^{N+1}_\alpha + \mathrm{i}\,\delta} + \sum_\alpha \frac{|L^\alpha_{1\sigma}|^2}{\omega - E^N + E^{N-1}_\alpha + \mathrm{i}\,\delta} \quad (72)$$

where $M^\alpha_{1\sigma} = \langle\psi^{N+1}_\alpha|\,\hat{c}^{\dagger}_{1\sigma}\,|\psi^N_0\rangle$, $L^\alpha_{1\sigma} = \langle\psi^{N-1}_\alpha|\,\hat{c}_{1\sigma}\,|\psi^N_0\rangle$, and $\delta > 0$ is infinitesimal. Here, α runs over all states of the $N \pm 1$-particle systems. The other components have analogous expressions. From any component of G, we find the corresponding spectral function

$$A(\omega) = -\Im G(\omega)/\pi \quad (73)$$

We represent the spectral function δ-function poles with lines whose height is proportional to the weights. Via a simple sum-rule [58], the sum of all weights in the spin-resolved spectral function is 1. There are four quasi-particle peaks for $N = 2$. These peaks are reflection-symmetric about $\omega = U/2$ for the symmetric dimer.

We also need to calculate the KS Green's function, $G_{\mathrm{S}}(\omega)$. This is done by simply taking the usual definition, equation (71), and applying it to the ground-state KS system. This means two non-interacting electrons sitting in the KS potential. The numerators vanish for all but single excitations. Thus the energy differences in the denominators become simply occupied and unoccupied orbital energies. Since there are

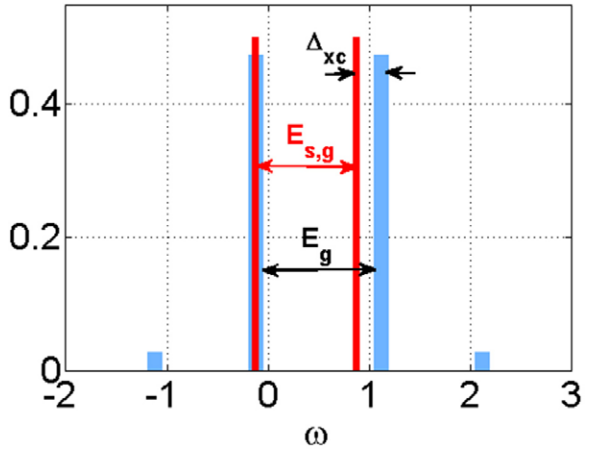

Figure 13. Spectral function of symmetric dimer for $U = 1$, $\Delta v = 0$, and $2\,t = 1$. The physical MB peaks are plotted in blue, the KS in red. Here $I = 0.1$, $A = -1.1$, and $\epsilon^{\mathrm{LUMO}} = 0.9$, corresponding to $\Delta v = 0$ in figure 11.

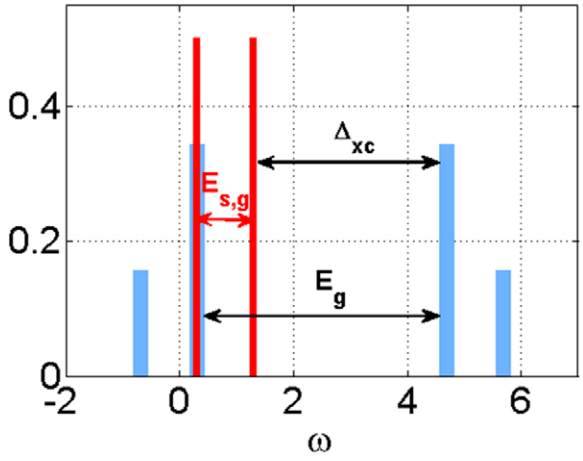

Figure 14. Same as figure 13, but now $U = 5$. Here $I = -0.3$, $A = -4.7$, and $\epsilon^{\mathrm{LUMO}} = 1.3$, corresponding to $\Delta v = 0$ in figure 12.

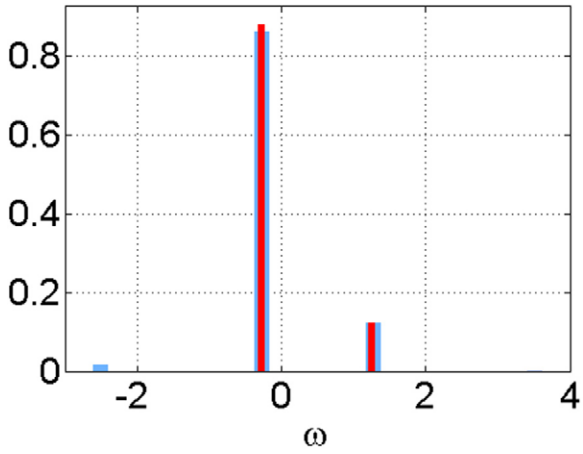

Figure 15. Same as figure 13, but now $U = 1$, $\Delta v = 2$. Here $I = 0.27$, $A = -1.27$, and $\epsilon^{\mathrm{LUMO}} = 1.25$, corresponding to $\Delta v = 2$ in figure 11.

only two distinct levels (the positive and negative combinations of atomic orbitals), there are only two peaks, positioned at the HOMO and LUMO levels, with weights:

$$M^{\alpha}_{1\sigma} = \frac{1}{2}\left(1 + \frac{\Delta v_{\mathrm{S}}/2}{\sqrt{(\Delta v_{\mathrm{S}}/2)^2 + t^2}}\right), \quad \text{(KS)} \qquad (74)$$

and the sign between the contributions on the right is negative in the L term. Thus the symmetric dimer has KS weights of 1/2.

In figure 13 we plot the spectral functions for the symmetric case, for $U = 1$, when $2\,t = 1$. Each pole contributes a delta function at a distinct transition frequency, which is represented by a line whose height represents the weight. The sum of all such weights adds to 1 as it should, and the peaks are reflection-symmetric about $U/2 = 0.5$. The gap is the distance between the highest negative pole (at $-I$) and the lowest positive pole (at $-A$). We see that the MB spectral function also has peaks that correspond to higher and lower quasi-particle excitations. If we now compare this to the *exact* KS Green's function G_{S}, we see that, by construction, G_{S} always has a peak at $-I$, whose weight need not match that of the MB function. It has only two peaks, the other being at ϵ^{LUMO}, which does not coincide with the position of the MB peak. This is so because the KS scheme is defined to reproduce the ground-state occupations, nothing else. But clearly, when U is sufficiently small, it is a rough mimic of the MB Green's function. The larger peaks in the MB spectral function each have KS analogs, with roughly the correct weights. One of them is even at exactly the right position. Thus if a system is weakly correlated, the KS spectral function can be a rough guide to the true quasiparticle spectrum.

On the other hand, when $U \gg 2\,t$, the KS spectral function is not even close to the true MB spectral function, as illustrated in figure 14. Now the two lowest-lying MB peaks approach each other, as do the two highest lying peaks, therefore increasing the quasi-particle gap. In addition, the weights tend to equilibrate with each other. In fact, when $U \to \infty$ and/or $t \to 0$, those two lowest-lying peaks gather together at $\omega = 0$, having both the same weight of 1/4. And similarly the two highest-lying peaks merge at $\omega = U$, also with a weight of 1/4. They are the precursors of the lower and upper Hubbard bands with a quasi-particle gap equal to U. If more sites are added to the symmetric dimer, other quasi-particle peaks appear, that also merge into the lower and upper Hubbard bands as $U \to \infty$. Notice that the spectral function has significant weights for transitions between states that differ from the HOMO and LUMO, and are forbidden in the KS spectral function for large U. In figure 14, we see that not only there is a large difference between the gaps in the two spectral functions, but also the KS weights are not close to the MB weights. The only 'right' thing about the KS spectrum is the position of the HOMO peak.

In figure 15, we plot the spectral functions for $\Delta v = 2$ and $U = 1$ for $2\,t = 1$, to see the effects of asymmetry on the spectral function. Now the system appears entirely uncorrelated, and the KS spectral function is very close to the true one, much more so than in the symmetric case. Here Δ_{XC} is negligible. The asymmetry of the potential strongly suppresses correlation effects. In figure 16, we see that the effects of strong U are largely quenched by a comparable Δv. Here Δ_{XC} is small

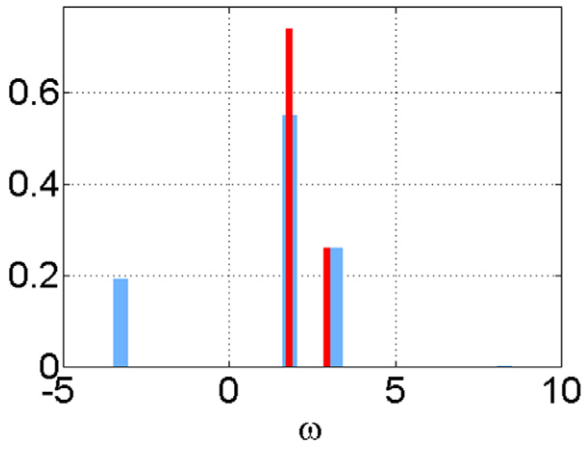

Figure 16. Same as figure 15, but now $U = 5$, $\Delta v = 5$. Here $I = -1.8$, $A = -3.2$, and $\epsilon^{\mathrm{LUMO}} = 3$, corresponding to $\Delta v = 5$ in figure 12.

compared to the gap, but not all KS peak heights are close to their MB counterparts.

The situation is interesting even for the 'simple' case, $N = 1$, in which the ground-state is open-shell [76]. Here the interacting spin-↑ and -↓ Green's functions differ. To understand why, we choose the $N = 1$ ground state to have spin ↑. This state has energy $E(1) = -\sqrt{t^2 + (\Delta v/2)^2}$. Adding a ↓-spin electron takes the system to the different singlet states at $N = 2$, and to the triplet state with $S_z = 0$. One of them is the ground state at $N = 2$ whose energy $E(2) < 0$ is given in equation (A.1) in the appendix. In contrast, adding an ↑-spin electron takes the interacting system to the triplet $N = 2$ state with $S_z = 1$, whose energy is trivially given by $E(2)_{\mathrm{trip}} = 0$. Annihilating an ↑-spin electron takes the system to the vacuum, while it is impossible to annihilate a ↓-spin electron. These clearly illustrates that the number and energy of the poles in $G_\uparrow$ and $G_\downarrow$ is different: $G_\uparrow$ has only two quasi-particle peaks, with trivial energies $E(2)_{\mathrm{trip}} - E(1) = \sqrt{t^2 + (\Delta v/2)^2}$ and $E(1) - E(0) = -\sqrt{t^2 + (\Delta v/2)^2}$. This last expression corresponds to the ionization energy $I = E(0) - E(1) = \sqrt{t^2 + (\Delta v/2)^2}$. $G_\downarrow$ has four quasiparticle peaks, all corresponding to adding a ↓-spin electron, with non-trivial energies. The lowest of these corresponds to the electron affinity $A = E(1) - E(2) = -\sqrt{t^2 + (\Delta v/2)^2} - E(2)$. In other words, ionization involves either removing an ↑-spin electron (hence seen as a pole in $G_\uparrow$) or adding a ↓-spin electron (hence seen as a pole in $G_\downarrow$). The interacting gap is $E_g = I - A = 2\sqrt{t^2 + (\Delta v/2)^2} + E(2)$.

We turn now to the KS Green's function. For $N = 1$, the KS on-site potentials equal the true on-site potentials, $\pm\Delta v/2$. So the ground-state (chosen again to have spin ↑) has energy $E_{\mathrm{S}}(1) = -\sqrt{t^2 + (\Delta v_{\mathrm{S}}/2)^2}$. Since the other state has energy $E_{\mathrm{S}}(1)$, and a second ↑-electron occupies that state, the total KS energy is $E(2)_{\mathrm{S}_z=1} = 0$. On the other hand, annihilating the ↑ electron costs an energy $E(1)$. This shows that the ↑-spin KS and interacting Green's functions are identical to one other and trivial for $N = 1$. Thus $I = -\epsilon^{\mathrm{HOMO}} = \sqrt{t^2 + (\Delta v/2)^2}$. This result is specific to this model.

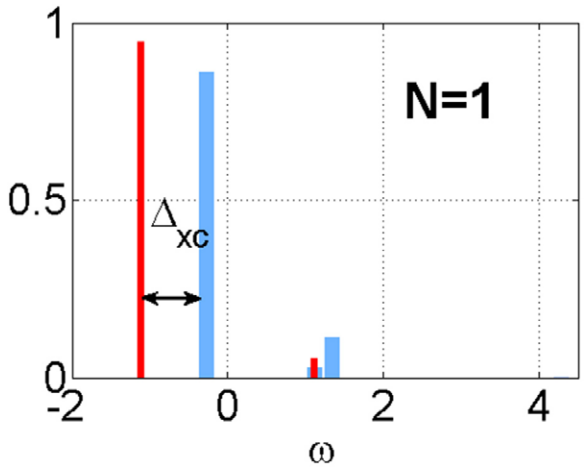

Figure 17. Spin-↓ resolved spectral function for $N = 1$ and $U = 1$, $\Delta v = 2$, ($2\,t = 1$). Here $I = 1.12$, $A = 0.27$, and $\epsilon^{\mathrm{LUMO}} = \epsilon^{\mathrm{HOMO}} = -1.12$.

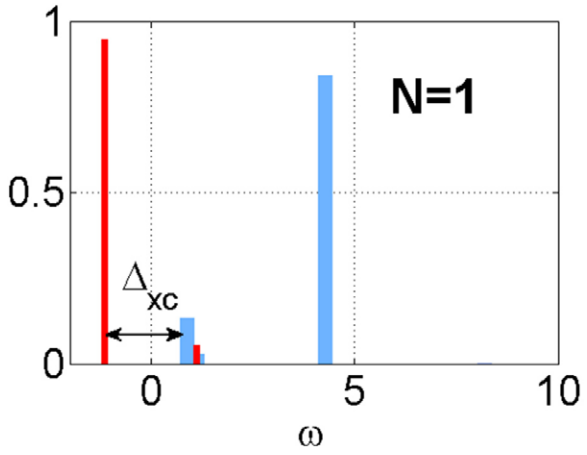

Figure 18. Spin-↓ resolved spectral function for $N = 1$ and $U = 5$, $\Delta v = 2$ ($2\,t = 1$). Here $I = 1.12$, $A = -0.90$, and $\epsilon^{\mathrm{LUMO}} = \epsilon^{\mathrm{HOMO}} = -1.12$.

Removing a ↓-spin KS electron is impossible, just as in the interacting case. However, adding it means having either two opposite-spin KS electrons with the same energy $-\sqrt{t^2 + (\Delta v_{\mathrm{S}}/2)^2}$, or having one with energy $-\sqrt{t^2 + (\Delta v_{\mathrm{S}}/2)^2}$ and another with energy $\sqrt{t^2 + (\Delta v_{\mathrm{S}}/2)^2}$. The first case corresponds to the KS ground-state with energy $-2\sqrt{t^2 + (\Delta v_{\mathrm{S}}/2)^2}$, while the second one is an excited state with energy 0. The KS value for the electron affinity is $A_{\mathrm{S}} = E_{\mathrm{S}}(1) - E_{\mathrm{S}}(2) = \sqrt{t^2 + (\Delta v_{\mathrm{S}}/2)^2}$, which differs from the interacting value. Furthermore, the KS gap $E_{gs} = 0$ is clearly an incorrect estimate of the true interacting gap, which is given by $I = \Delta_{xc}$.

Figures 17 and 18 show the spectral function associated with $G_\downarrow$ for the many-body and KS Green's functions for $N = 1$ and $\Delta v = 2$. In the first, $U = 1$, so it is relatively asymmetric, whereas in the second, $U = 5$, making it close to symmetric. Thus the HOMO is at the lowest red line, and matches exactly the LUMO, with a KS gap of zero. Thus Δ_{XC} *is* the gap of the interacting system. We see that in the first figure,

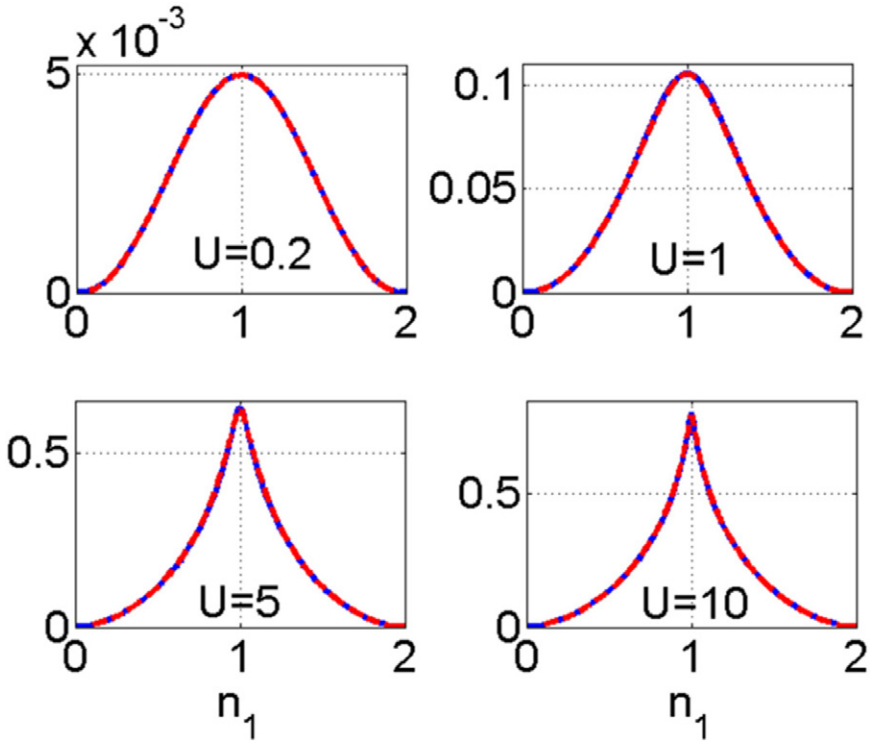

Figure 19. Plot of exact T_C (blue line) and $T_{C,par}$ (red dashed line) for different U and $2\,t = 1$.

correlations are weak and the KS spectral function mimics the physical one, but in the second figure ($U = 5$), they differ substantially, even though $N = 1$!

The difference in expressions for spin species is illustrated further by work analyzing Koopmans' and Janak's theorems for open-shell systems [75–77, 79]. Self-energy approximations beyond GW have been performed on the Hubbard dimer [190, 191], as well as a battery of many-body perturbation theory methods [162] though only for the symmetric case.

The bottom line message of this subsection is that the KS spectral function does not match the quasiparticle spectral function, because it is not supposed to. However, the main features of a weakly correlated system are loosely approximated by those of the KS function, with the gap error shifting the upper part of the spectrum relative to the lower part. This is the motivation behind the infamous scissors operator in solid-state physics. A very accurate DFT approximation can (at best) approximate the KS spectral function, not the many-body one. The exact XC functional does not reproduce the quasiparticle gap of the system. For strongly correlated systems, there are often substantial qualitative differences between the MB and KS spectral functions. These are some of the limitations of KS-DFT. that, e.g. DMFT is designed to overcome [69].

5. Correlation

5.1. Classifying correlation: strong, weak, dynamic, static, kinetic, and potential

There are as many different ways to distinguish weak from strong correlation as there are communities that study electronic structure. Due to the limited degrees of freedom (namely, one), these all overlap in the Hubbard dimer. We will discuss each.

The most important thing to realize is that correlation energy comes in two distinct contributions: kinetic and potential. These are entirely well-defined quantities within KS-DFT. The kinetic correlation energy is:

$$T_C = T - T_S \tag{75}$$

for a given density. Note that we could as easily call this the correlation contribution to the kinetic energy. The potential correlation energy is:

$$U_C = V_{ee} - E_{HX}, \tag{76}$$

and could also be called the correlation contribution to potential energy. For future notational convenience, we also define $U_X = E_X$, i.e. there is no kinetic contribution to exchange. Then, from equation (18), we see

$$E_C = T_C + U_C. \tag{77}$$

We can now use these to discuss the differences between weak and strong correlation. First note that, by construction, and as shown for our dimer in appendix C,

$$E_C < 0, \quad T_C > 0, \quad U_C < 0. \tag{78}$$

In figures 8 and 19, we plot both E_C and T_C, respectively, for several values of U (with $2\,t = 1$). When U is small, $T_C \approx -E_C$. However, for $U \gg 2\,t$, we see that although E_C becomes very large (in magnitude), T_C remains finite and in fact, T_C never exceeds $2\,t$ as proven in appendix C. We can define a measure of the nature of the correlation [29]:

$$\beta_{corr} \equiv \frac{T_C}{|E_C|}. \tag{79}$$

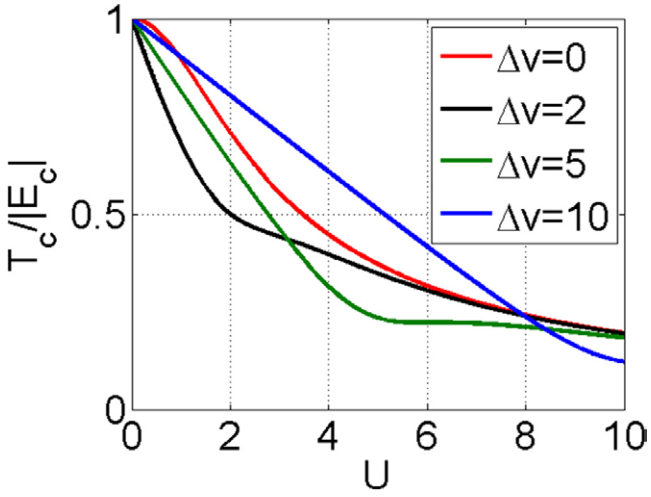

Figure 20. Plot of $\beta_{\rm corr} = T_{\rm C}/|E_{\rm C}|$ as a function of U with $2\,t = 1$.

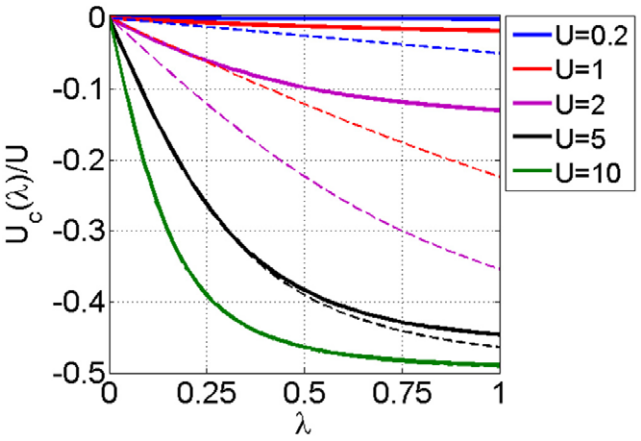

Figure 21. Adiabatic connection integrand divided by U for various values of U. The solid lines are $\Delta v = 2$ and the dashed lines $\Delta v = 0$. Asymmetry reduces the correlation energy but increases the fraction of kinetic correlation.

As $U \to 0$, $\beta_{\rm corr} \to 1$, while as $U \to \infty$, $\beta_{\rm corr} \to 0$. Thus $\beta_{\rm corr}$ close to 1 indicates weak correlation, β small indicates strong correlation. We plot $\beta_{\rm corr}$ as a function of U for several values of Δv in figure 20. Although $\beta_{\rm corr}$ is monotonically decreasing with U for $\Delta v = 0$, we see that the issue is much more complicated once we include asymmetry. The curve for each Δv remains monotonically decreasing with U. But consider $U = 2$ and different values of Δv. Then $\beta_{\rm corr}$ at first decreases with Δv, i.e. becoming *more* strongly correlated, but then increases again for $\Delta v > U$, ultimately appearing less correlated than $\Delta v = 0$.

Quantum chemists often refer to *dynamic* versus *static* correlation. Our precise prescription in KS-DFT loosely corresponds to their definition, replacing dynamic by kinetic, and static by potential. Thus, considering an H_2 molecule with a stretched bond, the Hubbard model applies. As the bond stretches, t vanishes, and $U/2\,t$ grows. Thus $\beta_{\rm corr} \to 0$ as $R \to \infty$. The exact wavefunction, the Heitler-London wavefunction [90], has only static correlation in this limit. In many-body language, it is strongly correlated. In DFT language, the fraction of correlation energy that is kinetic is vanishing.

5.2. Adiabatic connection

With the various contributions to correlation well-defined, we construct the adiabatic connection (AC) formula [80, 124] for the Hubbard dimer. The adiabatic connection has had enormous impact on the field of DFT as it allows both construction [4, 23, 23, 52, 175, 181], and understanding [29, 168, 174], of exact and approximate functionals solely from their potential contributions.

In many-body theory, one often introduces a coupling-constant in front of the interaction. In KS-DFT, a coupling constant λ is introduced in front of the electron–electron repulsion but, contrary to traditional many-body approaches, the density is held fixed as λ is varied (usually from 0 to 1). Via the Hohenberg–Kohn theorem, as long as there is more than 1 electron, this implies that the one-body potential must vary with λ, becoming $v^{\lambda}(\mathbf{r})$. By virtue of the density being held fixed, $v^{\lambda=0}(\mathbf{r}) = v_{\rm S}(\mathbf{r})$ while $v^{\lambda=1}(\mathbf{r}) = v(\mathbf{r})$. Thus λ interpolates between the KS system and the true many-body system. Additionally, $\lambda \to \infty$ results in the strictly correlated electron limit [70, 140, 148, 206, 207] which provides useful information about real systems that are strongly correlated.

The adiabatic connection for the Hubbard dimer is very simple. Define the XC energy at coupling constant λ by simply multiplying U by λ while keeping Δn fixed:

$$E^{\lambda}_{\rm XC}(U, \Delta n) = E_{\rm XC}(\lambda U, \Delta n). \tag{80}$$

Application of the Hellman–Feynman theorem [59] yields [80, 87, 124, 125]:

$$\frac{{\rm d}E_{\rm XC}(\lambda U, \Delta n)}{{\rm d}\lambda} = \frac{U_{\rm XC}(\lambda U, \Delta n)}{\lambda}, \tag{81}$$

where $U_{\rm XC}(U, \Delta n)$ is the potential contribution to the XC energy, i.e. $U_{\rm X} = E_{\rm X}$ and

$$U_{\rm C}(\lambda U) = V_{\rm ee}(\lambda U) - \lambda\, E_{\rm HX}(U). \tag{82}$$

Thus, we can extract $T_{\rm C}$ solely from our knowledge of $E_{\rm C}(U)$ via

$$T_{\rm C} = E_{\rm C} - U_{\rm C} = E_{\rm C} - \left.\frac{{\rm d}E^{\lambda}_{\rm C}}{{\rm d}\lambda}\right|_{\lambda=1}. \tag{83}$$

Thus, any formula for $E_{\rm C}$, be it exact or approximate, yields a corresponding result for $T_{\rm C}$ and $U_{\rm C}$, and vice versa [46]. We may then write

$$E_{\rm XC}(U, \Delta n) = \int_0^1 \frac{{\rm d}\lambda}{\lambda}\, U_{\rm XC}(\lambda U, \Delta n), \tag{84}$$

and this is the infamous adiabatic connection formula of DFT [80, 124]. We denote the integrand as $U_{\rm C}(\lambda)$, defined as

$$U_{\rm C}(\lambda) = \frac{U_{\rm C}(\lambda U)}{\lambda} = \frac{{\rm d}E_{\rm C}(\lambda U)}{{\rm d}\lambda}. \tag{85}$$

Plots of $U_{\rm C}(\lambda)$ from equation (85) are called adiabatic connection plots, and can be used to better understand both approximate and exact functionals. In figure 21, we plot a typical case for $U = 2\,t$ and $\Delta v = 0$. They have the nice interpretation that

the value at $\lambda = 1$ is the potential correlation energy, U_C, the area under the curve is E_C, and the area between the curve and the horizontal line at $U_C(1)$ is $-T_C$. Furthermore, one can also show [130]

$$\frac{dU_{XC}(\lambda)}{d\lambda} < 0, \tag{86}$$

from known inequalities for $T_C(\lambda)$ and $E_C(\lambda)$. This is proven for our problem in appendix C. Interestingly, such curves have always been found to be convex when extracted numerically for various systems [65, 186], but no general proof of this is known. The Hubbard dimer also exhibits this behavior. A proof for the dimer might suggest a proof for real-space DFT.

In figure 21 we plot $U_C(\lambda)/U$ for $\Delta v = 0$ and $\Delta v = 2$, with various values of U. From the above formulas, one can deduce that the area between the curve and the horizontal line at $U_C(1)$ is $-T_C$. Thus as U grows, the curve moves from being almost linear to decaying very rapidly, and β_{corr} varies from 1 down to 0.

In figure 21, we show U up to 10 (for $2\,t = 1$), to show the effect of stronger correlation. Not only has the magnitude of the correlation become larger, but the curve drops more rapidly toward its value at large λ. $\beta_{corr} \simeq 0.9$ for $\Delta v = 0$ and $U = 1$, but $\beta_{corr} \simeq 0.2$ for $\Delta v = 0$ and $U = 10$, reflecting the fact that the increase in correlation is of the static kind.

The weakly correlated limit has been much studied in DFT. Perturbation theory in the coupling constant is called Goerling-Levy perturbation theory [74]. For small λ,

$$U_C(\lambda U) = \lambda^2 U_C^{(2)} + \lambda^3 U_C^{(3)} + \ldots \quad (\lambda \to 0). \tag{87}$$

In appendix B.2, we show that

$$U_C^{(2)}(\Delta n) = -\frac{U^2}{8\,t}\left(1 - \left(\frac{\Delta n}{2}\right)^2\right)^{5/2}, \tag{88}$$

and

$$U_C^{(3)}(\Delta n) = \frac{3\,U^3}{32\,t^2}\left(\frac{\Delta n}{2}\right)^2\left(1 - \left(\frac{\Delta n}{2}\right)^2\right)^3 \tag{89}$$

for the dimer. This yields, for T_C,

$$T_C = -\frac{1}{2}\lambda^2 U_C^{(2)} - \frac{2}{3}\lambda^3 U_C^{(3)} - \frac{3}{4}\lambda^4 U_C^{(4)} - \ldots \tag{90}$$

showing that $\beta \to 1$ as U (or λ) vanishes. For any system, $U_C^{(2)}$ determines the initial slope of $U_C(\lambda)$.

On the other hand, in the strongly correlated limit, in real-space [71, 140].

$$E_C \to \lambda(B_0 + \lambda^{-1/2}B_1 + \lambda^{-1}B_2 \ldots), \quad (\lambda \to \infty) \tag{91}$$

where B_k ($k = 0, 1, 2\ldots$) are coupling-invariant functionals of $n(\boldsymbol{r})$ [141]. The dominant term is linear in U. Physically, it must exactly cancel the Hartree plus exchange contributions, since there is no electron–electron repulsion to this order when each electron is localized to separate sites. Correctly, such a term cancels out of T_C, so that its dominant contribution is $O(1)$. From appendix B.2, we see that the Hubbard dimer has a different form, involving only integer powers of λ:

$$E_C \to \lambda\, B_0 + \tilde{B}_1 + \tilde{B}_2/\lambda + \ldots \quad (\lambda \to \infty) \tag{92}$$

where

$$B_0(\Delta n) = -U(1 + \Delta n/2)^2/2, \tag{93}$$

$$\tilde{B}_1(\Delta n) = 2\,t\sqrt{1 + \Delta n/2}\,(\sqrt{1 - \Delta n/2} - \sqrt{-\Delta n}), \tag{94}$$

and

$$\tilde{B}_2(\Delta n) = (1 + \Delta n/2)t^2/U. \tag{95}$$

But both this term and the next cancel in the total energy (at half filling), so that the ground-state energy is $O(1/U)$, i.e. extremely small as U grows:

$$E \to -\frac{4t^2}{U} \tag{96}$$

This illustrates that, although the KS description is exact, it becomes quite contorted in the large U limit (see figure 2). This has been implicated in convergence difficulties of the KS equations, even with the exact XC functional, because the KS system behaves so differently from the physical system [235].

6. Accurate parametrization of correlation energy

Although the Hubbard dimer has an exact analytic solution when constructed from many-body theory, the dependence of $F(\Delta n)$ (or equivalently $E_C(\Delta n)$) is only given implicitly. While this is technically straightforward to deal with, in practice it would be much simpler to use if an explicit formula is available. In this section, we show how the standard machinery of DFT can be applied to develop an extremely accurate parametrization of the correlation energy functional.

An arbitrary antisymmetric wavefunction is characterized by 3 real numbers where $|12\rangle$ means an electron at site 1 and site 2, etc:

$$|\psi\rangle = \alpha\,(|12\rangle + |21\rangle) + \beta_1\,|11\rangle + \beta_2\,|22\rangle. \tag{97}$$

Normalization requires $2\alpha^2 + \beta_1^2 + \beta_2^2 = 1$. In terms of these parameters, the individual components of the energy are rather simple:

$$\begin{aligned} T &= -4\,t\,\alpha(\beta_1 + \beta_2) \\ V_{ee} &= U(\beta_1^2 + \beta_2^2) \\ V &= -\Delta v(\beta_1^2 - \beta_2^2), \end{aligned} \tag{98}$$

so that the variational principle may be written as

$$E = \min_{\substack{\alpha,\beta_1,\beta_2 \\ 1 = 2\alpha^2 + \beta_1^2 + \beta_2^2}} E(\alpha, \beta_1, \beta_2). \tag{99}$$

The specific values of these parameters for the ground-state wavefunction are reported in appendix A.

For this simple problem, we are fortunate that we can apply the Levy–Lieb constrained search method explicitly. A variation of this method was used for the derivation of the exact functional of the single- and double-site Anderson model and the symmetric Hubbard dimer [40], and a numerical version of this was used by Fuks *et al* [66]. Similar results were obtained by an alternative methods in [187].

The functional $F[n]$ is defined by minimizing the expectation value of $\hat{T}+\hat{V}_{ee}$ over all possible wavefunctions yielding a given $n(\mathbf{r})$. In real-space DFT, there are no easy ways of generating interacting wavefunctions for a given density. But here,

$$\Delta n = 2(\beta_2^2 - \beta_1^2), \tag{100}$$

which allows us to simply eliminate a parameter, e.g. β_1 in favor of Δn. Thus

$$F[\Delta n] = \min_{\alpha^2+\beta_2^2=\frac{1}{2}\left(1+\frac{|\Delta n|}{2}\right)} [T(\alpha,\beta_2,\Delta n) + V_{ee}(\alpha,\beta_2,\Delta n)]. \tag{101}$$

With normalization and the density constraint, only one parameter is left free. There exist several possible choices for this. If we choose $g = 2\alpha\,(\beta_1+\beta_2)$ which corresponds to the hopping term, then after some algebra the function(al) can be written nicely as

$$F(\rho) = \min_g f(\rho, g) \tag{102}$$

with the intermediate quantity

$$f(\rho, g) = -2\,t\,g + U h(g,\rho), \tag{103}$$

and

$$h(g,\rho) = \frac{g^2\left(1-\sqrt{1-g^2-\rho^2}\right)+2\rho^2}{2(g^2+\rho^2)}. \tag{104}$$

Note that both t and U appear linearly in $f(g,\rho)$. The minimization yields a sextic polynomial, equation (B.1), that g must satisfy. The weak-coupling, strong-coupling, symmetric, and asymmetric limits of g are given in appendix B.

Our construction begins with a simple approximation to $g(\rho)$:

$$g_0(\rho) = \sqrt{\frac{(1-\rho)\,(1+\rho\,(1+(1+\rho)^3 u a_1(\rho,u)))}{1+(1+\rho)^3 u a_2(\rho,u)}} \tag{105}$$

where

$$a_i(\rho,u) = a_{i1}(\rho) + u\,a_{i2}(\rho), \tag{106}$$

and

$$a_{21} = \frac{1}{2}\sqrt{(1-\rho)\rho/2}, \quad a_{11} = a_{21}(1+\rho^{-1}),$$
$$a_{12} = \frac{1}{2}(1-\rho), \qquad a_{22} = a_{12}/2. \tag{107}$$

These forms are chosen so g_0 is exact to second- and first-order in the weak- and strong-coupling limits respectively, and to first- and second- order in the symmetric and asymmetric limits respectively. Use of this g_0 to construct an approximation to F, $f(g_0(\rho),\rho)$, yields very accurate energetics. The maximum energy error, divided by U, is 0.002.

But for some of the purposes in this paper, such as calculations of T_C, even this level of error is unacceptable. We now improve on $g_0(\rho)$ using the adiabatic connection formula of section 5.2. Like F, we can define functions of two variables for each of the correlation components. Write

$$e_C(g,\rho) = f(g,\rho) - T_S(\rho) - E_{HX}(\rho). \tag{108}$$

where T_S and E_{HX} are from equations (53) and (52), respectively. The kinetic and the potential correlation are given by

$$t_C(g,\rho) = T - T_S = -2\,t\left(g - \sqrt{1-\rho^2}\right) \tag{109}$$

$$u_C(g,\rho) = V_{ee} - E_{HX} = U[h(g,\rho) - (1+\rho^2)/2], \tag{110}$$

and their sum yields $e_C(g,\rho)$. If we insert $g(\rho)$, the exact minimizer of $f(g,\rho)$, into any of these expressions, we get the exact answers.

But recall also that one can extract U_C from the derivative of E_C with respect to the coupling constant λ, i.e.

$$U_C = \mathrm{d}E_C(\lambda)/\mathrm{d}\lambda|_{\lambda=1}. \tag{111}$$

Now for any g and $e_C(g)$, we can find the λ dependence by replacing U by λU. Thus

$$\frac{\mathrm{d}e_C(g,\lambda)}{\mathrm{d}\lambda} = \frac{\partial E_C(\lambda)}{\partial\lambda} + \frac{\partial E_C(\lambda)}{\partial g}\frac{\partial g}{\partial\lambda} \tag{112}$$

Since T_S and E_{HX} do not depend on g, the minimization of f reduces to $\partial e_C/\partial g = 0$, so for the exact g the second term on the right of equation (112) is always zero. But it does not vanish for g_0.

Equating equations (111) and (112) and using the definitions, we find the following self-consistent equation for g:

$$g = -\frac{T}{2\,t} + \frac{1}{2\,t}\frac{\partial E_C}{\partial g}\frac{\partial g(\lambda)}{\partial\lambda}\bigg|_{\lambda=1}. \tag{113}$$

We may use this to improve our estimate for g. Simply evaluate the right-hand side at g_0, to find:

$$g_1 = g_0\left(u\frac{\partial h}{\partial g} - 1\right)\frac{\partial g(\lambda)}{\partial\lambda}\bigg|_{\lambda=1}, \tag{114}$$

where

$$\frac{\partial g(\lambda)}{\partial\lambda}\bigg|_{g_0} = \frac{(1-\rho)(1+\rho)^3\,[\rho(1+(1+\rho)^3 a_2(\lambda))a_1'(\lambda) - (1+\rho(1+\rho)^3 a_1(\lambda))a_2'(\lambda)]}{2g_0(1+(1+\rho)^3 a_2(\lambda))^2}. \tag{115}$$

The new F_{par} and $E_{C,par}$ are then obtained by using g_1 in equations (103) and (108). Using g_1, $\partial E_{C,par}/\partial g \neq 0$ still, but the error with g_1 is much lower than with g_0. We plot the the relative error, $(E_C - E_{C,par})/U$ for several U in figure 22. The maximum relative error is reduced by almost two orders of magnitude (from 2×10^{-3} to 5×10^{-5}) in the region $U\approx 2-6$, $|\Delta n|\approx 0.25$, where g_0 has the largest error. The other regions are also improved. For $(T_C - T_{C,par})/U$ and $(U_C - U_{C,par})/U$ the improvement is just of one order of magnitude (from 2×10^{-2} to 2×10^{-3} in both cases relative to the maximum), with different sign, so there is an error cancellation that yields the larger reduction of the E_C error. We anticipate that g could be improved even further by iteration.

To test the validity of our parametrization, we use it in the KS scheme to calculate the correlation energy of our Hubbard dimer *self-consistently*. If our parametrization were perfect,

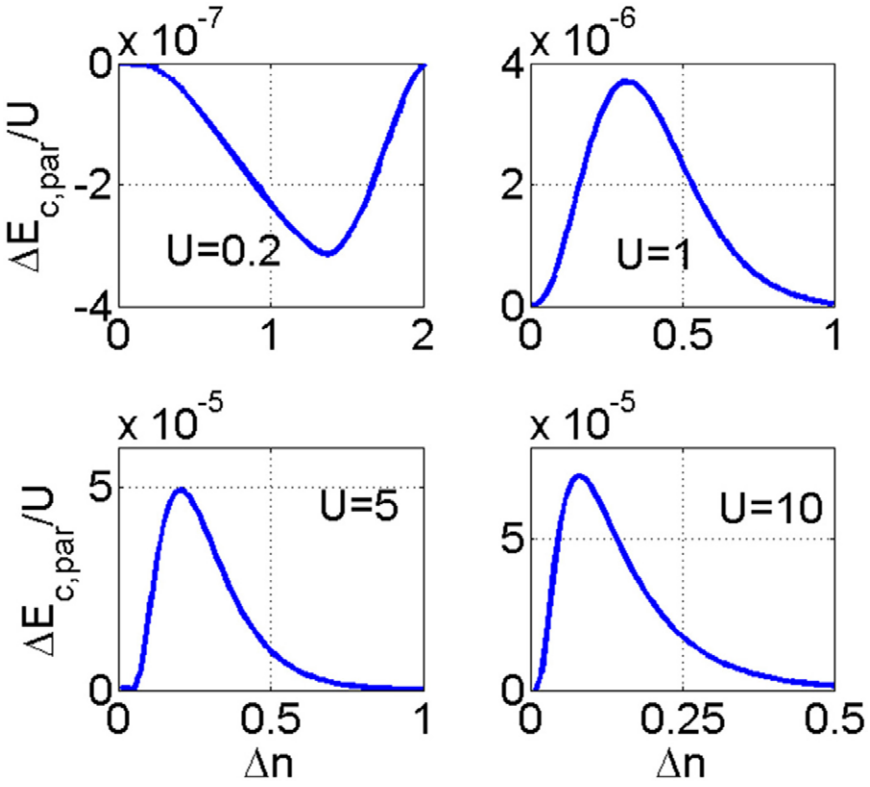

Figure 22. Error in $E_{\mathrm{C,par}}(\rho)/U$ for different U and $2\,t = 1$.

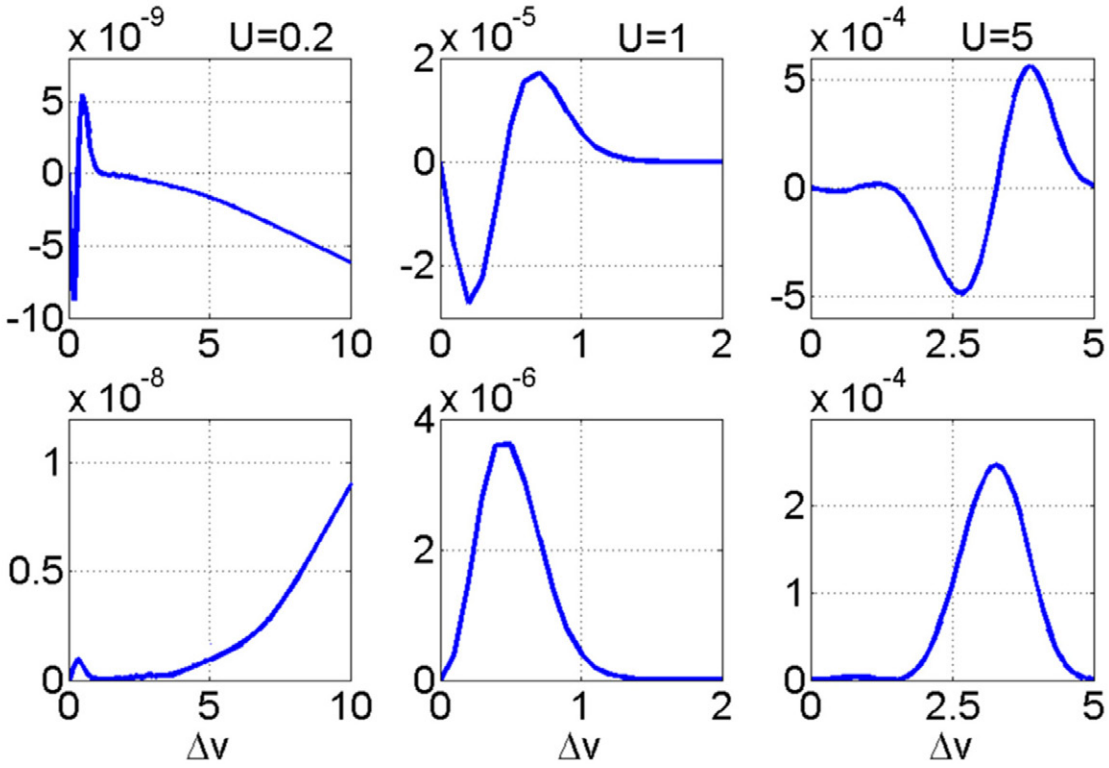

Figure 23. Top row: error in density as a function of Δv. Bottom row: error in ground-state energy as a function of Δv and $2\,t = 1$.

we would recover the exact densities and energies from our KS calculation without having to solve the many-body problem. These are plotted in figures 23, together with the absolute errors committed by the parametric function(al). Notice that in figures 8 and 19 the results obtained from the parametric function(al) are indistinguishable from the exact results. We recommend the use of g_0 for routine use, and g_1 for improved accuracy. We hope the methodology developed here might

prove useful to improve accuracy of correlation functionals in other contexts, e.g. using DFT to improve sampling in a Quantum Monte Carlo calculation [211].

We can define the starting point of our parametrization in a multitude of ways. In this section we defined it such that the parameter corresponds to the hopping term. Another possible choice favors the electron–electron term. Define

$$f_2(f,\rho) = -2\,t\,\sqrt{1-f}\left(\sqrt{f+\rho}+\sqrt{f-\rho}\right)+U\,f. \tag{116}$$

Another choice captures the asymmetric limit. Define,

$$f_3(l,\rho) = -2\,t\,\sqrt{2\,l-l^2-\rho^2}+U\,\frac{l^2+\rho^2}{2\,l}. \tag{117}$$

Then,

$$F(\rho) = \min_f f_2(f,\rho) = \min_l f_3(l,\rho). \tag{118}$$

These also yield high order polynomial equations when minimized. The present parametrization, equation (105), is quantitatively superior for nearly all values of U, and Δv of interest.

7. Approximations

The usefulness of KS-DFT derives from the use of approximations for the XC functional, not from the exact XC which is usually as expensive to calculate as direct solution of the many-body problem (or more so). While the field of real-space DFT is deluged by hundreds of different approximations [150] (relatively few of which are used in routine calculations [183]), few approximations exist that apply directly to the Hubbard dimer. The two we explore here are illustrative of many general principles.

7.1. Mean-field theory: broken symmetry

Since time immemorial, or at least the 1930's, folks have realized the limitations of restricted HF solutions for strongly correlated multi-center problems, and performed broken-symmetry calculations [45]. For example, in many-body theory, Anderson solved the Anderson impurity model for a magnetic atom in a metal [10] by allowing symmetry breaking, several years before Kondo's ground-breaking work [113]. In quantum chemistry, Coulson and Fischer identified the Coulson-Fischer point of the stretched H_2 molecule where the broken symmetry solution has lower energy than the restricted solution [45]. Modern quantum chemists like to spin-purify their wavefunctions, but DFT hardliners [178] claim the broken-symmetry solution is the 'correct' one (for an approximate functional). The exact KS functional, as shown in all previous sections, yields the exact energy and spin densities, while remaining in a spin singlet.

If we do not impose spin symmetry, the effective potential in mean-field theory becomes (section 2.2):

$$v_{i\sigma}^{\rm eff} = v_i + U\,n_{i\bar\sigma}, \tag{119}$$

with $\sigma=+1$ for spin up, $\sigma=-1$ for spin down and $\bar\sigma=-\sigma$, because the change in the effective field is caused by the other electron. Writing $n_i = n_{i,\uparrow}+n_{i,\downarrow}$, $m_i = n_{i,\uparrow}-n_{i\downarrow}$ and $\Delta m = m_2 - m_1$, and defining

$$\Delta v_\sigma^{\rm eff} = \Delta v + \frac{U}{2}\,(\Delta n - \sigma\,\Delta m), \tag{120}$$

and

$$t_\sigma^{\rm eff} = t\sqrt{1+(\Delta v_\sigma^{\rm eff}/2\,t)^2}, \tag{121}$$

we find the eigenvalues are:

$$\mathrm{e}_{\pm,\sigma}^{\rm MF} = \frac{U}{4}\,(N-\sigma\,M) \pm \frac{t_{\bar\sigma}^{\rm eff}}{2}, \tag{122}$$

where $N=2$ is the number of particles and M is the total magnetization. We find the ferromagnetic solution ($M=2$) to be everywhere above the antiferromagnetic solution ($M=0$), and for $M=0$:

$$E = \frac{U}{2}\left(1-\frac{\Delta n^2-\Delta m^2}{4}\right)-\frac{1}{2}(t_\uparrow^{\rm eff}+t_\downarrow^{\rm eff}), \tag{123}$$

where $\Delta m = 0$ is the paramagnetic (spin singlet) solution, and corresponds to our original mean-field or restricted Hartree–Fock solution. We minimize this energy with respect to Δn and Δm, given by

$$\Delta n = -\sum_\sigma \frac{\Delta v_\sigma^{\rm eff}}{t_\sigma^{\rm eff}}, \quad \Delta m = -\sum_\sigma \sigma\frac{\Delta v_\sigma^{\rm eff}}{t_\sigma^{\rm eff}}, \tag{124}$$

These antiferromagnetic (AFM) self-consistency equations always have the trivial solution $\Delta m = 0$, which corresponds to the restricted MF solution(RHF). However, there exists a non-trivial solution $\Delta m \neq 0$ for sufficiently large values of U.

In figure 24, we plot Δn for both restricted and unrestricted HF solutions for $U=5$. The solutions coincide for large Δv, but below a critical value of Δv, they differ. The UHF solution has a significantly lower Δn, which is much closer to the exact Δn.

In figure 25, we plot the energies, showing that the UHF solution does not rise above zero, and mimics the exact solution rather closely. For large U, at $n_1=1$, we can compare results analytically:

$$E \to \frac{U}{2}-2\,t\ \ (\text{RHF}),\ -\frac{2\,t^2}{U}\ \ (\text{UHF}),\ -\frac{4\,t^2}{U}\ \ (\text{exact}) \tag{125}$$

confirming that the UHF energy is far more accurate than the RHF energy, and recovers the dominant term in the strongly correlated limit. Note that the symmetric case is atypical: The constant terms vanish, both exactly and in UHF, so the leading terms is $O(1/U)$, and its coefficient in UHF is underestimated by a factor of 2. The slope of the exact result is two times larger than UHF. Of course, the exact solution is a spin-singlet, so the symmetry of the UHF solution is incorrect, but its energy is far better than that of RHF. This is called the symmetry dilemma in DFT [178]: Should I impose the right symmetry at the cost of a poor energy? Note that the exact KS wavefunction is also a singlet, so a broken-symmetry DFT solution produces the wrong symmetry for the KS wavefunction.

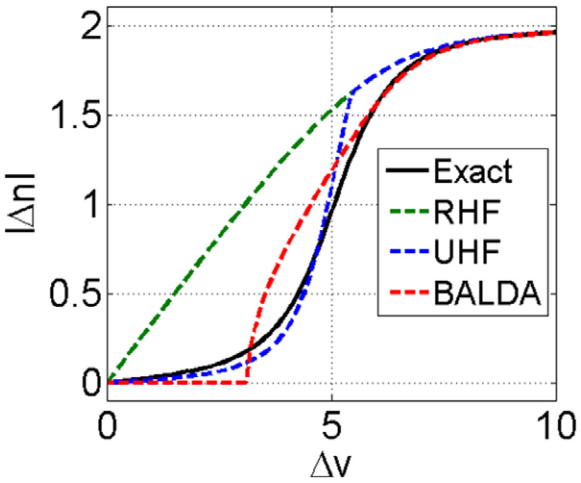

Figure 24. Plots of Δn for HF and BALDA as a function of Δv for $U = 5$ and $2\,t = 1$. The crossover from the charge-transfer to the Mott–Hubbard regime happens at $U \approx \Delta v$.

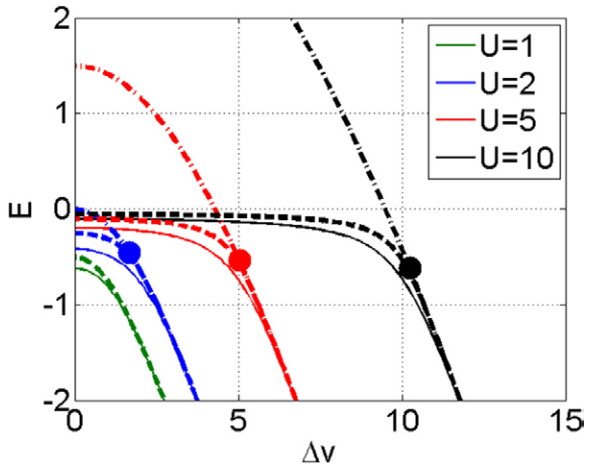

Figure 25. Ground-state energy of the unrestricted Hartree–Fock (thick dashed line), restricted Hartree–Fock (dot dashed line), and exact ground-state (thin solid line) of the Hubbard dimer as a function of Δv for several values of U and $2\,t = 1$. The dot shows the Coulson–Fischer point at which the symmetry breaks spontaneously. For smaller Δv the UHF energy is below RHF while for larger Δv they are the same.

7.2. BALDA

In real-space DFT, the local density approximation (LDA) was first suggested by Kohn and Sham [112], in which the XC energy is approximated at each point in a system by that of a uniform gas with the density at that point. Another way to think of this is that one decides to make a local approximation, and then chooses the uniform gas XC energy density to ensure exactness in the uniform limit. On the lattice, we must switch our reference system to incorporate Luttinger-liquid correlations instead of Fermi-liquid correlations [84]. The infinite homogeneous Hubbard chain plays the role of the uniform gas. This can be solved exactly via Bethe ansatz [134], and the corresponding LDA was first constructed and tested in [204]. Later, Capelle and collaborators [38, 63, 136, 137, 248] used the exact Bethe ansatz solution to create an explicit parametrization for the energy per site, and called this Bethe Ansatz LDA, or BALDA.

Since its inception, BALDA has been applied to many different problems including disorder and critical behavior in optical lattices [35, 241], spin-charge separation [231, 232] and effects of spatial inhomogeneity [135, 210] in strongly correlated systems, confined fermions both with attractive and repulsive interactions [33], current DFT on a lattice [6], electric fields and strong correlation [5], and various critical phenomena in 1D systems [2, 62]. Extensions to include spin-dependence (BALSDA) have been principally used for studying density oscillations [234, 242], and fermions in confinement [99, 243, 244]. A thermal DFT approximation on the lattice has been constructed using BALDA [245]. BALDA has also been used as an adiabatic approximation in TD-DFT to calculate excitations [108, 121, 131, 223, 227, 229] and also transport properties [123, 230], as well as using BALDA as a gateway to calculate time-dependent effects in 3D [105]. There has been significant interest in using BALDA to understand the derivative discontinuity in both DFT and TD-DFT [123, 245, 248, 252]. Additionally, the BALDA approach has been developed for other BA-solvable fermionic lattice systems aside from the Hubbard model [3, 156, 198, 246], such as the Anderson model [24, 122, 139], as well as bosonic systems [85, 238, 239].

We use here the semi-analytical approach to BALDA [137, 248] where the expressions are given in appendix D. In figure 26 we plot the BALDA ground-state energy as a function of Δv for several values of U. At first glance, it seems to do a good job in all regimes. In particular, for either very weak correlation ($U = 0.2$) or very strong correlation ($U = 100$), it is indistinguishable from the exact curves. However, for moderate correlation ($1 \lesssim U \lesssim 5$) where $\Delta v \lesssim U$, it appears to significantly underestimate the magnitude of E.

Even for the strong correlation regime, its behavior is not quite correct. For the symmetric case:

$$E^{\mathrm{BA}} \simeq 2\,t\left(\frac{4}{\pi} - 1\right) > 0 \qquad (U \gg 2\,t) \tag{126}$$

Thus, for $\Delta v = 0$ and $U = 100$ in figure 26, BALDA is in serious error, but this cannot be seen on the scale of the figure. The origin of this error is easy to understand. BALDA's reference system is an infinite homogeneous chain, and we are applying it to a finite inhomogeneous dimer. The error is in the correlation kinetic energy, which comes from the difference between the exact and KS kinetic energies. The tight-binding energy for an infinite homogeneous chain is different from that of the dimer, and this difference is showing up (incorrectly) in the correlation energy. We could, of course, reparametrize BALDA to use the homogeneous dimer energy, but the analog of real-space DFT is to use the homogeneous extended system (infinite Hubbard chain).

7.3. BALDA versus HF

Lastly we compare BALDA and both the restricted and unrestricted Hartree–Fock approximations. In figure 27, we plot the errors made in the ground-state energy of all three

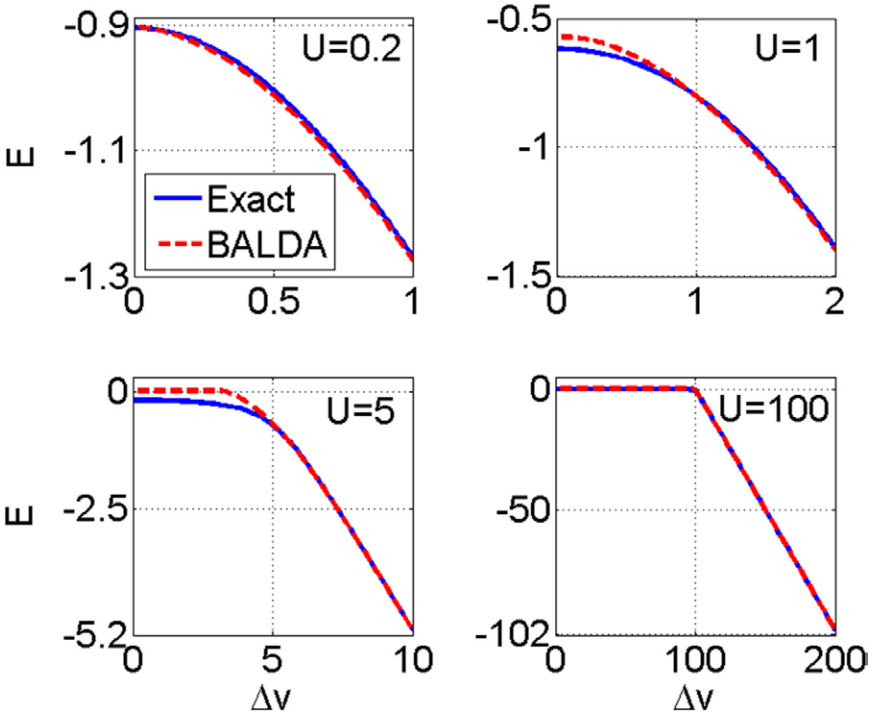

Figure 26. Ground-state energy versus Δv for several U, with $2\,t = 1$. The BALDA energies are evaluated self-consistently.

approximations. For $U \leqslant 1$, HF does not break symmetry, and so UHF = RHF. For very small U, the energy error is comparable to HF. For $U = 1$, BALDA is better than HF. For larger U, UHF produces a lower energy than HF, and almost everywhere is more accurate than BALDA. The sole exception is at precisely $U \approx \Delta v$, where BALDA is much better. In figure 24, we compare BALDA and UHF densities to the exact density for $U = 5$ as a function of Δv. Although BALDA does not have a symmetry-breaking point, it unfortunately has a critical value of Δv where Δn vanishes incorrectly. This is the origin of the cusp-like features in the BALDA energies of figures 26 and 27. In fact, the BALDA density appears somewhat worse than UHF for most Δv. But keep in mind that the main purpose of BALDA is to produce accurate energies *without* the artificial spin-symmetry breaking of UHF.

8. Fractional particle number

We will now show a way that one *can* extract the physical gap from ground-state DFT. This is done simply by changing the number of electrons, but now continuously, rather than just at integers. In fact, we already used this technology implicitly in section 4, but here we make this much more explicit.

8.1. Derivative discontinuity

An extremely important concept in DFT is that of the derivative discontinuity [43, 123, 157–159, 176, 177, 202, 250]. This is most famous for its implication for the Kohn–Sham gap of a solid, ensuring that the gap (in general) does *not* match the true fundamental (or charge) gap of the solid, as we saw in section 4. The expression itself refers to a plot of ground-state energy versus particle number N at zero temperature. In seminal work [171, 176, 177], it was shown that $E(\mathcal{N})$ consists of straight-line segments between integer values, where $\mathcal{N}$ is a real variable, where all quantities are now expectation values in a grand-canonical ensemble at zero temperature:

$$E(\mathcal{N}) = (1-w)\,E(N) + w\,E(N+1), \tag{127}$$

and

$$n_{\mathcal{N}}(\mathbf{r}) = (1-w)\,n_N(\mathbf{r}) + w\,n_{N+1}(\mathbf{r}), \tag{128}$$

where $\mathcal{N} = N + w$, i.e. both energy and ground-state density are piecewise linear, with a sudden change at integer values.

Then the chemical potential is

$$\begin{aligned} \mu = \mathrm{d}E/\mathrm{d}\mathcal{N} &= -I \qquad (\mathcal{N} < N) \\ &= -A \qquad (\mathcal{N} > N). \end{aligned} \tag{129}$$

When we evaluated everything at $N = 2$ in section 4, we really meant $N = 2^-$. Then Janak's theorem [103] shows that, for the KS system,

$$\begin{aligned} \mu = \mathrm{d}E/\mathrm{d}\mathcal{N} &= \epsilon^{\mathrm{HOMO}} \qquad (\mathcal{N} < N) \\ &= \epsilon^{\mathrm{LUMO}} \qquad (\mathcal{N} > N) \end{aligned} \tag{130}$$

This is the proof of the equivalence of I and $-\epsilon^{\mathrm{HOMO}}$.

Because the energy is in straight-line segments, the slope of $E(\mathcal{N})$, the chemical potential, $\mu(\mathcal{N})$, jumps discontinuously at integer values. Hence the name, derivative discontinuity. The jump in μ across an integer N is then $E_g = I - A$, the fundamental gap. In the KS system, since the energy is given in terms of orbitals and their occupations, that jump is simply the KS HOMO-LUMO gap, E_{gs}. Since the KS electrons have the non-interacting kinetic energy, and the external and Hartree potentials are continuous functionals of the density,

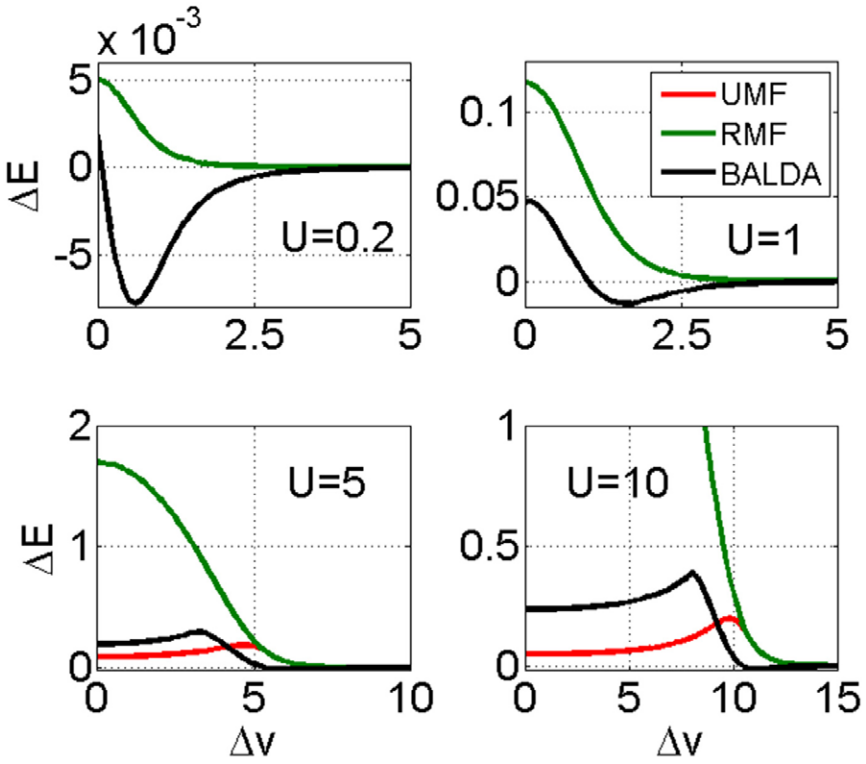

Figure 27. Plots of the RMF, UMF, and BALDA $\Delta E = E^{\text{approx}} - E^{\text{exact}}$ as a function of Δv for $U = 0.2,\ 1,\ 5$, and 10. For small U the RMF and UMF results are indistinguishable. Here $2\,t = 1$.

the difference is an XC effect. Moreover, it implies that v_{XC} jumps by this amount as one passes through N, an integer.

For solids, addition or removal of a single electron has an infinitesimal effect on the density, but the XC discontinuity shifts the conduction band upward by Δ_{XC} when an electron is added, contributing to the true gap. Since local and semilocal approximations to XC are usually smooth functionals of the density, they produce no such shift. They *do* yield accurate approximations to the KS gap of a solid, but *not* to the gap calculated by adding and removing an electron, because of this missing shift. Thus we have no general procedure for extracting accurate gaps using LDA and GGA. An important quality factor in more sophisticated approximations is whether or not they have a discontinuity. Orbital-dependent functionals, such as exact exchange (EXX in OEP) [72, 117, 120, 209, 217, 251] or self-interaction corrected LDA (SIC) [89, 104, 169, 170, 180], often capture effects due to the discontinuity quite accurately.

8.2. Hubbard dimer near integer particle numbers

In figure 28, we plot $E(\mathcal{N})$ for our Hubbard dimer. Real-space curves have always been found to be convex, although this has never been proven to be generally true. The vital part for us is that this equivalence of the HOMO level and $-I$ links the overall position of the KS levels to those of the many-body system. For fixed particle number, only the KS on-site energy difference is determined by the need to reproduce the exact site occupancies. But this condition also fixes the mean value of the KS on-site energy, $\bar{v}_{\text{S}}$, which in general is non-zero, even though we chose the actual mean on-site energy to be zero always. In figure 2, this is visible in the mean position of the two KS on-site potentials.

Another way to think about this is that function(al) derivatives at fixed $\mathcal{N}$ leave an undetermined constant in the potential, whereas that constant is determined if the particle number is allowed to change. We can write many equivalent formulas for the discontinuity:

$$\begin{aligned}\Delta_{\text{XC}} &= \frac{\partial E_{\text{XC}}}{\partial N}\bigg|_{N^+} - \frac{\partial E_{\text{XC}}}{\partial N}\bigg|_{N^-},\\ &= \bar{v}_{\text{XC}}(N^+) - \bar{v}_{\text{XC}}(N^-),\\ &= \bar{v}_{\text{S}}(N^+) - \bar{v}_{\text{S}}(N^-),\\ &= \epsilon_{\text{S}}(N^+) - \epsilon_{\text{S}}(N^-),\end{aligned} \tag{131}$$

all of which are true. Thus another way to find the gap from a KS system is to occupy it with an extra infinitesimal of an electron, and note the jump in potentials or eigenvalues. To illustrate this, in figure 29 we replot figure 11, but now for $N = 2^+$, showing that now the LUMO matches $-A$, and the difference between the HOMO and $-I$ is Δ_{XC}.

In figure 30 we plot Δ_{XC} for $N = 2$ for various U, as a function of Δv, scaling each variable by U. We see that the discontinuity always decreases with increasing Δv. In fact, the larger U is, the more abruptly it vanishes (on a scale of U) when $\Delta v > U$. In this sense, the greater the asymmetry, the less discontinuous the energy derivative is, and the KS gap will be closer to the true gap.

The situation is reversed when $N = 1$, as shown in figure 31. Now the discontinuity grows with increasing Δv. In

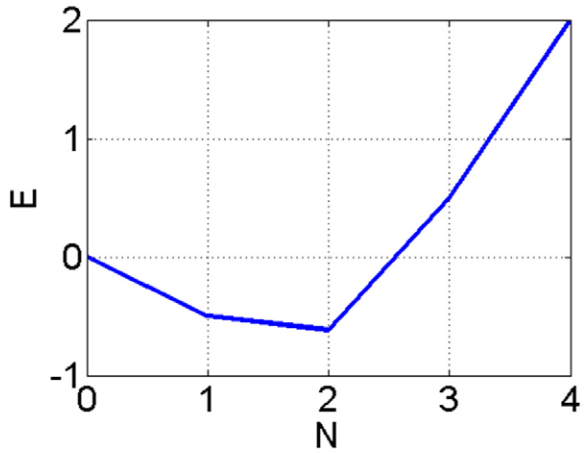

Figure 28. Plot of $E(\mathcal{N})$ for $U = 1$, $\Delta v = 0$ and $2\,t = 1$.

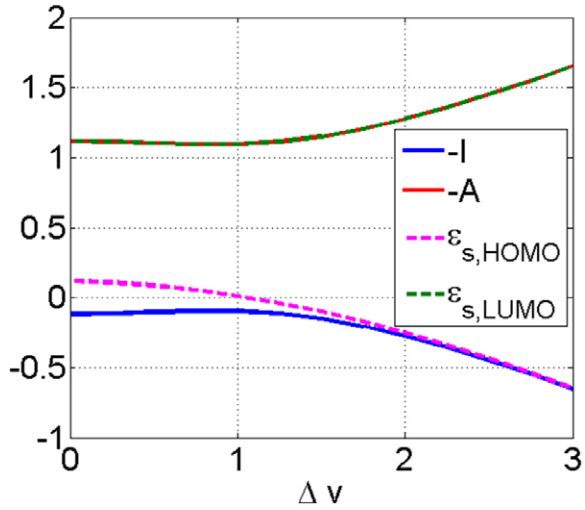

Figure 29. Same as figure 11 except with $N = 2^+$ instead of $N = 2^-$.

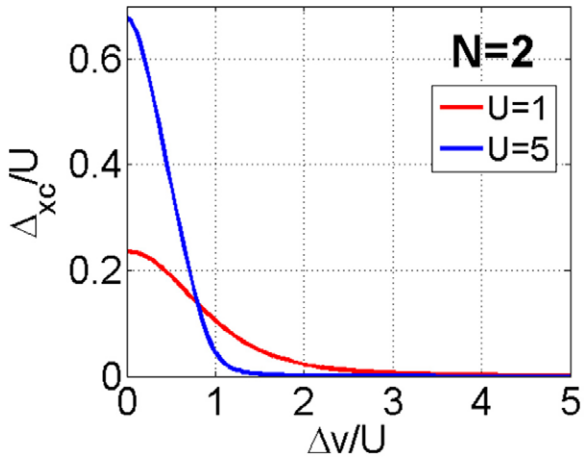

Figure 30. Derivative discontinuity as a function of Δv for $U = 1$, and $U = 5$.

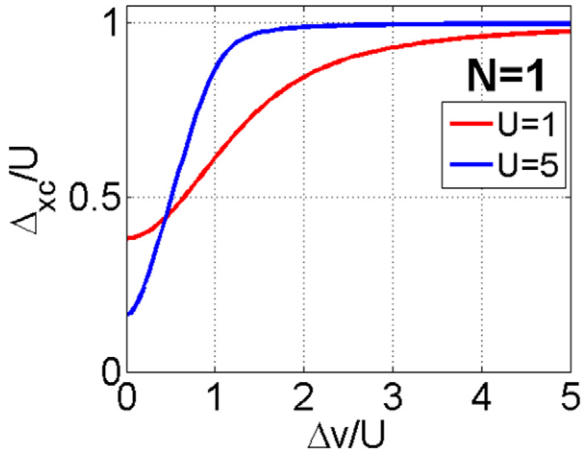

Figure 31. Derivative discontinuity for $N = 1$ as a function of Δv for $U = 1$, and $U = 5$.

this case, a large asymmetry puts the electron mostly on one site. When an infinitesimal of an electron is added, it goes to the same site, but paying an energy cost of U. On the other hand, if Δv is small, the first electron is spread over both sites, and so is the added infinitesimal, reducing the energy cost by a factor of 2. So $\Delta_{XC} \to U/2$ in the weakly correlated near-symmetric limit.

8.3. Discontinuity around $n_1 = 1$ for $N = 2$

The derivative discontinuity manifests itself in many different aspects of DFT. We have already seen how it affects both energies and potentials as N is continuously moved across an integer. Here we explore how it appears even at fixed particle number, as correlations become strong.

For our Hubbard dimer, with any finite Δv, if $U \gg \Delta v$, we know each n_i is close to 1. The overwhelmingly large U localizes each electron on opposite sites. In the limit as $U \to \infty$, all fluctuations are suppressed, and the dimer becomes two separate systems of one electron each. For large but finite U, and finite Δv, one is on the integer deficient side, and the other has slightly more than one electron. All the statements made above about $\mathcal{N}$ passing through 2 now apply as n_1 passes through 1.

We can see the effects in many of our earlier figures. In figure 7, the slope of F for $U = 10$ appears discontinuous at $n_1 = 1$. F contains the discontinuity in both T_S and E_{XC} in the limit $U \to \infty$. However, in reality, this curve is not really discontinuous. Zooming in on F near $n_1 = 1$, one sees that on a scale of $O(1/U)$, F is rounded.

The classic manifestation already appears in figure 4, the occupation difference as a function of Δv. To emphasize the point, in figure 32, we plot several curves for $U = 100$. This is the discontinuous change from having 1 particle on each site to 2 on one site that occurs. This is important because the common approximate density functionals miss this discontinuity effect. Explicit continuous functionals of the density cannot behave this way. For the SOFT case, this is embodied in the HF curves of figure 9: No matter how strong the value of U, these curves are linear. In RHF, Δn versus Δv never evolves the sudden step discussed above, as shown in figure 24. On the other hand, the BALDA approximation contains an explicit discontinuity at $n_1 = 1$ in its formulas, and

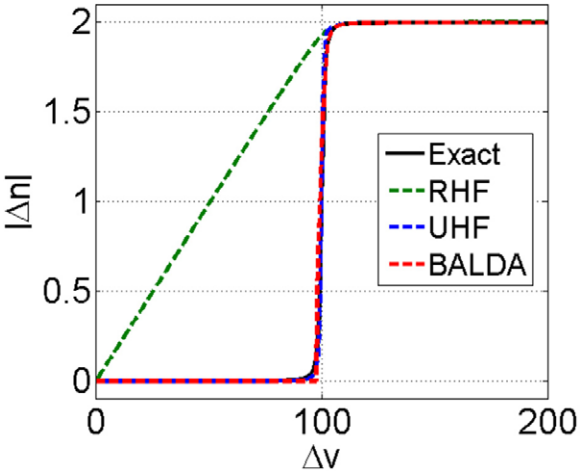

Figure 32. Plots of Δn in HF and BALDA as a function of Δv for $U = 100$ ($2\,t = 1$). The crossover from the charge-transfer to the Mott–Hubbard regime happens at about $U \approx \Delta v$.

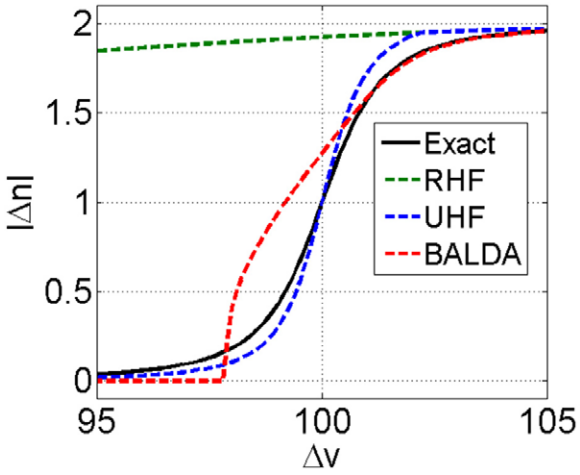

Figure 33. Same as figure 32.

so captures this effect, at least to leading-order in U. In this sense, both BALDA and UHF capture the most important effect of strong correlation. On the other hand, as discussed in section 7.3, UHF 'cheats', while BALDA retains the correct spin singlet. If BALDA's effects could be (legally) built into real-space approximations, they would be able to accurately dissociate molecules, overcoming perhaps approximate DFT's greatest practical failure.

However, in figure 33, we simply zoom in on the region of the plot near $\Delta v = U$. In fact, the exact curve is S-shaped, with a finite curvature on the scale of t. Now we see that, although both UHF and BALDA reproduce the discontinuous effect, the details are not quite right. UHF is admirably close in shape to the accurate curve, but its slope is too great at $n_1 = 1$. BALDA is accurate to leading order in $1/U$, and captures beautifully the region Δv a little larger than U, but is quite inaccurate below that. The presence of the gap in the BALDA potentials leads to the incorrect discontinuous behavior near $\Delta v = 98$. But once again we emphasize that the important feature is that these approximations do capture the dominant effect, and that BALDA does so without breaking symmetry.

9. Conclusions and discussion

So, what can we learn from this exercise in applying DFT methods to the simplest strongly correlated system? Perhaps the most important point is that there is a large cultural difference between many-body approaches and DFT methodology, and a considerable barrier to communication. In section 3.3, we saw that even the definition of exchange is different in the two communities. The greatest misunderstandings come not from using different words for the same thing, but rather from using the same word for two different things.

We can also see that the limitations of DFT calculations are often misunderstood in the broader community. For example, the exact ground-state XC functional has a HOMO-LUMO gap that does not, in general, match the fundamental gap. The KS eigenvalues are not quasiparticle eigenvalues in general, and are in fact, much closer to optical excitations [1]. Even the purpose of a DFT calculation is quite foreign to most solid-state physics. The modern art of DFT is aimed at producing extremely accurate (by physics standards) ground-state energies, and the many properties that can be extracted from those, rather than the response properties that are probed in most solid-state experiments, such as photoemission. (Flipping the coin, most quantum chemists would never describe DFT energies as extremely accurate, as traditional quantum chemical ab initio methods are hyper accurate on this scale.)

We also mention many aspects that we have *not* covered here. For example, time-dependent DFT is based on a distinct theorem (the Runge-Gross theorem [192]), and provides approximate optical excitations for molecular systems [32]. The Mermin theorem [155] generalizes the HK theorem to thermal ensembles [184]. There are many interesting features related to spin polarization and dynamics, but very little is relevant to the system discussed here. There are also many non-DFT approaches, such as *GW*, which could be tested on the asymmetric dimer.

We also take a moment to discuss how SOFT calculations can be related to real-space DFT. One can easily add more orbitals to each site and create an extended Hubbard model. For the H_2 molecule, adding just p_z orbitals and allowing them to scale yields a very accurate binding curve. But such an extension (beyond one basis function per site) is extremely problematic for SOFT [86, 201], because it is no longer clear how to represent the 'density'. With 2 basis functions, should one use just the diagonal occupations, or include off-diagonal elements? In fact, neither one is satisfactory, as neither approaches the real-space density functional in the infinite basis limit. An underlying important point of DFT is that it is applied to potentials that are diagonal in $\mathbf{r}$, i.e. $v(\mathbf{r})$, and not diagonal in an arbitrary basis. This is a key requirement of the HK theorem, and is the reason why the one-body density $n(\mathbf{r})$ is the corresponding variable on which to build the theory, and why the local density approximation is the starting point of all DFT approximations.

This inability to go from SOFT calculations to real-space DFT calculations should be regarded as a major caveat for those using SOFT to explore DFT. Here we have shown many

similarities in the behavior of SOFT functionals compared to real-space functionals. We have also proven some of the same basic theorems as those used in real-space DFT. But any results (especially unusual ones) that are found in SOFT calculations might not generalize to real-space DFT. The only way to be sure is to find a proof or calculation in real-space. On the other hand, SOFT calculations can be safely used to illustrate the basic physics behind real-space results [214].

Another limitation of SOFT can be seen already in our asymmetric Hubbard dimer. In a real heterogeneous diatomic molecule, say LiH with a pseudopotential for the core Li electrons, the values of U would be different on the two sites. But the real-space DFT is applied to interactions that are the same among all particles. And even if SOFT applies when both U and t become site-dependent, i.e. a one-to-one correspondence can be proven, it is unlikely that such studies would yield behavior that is even qualitatively similar to real-space DFT. Minimal models are usually designed to capture universal features and our Hubbard dimer captures the essential physics of the strongly correlated limit. However the SOFT function(al) is not the same as the DFT one.

Finally, we wish to emphasize once again the importance of testing ideas on the asymmetric Hubbard dimer. Much (but not all) of the SOFT literature tests ideas on homogeneous cases. The essence of DFT is the creation of a universal functional. i.e. $F[n]$ is the same no matter which specific problem you are trying to solve. The symmetric case is very special in several ways, and there are no difficulties in applying any method to the asymmetric case. We hope that some of the results presented here will make that easier.

Acknowledgments

We thank F Mila for his kind hospitality at EPFL where this collaboration began. We also thank our colleagues A Cohen, P Mori-Sánchez and J J Palacios for discussions on matters related to this article. Work at Universidad de Oviedo was supported by the Spanish MINECO project FIS2012-34858, and the EU ITN network MOLESCO. Work at UC Irvine was supported by the US Department of Energy (DOE), Office of Science, Basic Energy Sciences (BES) under award # DE-FG02-08ER46496. JCS acknowledges support through the NSF Graduate Research fellowship program under award # DGE-1321846.

Appendix A. Exact solution, components, and limits

In all appendices, we use dimensionless variables for brevity. Hence $\epsilon = E/2\,t$, $u = U/2\,t$, and $\nu = \Delta v/2\,t$. All the results in this appendix are already known, e.g. [187]. Then, the energy of the singlet-ground-state is

$$\epsilon = \frac{2}{3}\left(u - w\sin\left(\theta + \frac{\pi}{6}\right)\right) \tag{A.1}$$

where

$$w = \sqrt{3\,[1+\nu^2] + u^2}, \tag{A.2}$$

and

$$\cos(3\theta) = (9(\nu^2 - 1/2) - u^2)u/w^3. \tag{A.3}$$

The coefficients of the minimizing wavefunction, equation (97), are

$$\alpha = c\left(1 - \frac{u}{\epsilon}\right), \quad \beta_{1,2} = c\,(u - \epsilon \pm \nu), \tag{A.4}$$

$$c^{-2} = 2(\nu^2 + (\epsilon - u)^2(1 + \epsilon^{-2})). \tag{A.5}$$

The ground-state expectation values of the density difference and of the different pieces of the Hamiltonian are

$$\Delta n = 4\,c^2\,\nu\,(\epsilon - u) \tag{A.6}$$

$$V = \Delta v\,\Delta n/2, \tag{A.7}$$

$$T = 4\,c^2(\epsilon - u)^2/\epsilon, \tag{A.8}$$

$$V_{\rm ee} = 4\,c^2\,t\,u\,((\epsilon - u)^2 + \nu^2). \tag{A.9}$$

For fixed asymmetry ν, we can expand ε in the weakly and strongly correlated limits:

$$\epsilon^{w} = -\sqrt{1+\nu^2}\left(1 - \left(\frac{1}{2} + \nu^2\right)\tilde{u} + \left(\frac{1}{4} + \nu^2\right)\frac{\tilde{u}^2}{2} + \nu^4\frac{\tilde{u}^3}{2}\right) \tag{A.10}$$

where $\tilde{u} = u/(1+\nu^2)^{3/2}$. In the strongly correlated limit:

$$\epsilon^{st} = -u^{-1} + (1 - \nu^2)u^{-3} + O(u^{-5}). \tag{A.11}$$

We can also expand for fixed u around the symmetric limit:

$$\epsilon^{\rm sym} = \frac{1}{2}(u - r) + \frac{u - r}{r(u + r)}\nu^2, \tag{A.12}$$

where $r = \sqrt{u^2 + 4}$. And the asymmetric limit:

$$\epsilon^{\rm asy} = -\nu + u - (2\nu)^{-1} - u/2\nu^{-2} + (1 - 4u^2)(2\nu)^{-3}. \tag{A.13}$$

Appendix B. Many limits of $F(\Delta n)$

In this appendix we derive the limits that our parametrization in section 6 satisfies. Minimizing $\tilde{F}$ of equation (103) with respect to g, we obtain a sextic equation for g:

$$\begin{aligned}&(4 + u^2)\,g^6/4 + (\rho^2\,(3 + u^2) - 1)\,g^4\\ &+ 2\,u\,\rho^2\,g^3 + \rho^2\,(\rho^2\,(3 + u^2) - (2 + u^2))\,g^2\\ &-2\,u\,\rho^2\,(1 - \rho^2)\,g - \rho^4\,(1 - \rho^2) = 0\end{aligned} \tag{B.1}$$

where we define $\rho = |\Delta n|/2$. The solution defines $g_m(\rho)$, and $F(\rho) = F(g_m(\rho), \rho)$. Next we expand in several limits. and $F[U, \rho] = \tilde{F}[U, \rho, g_m]$. However, equation (B.1) can not be solved analytically in general.

B.1. Expansions for $g(\rho, u)$

We expand g in 4 different limits, which are built into g_0 of equation (105) in section 6.

The weakly correlated limit corresponds to $u \ll 1$. We thus expand $g(\rho, u)$ in powers of u for fixed ρ,

$$g(\rho, u) = \sum_{n=0}^{\infty} g^{(n)}(\rho)\, u^n / n\,!\,, \tag{B.2}$$

and insert the expansion into equation (B.1). The coefficients $g^{(n)}$ are found by canceling each term order by order in equation (B.1), yielding

$$\begin{aligned} g^{(0)} &= \sqrt{1-\rho^2}, \quad g^{(1)} = 0, \\ g^{(2)} &= -\frac{(1-\rho^2)^{5/2}}{4}, \quad g^{(3)} = \frac{3}{4}\rho^2 (1-\rho^2)^3, \\ g^{(4)} &= \frac{9}{16}(1-\rho^2)^{7/2}(1+7\rho^2-24\rho^4). \end{aligned} \tag{B.3}$$

Notice that $n_{1,2} = 1 \mp \mathrm{sign}(\Delta n)\,\rho$ so that to first order in U, equation (103) yields the non-interacting kinetic energy functional of equation (42).

For strongly correlated systems, we expand g in powers of $1/u$ while holding ρ fixed

$$g(\rho, u) = \sum_{n=0}^{\infty} \tilde{g}^{(n)}(\rho)\, u^{-n} / n\,!\,, \tag{B.4}$$

and substitute back into equation (B.1) to find the coefficients. The result is

$$\begin{aligned} \tilde{g}^{(0)} &= \sqrt{2\rho\,(1-\rho)}, \quad \tilde{g}^{(1)} = \frac{1-\rho}{2}, \\ \tilde{g}^{(2)} &= \frac{3\,(1-3\,\rho)}{8\rho}\,\tilde{g}^{(0)}. \end{aligned} \tag{B.5}$$

Notice that this expansion breaks down at the symmetric point $\rho = 0$.

The other kind of limit keeps u fixed. The symmetric limit is equivalent to $\rho \to 0$. We expand g in powers of ρ while holding u fixed.

$$g(\rho, u) = \sum_{n=0}^{\infty} \bar{g}^{(n)}(u)\, \rho^n / n\,!\,, \tag{B.6}$$

and substitute back into equation (B.1) to find the coefficients. The result is

$$\bar{g}^{(0)} = r^{-1}, \quad \bar{g}^{(2)} = \frac{1}{2}\left(u^2 + \frac{u^2/2\,(u^2/2+1) - 1}{r}\right) \tag{B.7}$$

where $r = \sqrt{1 + (u/2)^2}$.

The asymmetric limit is equivalent to $\rho \to 1$. We expand g in powers of $\bar{\rho} = 1 - \rho$ for fixed u:

$$g(\rho, u) = \sum_{n=0}^{\infty} \tilde{\bar{g}}^{(n)}(u)\, \bar{\rho}^n / n\,!\,, \tag{B.8}$$

and substitute back into equation (B.1). The result is

$$\begin{aligned} \tilde{\bar{g}}^{(1/2)} &= \sqrt{\pi/2}, \quad \tilde{\bar{g}}^{(3/2)} = -3\tilde{\bar{g}}^{(1/2)}/8 \\ \tilde{\bar{g}}^{(5/2)} &= \left(\frac{1}{16} + u^2\right) 5\tilde{\bar{g}}^{(3/2)} \\ \tilde{\bar{g}}^{(3)} &= 12\,u^3. \end{aligned} \tag{B.9}$$

B.2. Limits of the correlation energy functional

Now that we have expressions for g in all four limits we can use our expression for F, equation (103), T_{S}, and U_{H} to compute E_{C} in each regime:

$$e_{\mathrm{C}} = -g + uh(g, \rho) - \frac{u}{2}(1+\rho^2) + \sqrt{1-\rho^2}. \tag{B.10}$$

where $h(g, \rho)$ is defined in equation (104). Then, as $u \to 0$, $e_{\mathrm{C}} \to e_{\mathrm{C}}^{w}$, where

$$e_{\mathrm{C}}^{w}(\rho) = -\frac{u^2}{8}(1-\rho^2)^{5/2}\left(1 - u\,\rho^2\sqrt{1-\rho^2}\right). \tag{B.11}$$

Similarly, as $u \to \infty$, $e_{\mathrm{C}} \to e_{\mathrm{C}}^{\mathrm{str}}$, where

$$e_{\mathrm{C}}^{\mathrm{str}}(\rho) = -\frac{u}{2}(1-\rho)^2 + \sqrt{1-\rho}\left(\sqrt{1+\rho} - \sqrt{2\,\rho}\right) - \frac{1-\rho}{4\,u}. \tag{B.12}$$

An alternative expansion is to fix u and expand in ρ. As $\rho \to 0$, $e_{\mathrm{C}} \to e_{\mathrm{C}}^{\mathrm{sym}}$, where

$$\begin{aligned} e_{\mathrm{C}}^{\mathrm{sym}}(\rho) = 1 - \sqrt{1+\left(\frac{u}{2}\right)^2} \\ + \rho^2\left(\left(\frac{u}{2}\right)^3 - \frac{1}{2} + \sqrt{1+\left(\frac{u}{2}\right)^2}\left(\frac{1}{2} + \left(\frac{u}{2}\right)^2\right)\right). \end{aligned} \tag{B.13}$$

As $\rho \to 1$, $e_{\mathrm{C}} \to e_{\mathrm{C}}^{\mathrm{asym}}$, where

$$e_{\mathrm{C}}^{\mathrm{asym}}(\rho) = u^2\,\bar{\rho}^{5/2}\left(-\frac{1}{\sqrt{2}} + u\sqrt{\bar{\rho}}\right). \tag{B.14}$$

where $\bar{\rho} = 1 - \rho$.

B.3. Order of limits

Finally, we look at how these expressions behave when both parameters are extreme. The weakly correlated limit has no difficulties near the symmetric point:

$$\begin{aligned} e_{\mathrm{C}}^{w}(\rho \to 0) &= e_{\mathrm{C}}^{\mathrm{sym}}(u \to 0) \\ &= -\frac{u^2}{8}\left(1 - \frac{5\,\rho^2}{2}\right) + \frac{u^3\,\rho^2}{8}. \end{aligned} \tag{B.15}$$

In the asymmetric limit, there are also no problems:

$$\begin{aligned} e_{\mathrm{C}}^{w}(\rho \to 1) &= e_{\mathrm{C}}^{\mathrm{asym}}(u \to 0) \\ &= u^2\,\bar{\rho}^{5/2}\left(-\frac{1}{\sqrt{2}} + u\sqrt{\bar{\rho}}\right). \end{aligned} \tag{B.16}$$

Thus, the expansion in powers of u is well-behaved, and there are no difficulties using it for sufficiently small u. In the symmetric case, one sees explicitly that the radius of convergence of the expansion is $u = 2$.

On the other hand, the strong coupling limit is more problematic. Expanding the strong-couping functional around the symmetric limit, we find

$$e_{\mathrm{C}}^{\mathrm{str}}(\rho \to 0) = -\frac{u}{2} + 1 - \frac{1}{4\,u} - \sqrt{2\,\rho} + \rho\left(u + \frac{1}{4\,u}\right), \tag{B.17}$$

while reversing the order of limits yields:

$$e_{\rm C}^{\rm sym}(u\to\infty) = -\frac{u}{2} + 1 - \frac{1}{u} - \frac{\rho^2}{2}\left(1 - u - \frac{1}{2\,u} - \frac{u^3}{2}\right). \tag{B.18}$$

Note the difference beginning in the third terms, i.e. at first-order in $1/u$, even for $\rho = 0$. Thus for the Hubbard dimer, approximations based on expansions around the strong-coupling limit are likely to fail for some values of the density.

Appendix C. Proofs of energy relations

Using the notation established in section 6, we prove some simple relations about the energy and its components. Start with the general expression for the energy, equation (103) and (104),

$$\epsilon = \min_{\rho,g}[-g + uh(g,\rho) - \nu\rho]. \tag{C.1}$$

First take $\rho \to 0$. The second term reduces to $u\left(1-\sqrt{1-g^2}\right)/2$. Then let $g \to 0$, resulting in $h \to 0$. This yields $\epsilon \to 0$ and therefore the exact $\epsilon \leqslant 0$. This process corresponds to choosing a trial wavefunction, and by Rayleigh-Ritz, the ground-state wavefunction will produce a value equal to or below the trial result.

In Hartree–Fock, g reduces to $g_{\rm HF} = \sqrt{1-\rho^2}$. Then,

$$\epsilon^{\rm HF} = \min_{\rho} \epsilon(g_{\rm HF}(\rho),\rho) \geqslant \epsilon. \tag{C.2}$$

This shows that $\epsilon_{\rm C}^{\rm trad} = \epsilon - \epsilon^{\rm HF} \geqslant 0$, as in figure 6. The minimization can be performed analytically though it involves solving the quartic polynomial

$$\frac{\rho}{\sqrt{1-\rho^2}} + u\,\rho - \nu = 0. \tag{C.3}$$

Similarly, a DFT exact exchange (EXX) calculation is defined by

$$\epsilon^{\rm EXX} = \epsilon(g_{\rm HF}(\rho_m),\rho_m) \geqslant \min_{\rho} \epsilon(g_{\rm HF}(\rho),\rho) \tag{C.4}$$

where ρ_m is the minimizing density for the many-body problem. This yields $\epsilon_{\rm C}^{\rm DFT} = \epsilon - \epsilon^{\rm EXX}$, and $\epsilon_{\rm C}^{\rm trad} \geqslant \epsilon_{\rm C}^{\rm DFT}$ [78].

For the kinetic energy alone, $t = -g(\rho_m)$, and

$$t_{\rm S} = \min_{u\to 0,\rho}[-g(\rho)] = -\sqrt{1-\rho^2}. \tag{C.5}$$

This results in $t_{\rm C} \geqslant 0$ since the KS occupation difference is defined to minimize the hopping energy. This combined with the above implies $u_{\rm C} \leqslant 0$, as in equation (78).

For the adiabatic connection integrand, take a derivative of equation (110):

$$\frac{{\rm d}u_{\rm C}^{\lambda}}{{\rm d}\lambda} = \frac{u_{\rm C}(\rho,\lambda)}{\lambda} + \lambda u \frac{\partial h}{\partial g}\frac{\partial g}{\partial \lambda}. \tag{C.6}$$

The first term is less than zero by definition but the second needs more unraveling. To begin, from equation (103),

$$\frac{\partial f}{\partial g} = -1 + u\frac{\partial h}{\partial g}, \tag{C.7}$$

so, at the solution

$$\frac{\partial h}{\partial g} = \frac{1}{u}. \tag{C.8}$$

For λ near 1, Suppose $g(\lambda) \simeq g(1) + (\lambda-1)g'(1)$, and expand $\partial h/\partial g|_{g(\lambda)}$ in $g(\lambda)$ around $g(1)$:

$$\left.\frac{\partial h}{\partial g}\right|_{g(\lambda)} = \left.\frac{\partial h}{\partial g}\right|_{g(1)} + (\lambda-1)g'(1)\left.\frac{\partial^2 h}{\partial g^2}\right|_{g(1)} \tag{C.9}$$

The first term on the left is $1/(\lambda u) \approx (2-\lambda)/u$. After some algebra,

$$\left.\frac{\partial g}{\partial \lambda}\right|_{\lambda=1} = -\left(u\left.\frac{\partial^2 h}{\partial g^2}\right|_{g(1)}\right)^{-1} \tag{C.10}$$

Since the hopping term of f is linear in g, $\partial^2 f/\partial g^2 = \partial^2 h/\partial g^2$. The energy is a minimum at g so $\partial^2 f/\partial g^2 > 0$, thus $\partial g/\partial\lambda > 0$. Together, this results in

$${\rm d}U_{\rm C}^{\lambda}/{\rm d}\lambda < 0, \tag{C.11}$$

the adiabatic connection integrand is monotonically decreasing as seen in figure 21.

Appendix D. BALDA derivation

For an infinite homogeneous Hubbard chain of density $n = 1 + x$, the energy per site (in units of 2 t) is given approximately by

$$\bar{\epsilon}^{\rm unif} = u\,x\,\theta(x) + \alpha(x,\beta(U)) \tag{D.1}$$

where $\theta(x)$ is the Heaviside function and

$$\alpha(x,\beta) = -\frac{\beta}{\pi}\,\sin(\pi\,(1-|x|)/\beta)/\pi. \tag{D.2}$$

The function $\beta(u)$ varies smoothly from 1 at $u = 0$ to 2 as $u \to \infty$ [137], and satisfies

$$\alpha(0,\beta) = -4\int_0^{\infty} {\rm d}\,\xi\,\frac{J_0(\xi)\,J_1(\xi)}{\xi\,[1+\exp(u\,\xi))]} \tag{D.3}$$

This simple result is exact as $u \to 0$, $u \to \infty$ and at $n = 1$, and a good approximation (accurate to within a few percent) elsewhere [137] to the exact solution via Bethe ansatz [134]. In principle, β depends on n, and this dependence has been fit in later work [63]. Here, we use the simpler original version of a function of u only. In fact, the solution to equation (D.3) can be accurately fit (error below 1%) with a simple rational function,

$$\beta^{\rm fit}(u) = \frac{2 + au + bu^2}{1 + cu + bu^2} \tag{D.4}$$

with coefficients $a = 2c - \pi/4$ and $b = (a-c)/\log 2$ chosen to recover the small-u behavior to first-order, and the large u behavior to first order in $1/u$, and $c = 1.197\,963$ is fit to $\beta(u)$. This is useful for quick implementation of BALDA.

At $u = 0$, the hopping energy per site is just

$$\tilde{t}_{\rm S}^{\rm unif} = -\sin(\pi\,(1-|x|))/\pi, \tag{D.5}$$

while the Hartree-exchange energy per site is a simple local function:

$$\tilde{u}_{\rm HX}^{\rm unif} = u\,n^2/4. \tag{D.6}$$

Thus the correlation energy per site is just

$$\tilde{\epsilon}_{\rm C}^{\rm unif} = \tilde{\epsilon}^{\,\rm unif} - \tilde{t}_{\rm S}^{\rm unif} - \tilde{u}_{\rm HX}^{\rm unif}. \tag{D.7}$$

The BALDA approximation is then

$$\epsilon_{\rm XC}^{\rm BALDA} = \tilde{\epsilon}_{\rm XC}^{\rm unif}(n_1, U) + \tilde{\epsilon}_{\rm XC}^{\rm unif}(n_2, U). \tag{D.8}$$

Since the exchange is local, BALDA is exact for that contribution, and only correlation is approximated. Since $n_{1,2} = 1 \mp \Delta n/2$, $x = \mp\,\Delta n/2$ for sites 1 and 2 respectively. The BALDA HXC energy is then:

$$\epsilon_{\rm HXC}^{\rm BALDA} = 2\,(\alpha(\Delta n/2, U) - \alpha(\Delta n/2, 0)) + u|\Delta n|/2, \tag{D.9}$$

and was inserted into the KS equations (section 3.3) to find the results of section 7.2.

Appendix E. Mean-field derivation

The MF hamiltonian for the Hubbard dimer can be written in the number basis $|1\sigma, 2\sigma\rangle$ as follows

$$\hat{H}_\sigma^{\rm MF} = \begin{pmatrix} -\Delta v_\sigma^{\rm eff}/2 & -t \\ -t & \Delta v_\sigma^{\rm eff}/2 \end{pmatrix} \tag{E.1}$$

with $\sigma = \pm 1$ for spin up and down respectively. Setting $M = m_1 + m_2$ and $N = n_1 + n_2$ as the total magnetization and particle number of the system, the eigenvalues are

$$\begin{aligned} {\rm e}_{\pm,\sigma}^{\rm MF} &= \frac{U}{4}\,(N - \sigma\,M) \pm \frac{t_{\bar{\sigma}}^{\rm eff}}{2}, \\ t_\sigma^{\rm eff} &= 2\,t\sqrt{(\Delta v_\sigma^{\rm eff}/2\,t)^2 + 1}\,, \\ \Delta v_\sigma^{\rm eff} &= \Delta v + \frac{U}{2}\,(\Delta n - \sigma\,\Delta m). \end{aligned} \tag{E.2}$$

The total energy of the system is

$$E^{FM} = e_{-,\uparrow} + e_{+,\uparrow} - U_{\rm H} \tag{E.3}$$

$$E^{AFM} = e_{-,\uparrow} + e_{-,\downarrow} - U_{\rm H}, \tag{E.4}$$

where the Hartree term is written as

$$\begin{aligned} U_{\rm H} &= \frac{U}{4}(n_{1\uparrow}\,n_{1\downarrow} + n_{2\uparrow}\,n_{2\downarrow}) \\ &= \frac{U}{8}(N^2 - M^2 + \Delta n^2 - \Delta m^2). \end{aligned} \tag{E.5}$$

Depending on whether $E^{\rm AFM}$ is larger or smaller than $E^{\rm FM}$, the ground-state of the system may be ferromagnetic ($N = 2$, $|M| = 2$) or antiferromagnetic ($N = 2$, $M = 0$, $|\Delta m| \geqslant 0$). The paramagnetic state is a specific case of the AFM state with $\Delta m = 0$. Explicitly, for the ferromagnetic state we have the eigenstate energies and self-consistency equations

$$\Delta n = \Delta m = -\Delta v/\sqrt{4\,t^2 + \Delta v^2} \tag{E.6}$$

$$e_{\mp,\uparrow} = \mp\sqrt{4\,t^2 + \Delta v^2}/2 \tag{E.7}$$

On the other hand, the $M = 0$ state ($|\Delta m| > 0$ is AFM, $\Delta m = 0$ is PM) corresponds to the eigenvalues,

$$e_{-,\uparrow} = (U - t^{\rm eff}\Delta n)/2, \quad e_{-,\downarrow} = (U - t_\uparrow^{\rm eff})/2, \tag{E.8}$$

and self-consistency equations

$$\Delta n = -\sum_\sigma \frac{\Delta v_\sigma^{\rm eff}}{t_\sigma^{\rm eff}}, \quad \Delta m = -\sum_\sigma \sigma\frac{\Delta v_\sigma^{\rm eff}}{t_\sigma^{\rm eff}}, \tag{E.9}$$

and the expressions for $\Delta v_\sigma^{\rm eff}$ and $t_\sigma^{\rm eff}$ are given in equation (23). The self-consistency procedure needs to be carried out numerically in this case.

The total energy can also be written as

$$E^{\rm AFM,PM} = \frac{U}{2}\left(1 - \frac{\Delta n^2 - \Delta m^2}{4}\right) - \frac{t_\uparrow^{\rm eff} + t^{\rm eff}\Delta n}{2}. \tag{E.10}$$

In the PM case, the expressions can be simplified to give

$$\Delta n = \frac{-2\,\Delta v - U\,\Delta n}{\sqrt{(\Delta v + U\Delta n/2)^2 + 4\,t^2}} \tag{E.11}$$

for the occupations and

$$E^{\rm PM} = \frac{U}{2}\left(1 - \left(\frac{\Delta n}{2}\right)^2\right) - \sqrt{\left(\Delta v + \frac{U}{2}\,\Delta n\right)^2 + 4\,t^2}. \tag{E.12}$$

Appendix F. Relation between Hubbard model and real-space

To show how SOFT and real-space DFT are connected, begin with the one-electron dimer, H_2^+, with the protons separated by R. Use a basis of the exact atomic 1s orbitals, one on each site. This is a minimal basis in quantum chemistry. Then

$$\hat{h} = -\frac{1}{2}\nabla^2 - \frac{1}{r} - \frac{1}{|\mathbf{r} - R\mathbf{z}|} \tag{F.1}$$

where the bond is along the z-axis. Then the matrix elements of $\hat{h}$ in the basis set of atomic orbitals are:

$$v_1 = v_2 = \epsilon_A + j(R), \quad t = s(R)\,\epsilon_A + k(R) \tag{F.2}$$

where ϵ_A is the atomic energy (one Rydberg here) and

$$\begin{aligned} s(R) &= \langle A|B\rangle = {\rm e}^{-R}(1 + R + R^2/3) \\ j(R) &= \langle A|\frac{1}{|\mathbf{r} - R\mathbf{z}|}|A\rangle = -(1/R - {\rm e}^{-2R}(1 + 1/R)) \\ k(R) &= \langle A|\frac{1}{|\mathbf{r} - R\mathbf{z}|}|B\rangle = -{\rm e}^{-R}(1 + R), \end{aligned} \tag{F.3}$$

yielding the textbook eigenvalues (for the generalized eigenvalue problem):

$$\epsilon_\pm = \epsilon_A + (j \pm k)/(1 \pm s). \tag{F.4}$$

Of course, the orbitals can always be symmetrically orthogonalized in advance [146], in which case

$$v_{\text{ortho}} = \epsilon_A + (-j + ks)/(s^2 - 1), \tag{F.5}$$

$$t_{\text{ortho}} = -(sj - k)/(s^2 - 1). \tag{F.6}$$

Although physics textbooks often set the overlap to zero, this is inconsistent, as the size of the overlap is comparable to $k(R)$, say. Setting the on-site potential to zero (but re-adding its value to the energy) and using t_{ortho}, makes the solution equation (29) of the text produce the exact electronic energy in this minimal basis.

But quantum chemistry textbooks note that this calculation is horribly inaccurate, yielding a bond-length of 2.5 Bohr and a well depth of 2.75 eV. Inclusion of a p_z orbital on each site, and allowing the lengthscale of each orbital to vary, produces almost exact results of 2.00 Bohr and 4.76 eV. Thus, even in this simple case, more than one orbital per site is needed to converge to the real-space limit.

Next we consider repeating the minimal-basis calculation with one nuclear charge replaced by value Z. This yields an asymmetric tight-binding problem for which the orbitals can be orthogonalized and values of Δv and t deduced as a function of R. But note that changing Z will change both Δv and t simultaneously, unlike our asymmetric SOFT dimer, where only Δv changes. In real-space DFT, the kinetic energy functional remains the same, T_{S}^{W} of equation (20), for all R and every Z.

The situation is even more complicated for H_2 and its asymmetric variants. Clearly U becomes a function of R, but there are also several independent off-diagonal matrix elements that are R dependent. Again, all change as a function of both R and Z, but none of this occurs in SOFT. In real-space DFT, T_{S} is still the von Weisacker functional, U_H is always the Hartree energy, and the exact $E_{\text{XC}}[n]$ is independent of R and Z, but always produces the exact energy when iterated in the KS equations. In [41], they take a different approach by including a nearest-neighbor Hubbard U.

References

[1] Savin A, Gonze X and Umrigar C J 1998 *Chem. Phys. Lett.* **288** 391
[2] Abedinpour S, Bakhtiari M, Xianlong G, Polini M, Rizzi M and Tosi M 2007 *Laser Phys.* **17** 162
[3] Abedinpour S H, Polini M, Xianlong G and Tosi M P 2007 *Phys. Rev.* A **75** 015602
[4] Adamo C and Barone V 1999 *J. Chem. Phys.* **110** 6158
[5] Akande A and Sanvito S 2010 *Phys. Rev.* B **82** 245114
[6] Akande A and Sanvito S 2012 *J. Phys.: Condens. Matter* **24** 055602
[7] Alcaraz F C and Capelle K 2007 *Phys. Rev.* B **76** 035109
[8] Almbladh C-O and von Barth U 1985 *Phys. Rev.* B **31** 3231
[9] Almbladh C O and Pedroza A C 1984 *Phys. Rev.* A **29** 2322
[10] Anderson P W 1961 *Phys. Rev.* **124** 41
[11] Anderson P W 1987 *Science* **235** 1196
[12] Anisimov V I, Aryasetiawan F and Lichtenstein A I 1997 *J. Phys.: Condens. Matter* **9** 767
[13] Anisimov V I, Poteryaev A I, Korotin M A, Anokhin A O and Kotliar G 1997 *J. Phys.: Condens. Matter* **9** 7359
[14] Aryasetiawan F and Gunnarsson O 1998 *Rep. Prog. Phys.* **61** 237
[15] Aryasetiawan F and Gunnarsson O 2002 *Phys. Rev.* B **66** 165119
[16] Aryasetiawan F, Gunnarsson O and Rubio A 2002 *Europhys. Lett.* **57** 683
[17] Hammer B, Morikawa Y and Nørskov J 1996 *Phys. Rev. Lett.* **76** 2141
[18] Baerends E 2001 *Phys. Rev. Lett.* **87** 133004
[19] Baerends E J, Gritsenko O V and van Meer R 2013 *Phys. Chem. Chem. Phys.* **15** 16408
[20] von Barth U and Hedin L 1972 *J. Phys. C: Solid State Phys.* **5** 1629
[21] Bartlett R J and Musial M 2007 *Rev. Mod. Phys.* **79** 291
[22] Becke A D 1988 *Phys. Rev.* A **38** 3098
[23] Becke A D 1993 *J. Chem. Phys.* **98** 5648
[24] Bergfield J P, Liu Z-F, Burke K and Stafford C A 2012 *Phys. Rev. Lett.* **108** 066801
[25] Bickelhaupt F and Baerends E 2000 *Rev. Comput. Chem.* **15** 1
[26] Bickers N E and Scalapino D J 1989 *Ann. Phys.* **193** 206
[27] Bickers N E, Scalapino D J and White S R 1989 *Phys. Rev. Lett.* **62** 961
[28] Burke K 2012 *J. Chem. Phys.* **136** 150901
[29] Burke K, Ernzerhof M and Perdew J P 1997 *Chem. Phys. Lett.* **265** 115
[30] Burke K, Perdew J P and Ernzerhof M 1998 *J. Chem. Phys.* **109** 3760
[31] Burke K and Wagner L O 2013 *Int. J. Quant. Chem.* **113** 96
[32] Burke K, Werschnik J and Gross E K U 2005 *J. Chem. Phys.* **123** 062206
[33] Campo V L and Capelle K 2005 *Phys. Rev.* A **72** 061602
[34] Campo V L, Capelle K, Hooley C, Quintanilla J and Scarola V W 2012 *Phys. Rev.* A **85** 033644
[35] Campo V L Jr, Quintanilla J and Hooley C 2009 *Phys. B: Condens. Matter* **404** 3328 (*Proc. Int. Conf. on Strongly Correlated Electron Systems*)
[36] Capelle K 2006 *Braz. J. Phys.* **36** 1318
[37] Capelle K and Campo V L Jr 2013 *Phys. Rep.* **528** 91
[38] Capelle K, Lima N, Silva M and Oliveira L 2003 *The Fundamentals of Electron Density, Density Matrix and Density Functional Theory in Atoms, Molecules and the Solid State* (*Progress in Theoretical Chemistry and Physics* vol 14) ed N Gidopoulos and S Wilson (Berlin: Springer) pp 145–68
[39] Capelle K, Vignale G and Ullrich C A 2010 *Phys. Rev.* B **81** 125114
[40] Carrascal D J and Ferrer J 2012 *Phys. Rev.* B **85** 045110
[41] Chiappe G, Louis E, SanFabián E and Verges J A 2007 *Phys. Rev.* B **75** 195104
[42] Cohen A J and Mori-Sánchez P 2015 arXiv:1506.02230
[43] Cohen A, Mori-Sánchez P and Yang W 2008 *Phys. Rev.* B **77** 115123
[44] Cohen A J, Mori-Sánchez P and Yang W 2008 *Science* **321** 792
[45] Coulson C and Fischer I 1949 *Phil. Mag.* **40** 386
[46] Frydel D, Terilla W M and Burke K 2000 *J. Chem. Phys.* **112** 5292
[47] Dagotto E 1994 *Rev. Mod. Phys.* **66** 763
[48] Daul S and Noack R M 1998 *Phys. Rev.* B **58** 2635
[49] Dreizler R M and Gross E K U 1990 *Density Functional Theory: an Approach to the Quantum Many-Body Problem* (Berlin: Springer)
[50] Duffy D and Moreo A 1995 *Phys. Rev.* B **52** 15607
[51] Engel E and Dreizler R M 2011 *Density Functional Theory: an Advanced Course* (Berlin: Springer)
[52] Ernzerhof M and Scuseria G E 1999 *J. Chem. Phys.* **110** 5029
[53] Essler F, Korepin V and Schoutens K 1992 *Phys. Rev. Lett.* **68** 2960
[54] Essler F H L, Frahm H, Göhmann F, Klümper A and Korepin V E 2005 *The One-Dimensional Hubbard Model* (Cambridge: Cambridge University Press)

[55] Farzanehpour M and Tokatly I V 2012 *Phys. Rev.* B **86** 125130
[56] Feller D and Peterson K A 2007 *J. Chem. Phys.* **126** 114105
[57] Fermi E 1928 *Z. Phys.* A **48** 73
[58] Fetter A L and Walecka J D 1971 *Quantum Theory of Many-Particle Systems* (New York: McGraw-Hill)
[59] Feynman R P 1939 *Phys. Rev.* **56** 340
[60] Filippi C and Umrigar C J 1996 *J. Chem. Phys.* **105** 213
[61] Fradkin E 2013 *Field Theories of Condensed Matter Physics* 2nd edn (Cambridge: Cambridge University Press)
[62] Franca V V, Hörndlein D and Buchleitner A 2012 *Phys. Rev.* A **86** 033622
[63] Franca V V, Vieira D and Capelle K 2012 *New J. Phys.* **14** 073021
[64] Friesner R A 2005 *Proc. Natl Acad. Sci. USA* **102** 6648
[65] Fuchs M, Niquet Y-M, Gonze X and Burke K 2005 *J. Chem. Phys.* **122** 094116
[66] Fuks J I, Farzanehpour M, Tokatly I V, Appel H, Kurth S and Rubio A 2013 *Phys. Rev.* A **88** 062512
[67] Fuks J I and Maitra N T 2014 *Phys. Chem. Chem. Phys.* **16** 14504
[68] Fuks J I and Maitra N T 2014 *Phys. Rev.* A **89** 062502
[69] Georges A, Kotliar G, Krauth W and Rozenberg M J 1996 *Rev. Mod. Phys.* **68** 13
[70] Gori-Giorgi P and Seidl M 2010 *Phys. Chem. Chem. Phys.* **12** 14405
[71] Gori-Giorgi P, Seidl M and Vignale G 2009 *Phys. Rev. Lett.* **103** 166402
[72] Görling A 2005 *J. Chem. Phys.* **123** 062203
[73] Görling A and Ernzerhof M 1995 *Phys. Rev.* A **51** 4501
[74] Görling A and Levy M 1993 *Phys. Rev.* B **47** 13105
[75] Gritsenko O V and Baerends E J 2002 *J. Chem. Phys.* **117** 9154
[76] Gritsenko O V and Baerends E J 2004 *J. Chem. Phys.* **120** 8364
[77] Gritsenko O V, Braïda B and Baerends E J 2003 *J. Chem. Phys.* **119** 1937
[78] Gross E K U, Petersilka M and Grabo T 1996 *Chem. Appl. Density-Funct. Theory* **629** 42
[79] Grüning M, Gritsenko O V and Baerends E J 2003 *J. Chem. Phys.* **118** 7183
[80] Gunnarsson O and Lundqvist B 1976 *Phys. Rev.* B **13** 4274
[81] Gunnarsson O and Schönhammer K 1986 *Phys. Rev. Lett.* **56** 1968
[82] Ha Z 1996 *Quantum Many-body Systems in One Dimension* (*Series in Algebra*) (Singapore: World Scientific)
[83] Hafner J, Wolverton C and Ceder G 2011 *MRS Bull.* **31** 659
[84] Haldane F D M 1981 *J. Phys. C: Solid State Phys.* **14** 2585
[85] Hao Y and Chen S 2009 *Phys. Rev.* A **80** 043608
[86] Harriman J E 1986 *Phys. Rev.* A **34** 29
[87] Harris J and Jones R 1974 *J. Phys.* F **4** 1170
[88] Head-Gordon M 1996 *J. Phys. Chem.* **100** 13213
[89] Heaton R A, Harrison J G and Lin C C 1983 *Phys. Rev.* B **28** 5992
[90] Heitler W and London F 1927 *Z. Phys.* **44** 455
[91] Helgaker T, Ruden T A, Jørgensen P, Olsen J and Klopper W 2004 *J. Phys. Org. Chem.* **17** 913
[92] Hellgren M, Caruso F, Rohr D R, Ren X, Rubio A, Scheffler M and Rinke P 2015 *Phys. Rev.* B **91** 165110
[93] Herbut I 2006 *Phys. Rev. Lett.* **97** 146401
[94] Heyd J, Scuseria G E and Ernzerhof M 2003 *J. Chem. Phys.* **118** 8207
[95] Himmetoglu B, Floris A, de Gironcoli S and Cococcioni M 2014 *Int. J. Quantum Chem.* **114** 14
[96] Hirsch J E 1989 *Phys. Rev.* B **40** 2354
[97] Hirsch J E 1993 *Phys. Rev.* B **48** 3327
[98] Hohenberg P and Kohn W 1964 *Phys. Rev.* **136** B864
[99] Hu J-H, Wang J-J, Xianlong G, Okumura M, Igarashi R, Yamada S and Machida M 2010 *Phys. Rev.* B **82** 014202
[100] Hubbard J 1963 *Proc. R. Soc.* A **276** 238
[101] Ijäs M and Harju A 2010 *Phys. Rev.* B **82** 235111
[102] Perdew J P, Vosko S H, Jackson K A, Pederson M R, Singh D J, Chevary J A and Fiolhais C 1992 *Phys. Rev.* B **46** 6671
[103] Janak J 1978 *Phys. Rev.* B **18** 7165
[104] Johnson B G, Gonzales C A, Gill P M W and Pople J A 1994 *Chem. Phys. Lett.* **221** 100
[105] Karlsson D, Privitera A and Verdozzi C 2011 *Phys. Rev. Lett.* **106** 116401
[106] Karlsson D, Verdozzi C, Odashima M M and Capelle K 2011 *Europhys. Lett.* **93** 23003
[107] Kartsev A, Karlsson D, Privitera A and Verdozzi C 2013 *Sci. Rep.* **3** 2570
[108] Khosravi E, Uimonen A-M, Stan A, Stefanucci G, Kurth S, van Leeuwen R and Gross E K U 2012 *Phys. Rev.* B **85** 075103
[109] Kohn W 1964 *Phys. Rev.* **133** A171
[110] Kohn W 1999 *Rev. Mod. Phys.* **71** 1253
[111] Kohn W, Becke A and Parr R 1996 *J. Phys. Chem.* **100** 12974
[112] Kohn W and Sham L J 1965 *Phys. Rev.* **140** A1133
[113] Kondo J 1964 *Prog. Theor. Phys.* **32** 37
[114] Korepin V E and Essler F H 1994 *Exactly Solvable Models of Strongly Correlated Electrons* vol 18 (Singapore: World Scientific)
[115] Kotliar G, Savrasov S Y, Haule K, Oudovenko V S, Parcollet O and Marianetti C A 2006 *Rev. Mod. Phys.* **78** 865
[116] Kotliar G and Vollhardt D 2004 *Phys. Today* **57** 53
[117] Krieger J B, Li Y and Iafrate G J 1992 *Phys. Rev.* A **46** 5453
[118] Kulik H J 2015 *J. Chem. Phys.* **142** 240901
[119] Kulik H J and Marzari N 2010 *J. Chem. Phys.* **133** 114103
[120] Kümmel S and Kronik L 2008 *Rev. Mod. Phys.* **80** 3
[121] Kurth S and Stefanucci G 2011 *Chem. Phys.* **391** 164 (open problems and new solutions in time dependent density functional theory)
[122] Kurth S and Stefanucci G 2013 *Phys. Rev. Lett.* **111** 030601
[123] Kurth S, Stefanucci G, Khosravi E, Verdozzi C and Gross E K U 2010 *Phys. Rev. Lett.* **104** 236801
[124] Langreth D and Perdew J 1975 *Solid State Commun.* **17** 1425
[125] Langreth D and Perdew J 1977 *Phys. Rev.* B **15** 2884
[126] Lee C, Yang W and Parr R G 1988 *Phys. Rev.* B **37** 785
[127] Lee P A, Nagaosa N and Wen X-G 2006 *Rev. Mod. Phys.* **78** 17
[128] Lee T J and Scuseria G E 1995 *Quantum Mechanical Electronic Structure Calculations with Chemical Accuracy* (*Understanding Chemical Reactivity* vol 13) ed S Langhoff (Berlin: Springer) pp 47–108
[129] Levy M 1979 *Proc. Natl Acad. Sci. USA* **76** 6062
[130] Levy M and Perdew J 1985 *Phys. Rev.* A **32** 2010
[131] Li W, Xianlong G, Kollath C and Polini M 2008 *Phys. Rev.* B **78** 195109
[132] Lieb E H 1983 *Int. J. Quantum Chem.* **24** 243
[133] Lieb E H and Wu F 2003 *Physica* A **321** 1 (statphys-Taiwan-2002: lattice models and complex systems)
[134] Lieb E H and Wu F Y 1968 *Phys. Rev. Lett.* **20** 1445
Lieb E H and Wu F Y 1968 *Phys. Rev. Lett.* **21** 192
[135] Lima N, Malvezzi A and Capelle K 2007 *Solid State Commun.* **144** 557 (fundamental phenomena in low-dimensional electron systems)
[136] Lima N A, Oliveira L N and Capelle K 2002 *Europhys. Lett.* **60** 601
[137] Lima N A, Silva M F, Oliveira L N and Capelle K 2003 *Phys. Rev. Lett.* **90** 146402
[138] Lin H and Hirsch J 1987 *Phys. Rev.* B **35** 3359
[139] Liu Z-F, Bergfield J P, Burke K and Stafford C A 2012 *Phys. Rev.* B **85** 155117
[140] Liu Z-F and Burke K 2009 *J. Chem. Phys.* **131** 124124
[141] Liu Z-F and Burke K 2009 *Phys. Rev.* A **79** 064503

[142] López-Sandoval R and Pastor G M 2000 *Phys. Rev.* B **61** 1764
[143] López-Sandoval R and Pastor G M 2002 *Phys. Rev.* B **66** 155118
[144] López-Sandoval R and Pastor G M 2003 *Phys. Rev.* B **67** 035115
[145] López-Sandoval R and Pastor G M 2004 *Phys. Rev.* B **69** 085101
[146] Löwdin P-O 1950 *J. Chem. Phys.* **18** 365
[147] Magyar R J 2009 *Phys. Rev.* B **79** 195127
[148] Malet F and Gori-Giorgi P 2012 *Phys. Rev. Lett.* **109** 246402
[149] Mancini L, Ramsden J D, Hodgson M J P and Godby R W 2014 *Phys. Rev.* B **89** 195114
[150] Marques M A, Oliveira M J and Burnus T 2012 *Comput. Phys. Commun.* **183** 2272
[151] Marques M A L, Maitra N T, Nogueira F M S, Gross E K U and Rubio A (ed) 2012 *Fundamentals of Time-Dependent Density Functional Theory* (*Lecture Notes in Physics* vol 837) (Berlin: Springer)
[152] Martin R 2004 *Electronic Structure* (Cambridge: Cambridge University Press)
[153] Mattis D C 1993 *The Many-Body Problem: an Encyclopedia of Exactly Solved Models in One Dimension* 1st edn (Singapore: World Scientific)
[154] McLean A D, Weiss A and Yoshimine M 1960 *Rev. Mod. Phys.* **32** 211
[155] Mermin N D 1965 *Phys. Rev.* A **137** 1441
[156] Mirjani F and Thijssen J M 2011 *Phys. Rev.* B **83** 035415
[157] Mori-Sánchez P, Cohen A and Yang W 2008 *Phys. Rev. Lett.* **100** 146401
[158] Mori-Sanchez P and Cohen A J 2014 *Phys. Chem. Chem. Phys.* **16** 14378
[159] Mori-Sánchez P, Cohen A J and Yang W 2009 *Phys. Rev. Lett.* **102** 066403
[160] Murmann S, Bergschneider A, Klinkhamer V M, Zürn Z, Lompe T and Jochim S 2015 *Phys. Rev. Lett.* **114** 080402
[161] Ochterski J W, Petersson G A and Wiberg K B 1995 *J. Am. Chem. Soc.* **117** 11299
[162] Olsen T and Thygesen K S 2014 *J. Chem. Phys.* **140** 16
[163] Onida G, Reining L and Rubio A 2002 *Rev. Mod. Phys.* **74** 601
[164] O'Regan B and Graetzel M 1991 *Nature* **353** 737
[165] Over H, Kim Y, Seitsonen A, Wendt S, Lundgren E, Schmid M, Varga P, Morgante A and Ertl G 2000 *Science* **287** 1474
[166] Parr R G and Yang W 1989 *Density Functional Theory of Atoms and Molecules* (Oxford: Oxford University Press)
[167] Parr R G and Yang W 1995 *Annu. Rev. Phys. Chem.* **46** 701
[168] Peach M J G, Miller A M, Teale A M and Tozer D J 2008 *J. Chem. Phys.* **129** 6
[169] Pederson M R, Ruzsinszky A and Perdew J P 2014 *J. Chem. Phys.* **140** 121103
[170] Pemmaraju C, Archer T, Sanchez-Portal D and Sanvito S 2007 *Phys. Rev.* B **75** 045101
[171] Perdew J 1985 What do the kohn-sham orbitals mean? how do atoms dissociate? *Density Functional Methods in Physics* ed R Dreizler and J da Providencia (New York: Plenum) p 265
[172] Perdew J 1986 *Phys. Rev.* B **33** 8822
[173] Perdew J 1986 *Int. J. Quantum Chem. Symp.* **19** 497
[174] Perdew J P, Burke K and Ernzerhof M 1996 *Phys. Rev. Lett.* **77** 3865
Perdew J P, Burke K and Ernzerhof M 1996 *Phys. Rev. Lett.* **78** 1396
[175] Perdew J P, Ernzerhof M and Burke K 1996 *J. Chem. Phys.* **105** 9982
[176] Perdew J P and Levy M 1983 *Phys. Rev. Lett.* **51** 1884
[177] Perdew J P, Parr R G, Levy M and Balduz J L 1982 *Phys. Rev. Lett.* **49** 1691
[178] Perdew J P, Savin A and Burke K 1995 *Phys. Rev.* A **51** 4531
[179] Perdew J P and Wang Y 1992 *Phys. Rev.* B **45** 13244
[180] Perdew J P and Zunger A 1981 *Phys. Rev.* B **23** 5048
[181] Mori-Sánchez P, Cohen A and Yang W 2006 *J. Chem. Phys.* **124** 091102
[182] Pollehn T J, Schindlmayr A and Godby R W 1998 *J. Phys.: Condens. Matter* **10** 1273
[183] Pribram-Jones A, Gross D A and Burke K 2015 *Annu. Rev. Phys. Chem.* **66** 283–304
[184] Pribram-Jones A, Pittalis S, Gross E and Burke K 2014 *Frontiers and Challenges in Warm Dense Matter* (*Lecture Notes in Computational Science and Engineering* vol 96) ed F Graziani *et al* (Berlin: Springer) pp 25–60
[185] Purvis G D and Bartlett R J 1982 *J. Chem. Phys.* **76** 1910
[186] Puzder A, Chou M and Hood R 2001 *Phys. Rev.* A **6402** 2501
[187] Requist R and Pankratov O 2008 *Phys. Rev.* B **77** 235121
[188] Requist R and Pankratov O 2010 *Phys. Rev.* A **81** 042519
[189] Robert J, Niels S, Kenneth G, Henning M and Tilman E 2008 *Nature* **455** 204
[190] Romaniello P, Bechstedt F and Reining L 2012 *Phys. Rev.* B **85** 155131
[191] Romaniello P, Guyot S and Reining L 2009 *J. Chem. Phys.* **131** 154111
[192] Runge E and Gross E K U 1984 *Phys. Rev. Lett.* **52** 997
[193] Sagvolden E and Perdew J P 2008 *Phys. Rev.* A **77** 012517
[194] Sahni V and Levy M 1986 *Phys. Rev.* B **33** 3869
[195] Saubanère M and Pastor G M 2011 *Phys. Rev.* B **84** 035111
[196] Saubanère M and Pastor G M 2014 *Phys. Rev.* B **90** 125128
[197] Schaefer H 2012 *Quantum Chemistry: The Development of Ab Initio Methods in Molecular Electronic Structure Theory* (*Dover Books on Chemistry*) (New York: Dover)
[198] Schenk S, Dzierzawa M, Schwab P and Eckern U 2008 *Phys. Rev.* B **78** 165102
[199] Schenk S, Schwab P, Dzierzawa M and Eckern U 2011 *Phys. Rev.* B **83** 115128
[200] van Schilfgaarde M, Kotani T and Faleev S 2006 *Phys. Rev. Lett.* **96** 226402
[201] Schindlmayr A and Godby R W 1995 *Phys. Rev.* B **51** 10427
[202] Schönhammer K and Gunnarsson O 1987 *J. Phys. C: Solid State Phys.* **20** 3675
[203] Schönhammer K and Gunnarsson O 1988 *Phys. Rev.* B **37** 3128
[204] Schönhammer K, Gunnarsson O and Noack R M 1995 *Phys. Rev.* B **52** 2504
[205] Schulz H J 1990 *Phys. Rev. Lett.* **65** 2462
[206] Seidl M, Gori-Giorgi P and Savin A 2007 *Phys. Rev.* A **75** 042511
[207] Seidl M, Perdew J P and Levy M 1999 *Phys. Rev.* A **59** 51
[208] Sham L J and Schlüter M 1983 *Phys. Rev. Lett.* **51** 1888
[209] Sharp R and Horton G 1953 *Phys. Rev.* **90** 317
[210] Silva M F, Lima N A, Malvezzi A L and Capelle K 2005 *Phys. Rev.* B **71** 125130
[211] Site L D 2015 *Chem. Phys. Lett.* **619** 148
[212] Solovyev I V 2008 *J. Phys.: Condens. Matter* **20** 293201
[213] Stanton J F 1997 *Chem. Phys. Lett.* **281** 130
[214] Stoudenmire E M, Wagner L O, White S R and Burke K 2012 *Phys. Rev. Lett.* **109** 056402
[215] Szabo A and Ostlund N S 1996 *Modern Quantum Chemistry* (New York: Dover)
[216] Takahashi M 2005 *Thermodynamics of One-Dimensional Solvable Models* (Cambridge: Cambridge University Press)
[217] Talman J and Shadwick W 1976 *Phys. Rev.* A **14** 36
[218] Thackeray M M, Wolverton C and Isaacs E D 2012 *Energy Environ. Sci.* **5** 7854
[219] Thomas L H 1927 *Math. Proc. Camb. Phil. Soc.* **23** 542
[220] Tokatly I V 2011 *Phys. Rev.* B **83** 035127
[221] Töws W and Pastor G M 2011 *Phys. Rev.* B **83** 235101
[222] Turkowski V and Rahman T S 2014 *J. Phys.: Condens. Matter* **26** 022201

[223] Uimonen A-M, Khosravi E, Stan A, Stefanucci G, Kurth S, van Leeuwen R and Gross E K U 2011 *Phys. Rev.* B **84** 115103
[224] Ullrich C A 2012 *Time-Dependent Density-Functional Theory* (Oxford: Oxford University Press)
[225] Umrigar C J and Gonze X 1994 *Phys. Rev.* A **50** 3827
[226] Umrigar C J and Nightingale M 1999 *Quantum Monte Carlo Methods in Physics and Chemistry* vol 525 (Berlin: Springer)
[227] Verdozzi C 2008 *Phys. Rev. Lett.* **101** 166401
[228] Verdozzi C, Godby R W and Holloway S 1995 *Phys. Rev. Lett.* **74** 2327
[229] Verdozzi C, Karlsson D, von Friesen M P, Almbladh C-O and von Barth U 2011 *Chemical Physics* **391** 37 (open problems and new solutions in time dependent density functional theory)
[230] Vettchinkina V, Kartsev A, Karlsson D and Verdozzi C 2013 *Phys. Rev.* B **87** 115117
[231] Vieira D 2012 *Phys. Rev.* B **86** 075132
[232] Vieira D 2014 *J. Chem. Theory Comput.* **10** 3641
[233] Vieira D and Capelle K 2010 *J. Chem. Theory Comput.* **6** 3319
[234] Vieira D, Freire H J, Campo V L Jr and Capelle K 2008 *J. Magn. Magn. Mater.* **320** e418 (VIII Latin American Workshop on Magnetism, Magnetic Materials and their Applications)
[235] Wagner L O, Baker T E, Stoudenmire E M, Burke K and White S R 2014 *Phys. Rev.* B **90** 045109
[236] Wagner L O, Stoudenmire E, Burke K and White S R 2012 *Phys. Chem. Chem. Phys.* **14** 8581
[237] Wagner L O, Stoudenmire E M, Burke K and White S R 2013 *Phys. Rev. Lett.* **111** 093003
[238] Wang H, Hao Y and Zhang Y 2012 *Phys. Rev.* A **85** 053630
[239] Wang H and Zhang Y 2013 *Phys. Rev.* A **88** 023626
[240] Weizsäcker C F V 1935 *Z. Phys.* A **96** 431
[241] Xianlong G 2008 *Phys. Rev.* B **78** 085108
[242] Xianlong G 2012 *Phys. Rev.* A **86** 023616
[243] Xianlong G 2013 *Phys. Rev.* A **87** 023628
[244] Xianlong G and Asgari R 2008 *Phys. Rev.* A **77** 033604
[245] Xianlong G, Chen A-H, Tokatly I V and Kurth S 2012 *Phys. Rev.* B **86** 235139
[246] Xianlong G, Polini M, Asgari R and Tosi M P 2006 *Phys. Rev.* A **73** 033609
[247] Xianlong G, Polini M, Tanatar B and Tosi M P 2006 *Phys. Rev.* B **73** 161103
[248] Xianlong G, Polini M, Tosi M P, Campo V L, Capelle K and Rigol M 2006 *Phys. Rev.* B **73** 165120
[249] Yang J, Hu W, Usvyat D, Matthews D, Schütz M and Chan G K-L 2014 *Science* **345** 640
[250] Yang W, Cohen A J and Mori-Sanchez P 2012 *J. Chem. Phys.* **136** 204111
[251] Yang W and Wu Q 2002 *Phys. Rev. Lett.* **89** 143002
[252] Ying Z-J, Brosco V and Lorenzana J 2014 *Phys. Rev.* B **89** 205130